IN-SITU MONITORING OF THE MECHANICAL PROPERTIES DURING THE PHOTOPOLYMERIZATION OF ACRYLATE RESINS USING PARTICLE TRACKING MICRORHEOLOGY

A Dissertation
Presented to
The Academic Faculty

By
Ryan Patrick Slopek

In Partial Fulfillment
of the Requirements for the Degree
Doctor of Philosophy in the
School of Chemical and Biomolecular Engineering

Georgia Institute of Technology
May 2008

IN-SITU MONITORING OF THE MECHANICAL PROPERTIES DURING THE PHOTOPOLYMERIZATION OF ACRYLATE RESINS USING PARTICLE TRACKING MICRORHEOLOGY

Approved by:

Dr. Victor Breedveld, Thesis Chair
School of Chemical and Biomolecular Engineering
Georgia Institute of Technology

Dr. Cliff Henderson
School of Chemical and Biomolecular Engineering
Georgia Institute of Technology

Dr. Pete Ludovice
School of Chemical and Biomolecular Engineering
Georgia Institute of Technology

Dr. David Rosen
George W. Woodruff School of Mechanical Engineering
Georgia Institute of Technology

Dr. Sai Kumar
AccuRx, Inc.

Date Approved: January 25, 2008

In the depths of winter I finally learned
that there was in me an invincible
summer.

-Albert Camus (1913-1960)

ACKNOWLEDGEMENTS

I would to thank my research advisor, Dr. Victor Breedveld, for his guidance, insight, patience, and time. His encouragement and advice greatly contributed to the success of this research. I would also like to thank Dr. Cliff Henderson for sharing his knowledge of photo-induced curing and for allowing me the use of several key pieces of research equipment. In addition, I would like to thank Dr. Pete Ludovice and Dr. David Rosen for taking the time and agreeing to be a part of my committee. Your suggestions and insight were invaluable to the advancement of my research. I also want to thank Dr. Sai Kumar, a former supervisor and member of my committee, for teaching me to never stop asking questions.

I am also eternally grateful to many others for directly helping with this research. Specifically, I would like to thank Haris McKinley for the time and knowledge he invested in starting this research project. I am grateful to Gökcen Altun and Dr. Yanyan Tang, for answering my questions and allowing me the opportunity to compare my experimental results to their modeled results. I will forever be indebted to Dr. Jun Sato and the rest of the complex fluids group for the countless times they helped out along the way.

I would like to thank my good friends for making the best of the worst times—thank you all so much. I am especially grateful to Akua, Ayanna, and Krista, who stuck with me in good times and bad—you'll always remain in my thoughts and prayers.

Finally, I would like to thank my parents for their unbounded support and encouragement—words cannot thank you enough.

TABLE OF CONTENTS

LIST OF TABLES

LIST OF FIGURES

SUMMARY

Photopolymerization is the basis of several multi-million dollar industries including films and coating, rapid prototyping, inks, adhesives, fiber optics, and biomaterials. The fundamentals of the photopolymerization process, however, are not well understood. As a result, issues affecting the cure speed and overall quality of the final product (shape, size, and surface finish) of photopolymerization impose significant limitations on applications that require fast processing and high spatial resolution.

To address this issue, microrheology was employed to perform in-situ monitoring of the liquid-to-gel transition during free-radical photopolymerization. Photosensitive acrylate and hydrogel resins were exposed to ultraviolet light, while the Brownian motion of micrometer sized, inert fluorescent tracer particles was tracked via optical videomicroscopy. Statistical analysis of particle motion yielded the rheological properties of the embedding medium as a function of time and location, thereby relating UV exposure to the progress of polymerization and gelation.

The microrheological setup enabled a detailed study of three-dimensional gelation profiles; other experimental parameters that were initially varied include photoinitiator concentration, monomer composition, and light intensity. Significant changes in gelation time were observed with varying UV intensity and UV penetration depth into the sample. In addition, oxygen inhibition was found to significantly impact the cure speed of monomeric resins. The preliminary results were used to test the accuracy of the energy

threshold model, which is often used to empirically predict the outcome of photopolymerization reactions.

By using lithographic masks to generate well-defined UV illumination patterns with characteristic dimensions of tens of micrometers, it could be shown unambiguously that the diffusion of oxygen, an inhibitor, plays a critical role in the polymerization reaction. The experiments are in excellent agreement with a simple two-step model of oxygen consumption followed by polymerization.

The use of high-speed electronic shutters in the UV light path enabled us to control the illumination time of the samples with high precision. Microrheological analysis could be used to reconstruct three-dimensional profiles of partially polymerized samples. Traditional photorheometry is not capable of resolving the evolution of sample rheology with such spatial resolution. In addition, experiments with pulsed illumination were used to quantify the role of dark reactions due to residual free radicals after termination of UV illumination.

These microrheology experiments provided unique information that is unattainable with other characterization methods typically used to study photopolymerization (FTIR, DSC) and this knowledge can be used to develop a more quantitative understanding of the process.

CHAPTER 1

INTRODUCTION

In this chapter, the importance of photopolymerization to both industry and the consumer will be stressed, along with the current issues that limit the application of photopolymerization. In addition, a brief review of the techniques used to study photopolymerization will be offered. The method and theory behind microrheology, the technique employed in this research, will be explained in detail. Finally, the goals of this research project will be formulated to investigate and resolve some of the present limitations of photopolymerization.

1.1. Photopolymerization

UV-initiated free-radical photopolymerization of multifunctional liquid monomers in the presence of a photoinitiator is one of the most efficient methods to produce solid coatings and objects. The process results in the almost instantaneous transformation of a liquid resin into a highly cross-linked solid polymer that is insoluble in organic solvents and resistant to both heat and mechanical treatments. Several books [1-6] and reviews [7-10] have been written on the subject of photopolymerization.

Besides the high cure speed, light-induced polymerization has a number of other favorable features such as solvent-free formulation, low energy consumption, ambient temperature operation, and tunable properties like color, flexibility, clarity, and surface characteristics of the final products. Because of its distinct advantages, this technology

has experienced a steady growth over the last few decades. UV-curing has become an established technology for a large variety of commercial applications, primarily in the coating and printing industries, but also in photolithography, biomaterials, the manufacture of adhesives, and restorative dental materials.

Currently, issues affecting the cure speed and overall quality of the final product (shape, size, and surface finish) are limiting the use of photo-polymerization in certain fields. For example, inhibition by oxygen in free-radical polymerization leads to a significant decrease in cure speed and complicates the overall reaction chemistry. Another disadvantage is the inability of many lasers and UV exposure tools to homogeneously cure thick or strongly absorbing samples. Finally, the problem of inhomogeneity in the cure of polymer negatively impacts mechanical properties and the stability of the final polymer product. All of these limitations are the result of a general lack of understanding and control of the photopolymerization process.

1.1.1. Photopolymerization Systems

Photopolymerization systems usually contain three main components: monomer, initiator, and additives used to impart desired properties. Unsaturated monomers containing a carbon-carbon double bond are extensively used in photoinduced free-radical polymerizations. The free-radical active center reacts with the unsaturated monomer by opening the carbon-carbon double bond and adding the molecule to the growing polymer chain. The three main free-radical photopolymerization systems used are and (meth-)acrylate, thiol-ene, and unsaturated polyester systems.

Acrylate and methacrylate monomers are by far the most widely used in free-radical photopolymerization processes [9]. The successful commercial use of these UV-

curable resins can be attributed to their high reactivity and ability to form a large variety of cross-linked polymers with tailor made properties such as color, flexibility and surface characteristics. The generalized structure of these monomers and their corresponding polymer is shown in Figure 1.1.

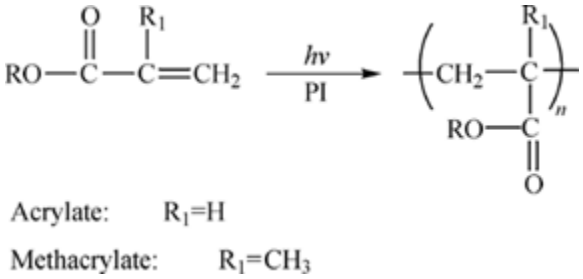

Figure 1.1: Molecular structure of a generalized acrylate monomer and its corresponding polymer repeat unit; the R side group may vary.

Studies have shown that acrylates have faster reaction rates then their methacrylate counterparts [11]. The functionality of acrylate monomers plays a key role in rheological properties and curing speed, with higher functional monomers having a higher viscosity and faster cure speed [4]. Linear acrylates are generally used as reactive diluents to reduce the viscosity of the unpolymerized liquid for ease of processing. Multifunctional acrylates increase the mechanical strength and solvent resistance of the polymer product by forming cross-linked networks rather than linear polymer chains [9, 10].

Acrylate and methacrylate systems have several drawbacks, including relatively large polymerization shrinkage and high toxicity of some monomers. Methacrylates are considered less toxic and volatile than their acrylate counterparts [2]. Shrinkage causes stress in the polymer parts, which ultimately affects performance; it is a result of the formation of covalent bonds between monomer molecules. Covalent bonds decrease the

distance between monomer molecules by approximately half compared to two molecules experiencing van der Waal's forces. Shrinkage results in a 5-25% loss in volume (2-8% in linear dimensions) [2, 10]. Thus, shrinkage places a financial burden on industries that rely on acrylate and methacrylate photopolymerization systems. The effects of shrinkage can be minimized by using oligomeric acrylates, which contain 1 to12 repeat units formed via step-growth polymerization [2, 3, 9, 10].

Since most of the commonly used monomers do not produce free-radicals when exposed to UV light, it is necessary to include photoinitiators to initiate the polymerization process by producing free-radicals upon illumination. Upon absorption of light with a specific frequency, the photoinitiator molecule is promoted from the ground electronic state to either a singlet or triplet excited electronic state. These excited molecules then undergo cleavage or react with another molecule to produce initiating free radicals [1]. The photoinitiator plays a key role in that it governs both the rate of initiation and the penetration of the incident light into the sample as a result of absorption, and therefore cure depth [9]. Only free-radical photoinitiator systems, commonly classified as type I and type II, will be described here.

Type I photoinitiators are usually termed unimolecular because the initiation system involves only one molecular species interacting with the light and producing free-radicals. One class involves photoinitiators that form radicals through cleavage of the initiator molecule as shown in Figure 1.2 [9]. This cleavage may take place at the α or β position with respect to the carbonyl group. Cleavage occurs mainly in aromatic carbonyl compounds; α-cleavage occurs if the bond adjacent to the carbonyl is broken to produce two free radicals, one benzoyl and one fragment radical [1, 10]. The

benzoyl radical is the major initiating species, while the fragment in some cases may or may not contribute to the initiation [10]. β-cleavage occurs predominately in photoinitiators with a carbon-sulfur bond or a carbon-oxygen bond adjacent to the benzoyl chromophore [1, 10]. A second class of unimolecular photoinitiator includes those that form biradicals through intramolecular hydrogen abstraction as shown in Figure 1.3 [10]. This mechanism commonly occurs in ketones and results in a ketyl radical, which participates in termination, and another radical that induces growth of the polymer chain.

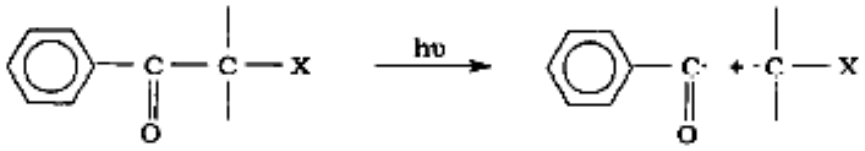

Figure 1.2: Cleavage mechanism of unimolecular photoinitiator free-radical generation [9].

Figure 1.3: Hydrogen abstraction mechanism of unimolecular photoinitiator free-radical generation between the photoinitiator benzophenone and the hydrogen donor tetrahydrofuran [10].

If the photoinitiator in its excited state interacts with a second co-initiating molecule to generate radicals by a bimolecular reaction as shown in Figure 1.4 [10], the initiating system is termed bimolecular or Type II. Once the photoinitiator is in the excited state, the co-initiator, which is usually an ether or an alcohol, serves as a hydrogen or electron donor. The reaction results in the formation of free-radicals, one or more of which may actually begin the photopolymerization process. Photoinitiator

families of this class include benzophenone derivatives, thioxanthones, camphorquinones, benzyls, and ketocoumarins [9, 10].

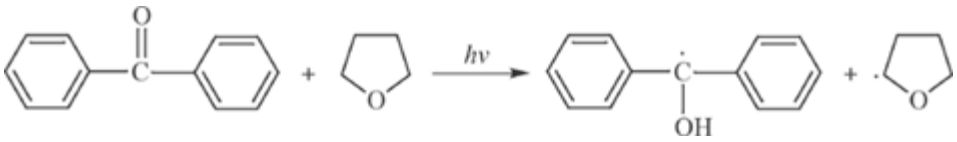

Figure 1.4: General bimolecular photoinitiator free-radical generation mechanism shown for intramolecular H-abstraction of photoinitiator 1-phyenyl-butan-1-one [6].

Bimolecular systems require longer wavelengths and, therefore, less energy than unimolecular systems, which are typically constrained to use in the UV region of the spectrum because of the absorption characteristics of the benzoyl chromophore. The production of free-radicals in bimolecular systems, however, decreases in vitrifying systems because diffusion of the initiator and co-initiator molecules is strongly suppressed [1, 10].

1.1.2. Photopolymerization Kinetics

A description of free-radical kinetics must take into account three basic steps: initiation, which creates free-radical active centers; propagation, which grows the polymer chains; and termination, which destroys the active centers and ends chain growth. The kinetics of linear and multifunctional monomer systems vary only in the way the chain is propagated and free-radicals are terminated. Figure 1.5 [9] outlines the basic steps of free-radical photopolymerization of a linear photoresin. The kinetics of a multifunctional photoresin are more complicated and include cross-linking as shown in Figure 1.6 [9]. Another important aspect of free-radical kinetics is the inhibition of the process. Discussion of photopolymerization kinetics will be limited to free-radical

photopolymerizations since the kinetics of cationic photopolymerization are not well understood.

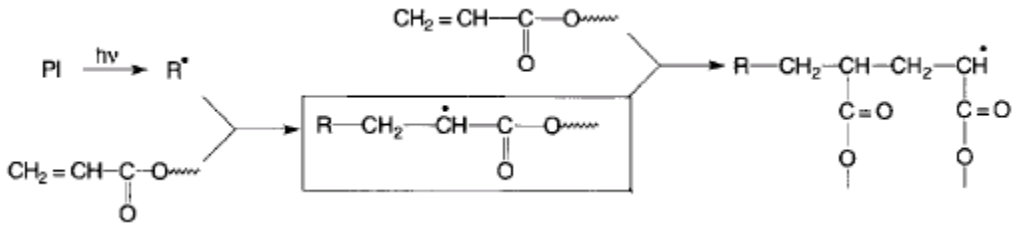

Figure 1.5: Schematic representation of linear photopolymerization kinetics [9].

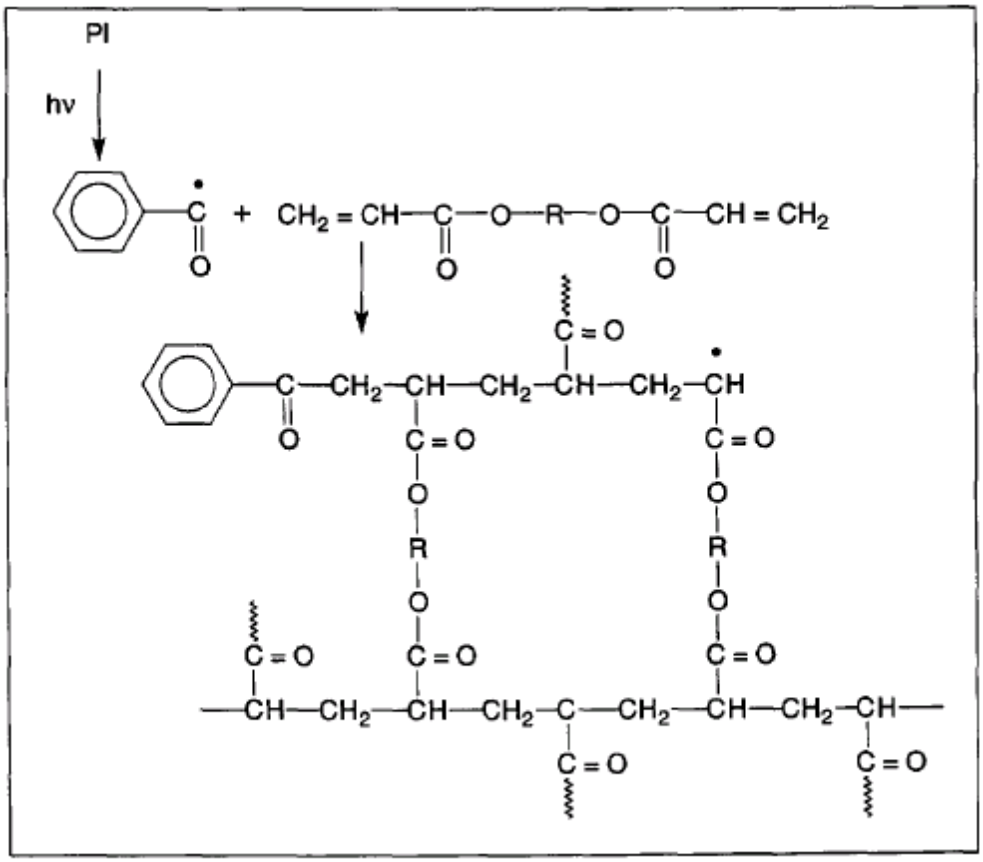

Figure 1.6: Schematic representation of the kinetics of a multifunctional photopolymerization reaction [9].

In photoinduced free-radical polymerization, the rate of initiation depends on two processes: the dissociation of the initiator and the initiation of the propagating chain. The basic equations for initiation are:

$$In \xrightarrow{h\nu} R^{\bullet} \tag{1.1}$$

$$R^{\bullet} + M \xrightarrow{k_i} M_n^{\bullet} \tag{1.2}$$

where *In* is the photoinitiator and $R^{\bullet}$ is a growing free-radical. The main mechanisms of radical generation are by photocleavage of aromatic carbonyl compounds, which undergo a Norrish type 1 bond scission and by hydrogen abstraction from a hydrogen donating molecule, to generate a ketyl radical and a donor radical [1, 9].

The rate at which photons are absorbed at a specific wavelength will determine the decomposition rate of photoinitiators, and ultimately the initiation of the propagating chain. An important parameter in the rate of initiation is the amount of photons absorbed by the photoinitiator molecules, I_a, which is commonly expressed in (mol photon/L•s). Beer's Law, which relates the absorption of light to the concentration of the absorbing species, is used to define I_a for a specified wavelength of light. Beer's Law originates from the partial differential equation used to describe the intensity of light passing through an absorbing medium:

$$\frac{dI}{dx} = -kI \tag{1.3}$$

where I is the intensity and k is the absorption coefficient. The absorption coefficient combines the terms of molar absorptivity, ε, (in cm^{-1} M^{-1}) and concentration of absorbing species [I] (in M) into a single term with the units of inverse centimeters [1, 10]. Equation 1.3 can be integrated to ultimately yield:

$$I_a = I_0 \exp(-kx) \tag{1.4}$$

where I_0 is the intensity of the incident light [1, 6]. Essentially, Beer's Law states that there is an exponential dependence between the transmission of light through an absorbing medium and the absorption coefficient, k, which is often a linear function of

the concentration of the absorbing species. Analysis of Beer's Law with respect to photopolymerization has shown that the optimum value of I_a depends on the concentration of photoinitiator [1]. For example, in a thick sample simply increasing the amount of photoinitiator does not result in a homogeneous reaction rate since upper layers of the sample will absorb the largest fraction of incident light, limiting initiation near the bottom of the sample.

Free-radical photoinitiated polymerization usually follows chain growth polymerization kinetics; therefore, propagation involves the addition of monomer to the growing polymer chain as shown in the following basic equation:

$$M_n^{\bullet} + M \xrightarrow{k_p} M_{n+1}^{\bullet} \tag{1.5}$$

where M is the monomeric photoresin and $M_n^{\bullet}$ represents a growing polymer chain. The propagation step is where physical and chemical changes in the photopolymerization system begin to become more evident. The rate of propagation is primarily dependent on the functionality of the monomer [5]. For linear monomers the propagation step is marked by a steady increase in both viscosity and elastic modulus resulting from spatial hindrance associated with continued chain elongation. Multifunctional monomers undergo a more rapid change in both viscosity and elastic modulus due to the formation of dense cross-linked networks, which ultimately leads to the creation of a solid polymer. Increasing the monomer functionality accelerates the curing reaction, but also reduces the final degree of conversion, because gelation of the irradiated sample restricts the mobility of the reactive species and prevents completion of the polymerization reaction [1].

Termination of free-radical active centers may occur either by combination or by disproportionation [1, 5, 6]. In termination by combination, two propagating chains unite to form one long polymer molecule:

$$M_n^{\bullet} + M_m^{\bullet} \xrightarrow{k_{tc}} M_{n+m} \tag{1.6}$$

In termination by disproportionation, one propagating chain abstracts a hydrogen atom from a neighboring propagating chain, resulting in two polymer molecules, one of them having a terminal double bond:

$$M_n^{\bullet} + M_m^{\bullet} \xrightarrow{k_{td}} M_n + M_m \tag{1.7}$$

The rate of termination for linear monomers, which is generally assumed to be independent of chain length, equals the rate of destruction of propagating active centers [1]. Termination mechanisms are more complex for multifunctional monomers because free-radical center trapping and effects of reaction—diffusion must be considered [5]. As a result of cross-linking in multifunctional monomers, free-radicals often become trapped in the network and are unable to react further. This often leaves a substantial amount of unterminated active centers and unreacted double bonds in cross-linked polymer systems [1].

One of the major disadvantages of free-radical photopolymerization is its susceptibility to oxygen inhibition. This inhibition is particularly problematic in thin-film and coating applications where oxygen diffusion plays a significant role in increasing cure times, which often results in incomplete conversion at exposed surfaces [8, 9]. When oxygen, which is essentially a biradical in its electronic ground state, reacts with a free-radical, it forms a peroxy radical, which is much less reactive [1]:

$$M^{\bullet} + O_2 \xrightarrow{k_o} M - O - O^{\bullet} \quad (1.8)$$

$$M - O - O^{\bullet} + M \longrightarrow No \;\; Rxn \quad (1.9)$$

Hence, oxygen effectively acts as a chain terminator and reduces the rate of polymerization until all oxygen in the system has been consumed [1].

Costs associated with combating the effects of oxygen inhibition are high. One way to minimize the effect is to blanket the system with an inert gas such as nitrogen, carbon dioxide, or argon [12, 13]. Waxes or shielding films may also be used to prevent oxygen from entering the system. Other methods include adding oxygen scavengers, dye sensitizers, or antioxidants to capture oxygen and prevent it from reacting with propagating chains [1]. High concentrations of photoinitiator or increased light intensity may also be used to increase the production of free-radicals in order to consume the oxygen within the system more rapidly. The last method, however, is ineffective close to the surface because it becomes difficult to consume the oxygen faster than it diffuses into the sample [12, 13].

Formulators knowingly introduce polymerization inhibitors, such as hydroquinone (HQ) and hydroquinone monomethyl ether (MEHQ), in order to promote process and shelf stability of highly reactive acrylate monomer based formulations. The inhibitors act by reacting with the initiating and propagating free-radicals and converting them either to nonradical species or low reactive radicals that are unable to promote propagation:

$$M^{\bullet} + Z \xrightarrow{k_z} M + Z^{\bullet} \quad (1.10)$$

$$M^{\bullet} + Z \xrightarrow{k_z} MZ^{\bullet} \quad (1.11)$$

$$M + Z^{\bullet} or\, MZ^{\bullet} + M \longrightarrow No \;\; Rxn \quad (1.13)$$

When used in small amounts, inhibitors can scavenge free-radicals that form during the manufacturing process or storage, without negatively effecting cure time or final properties. The concentration of inhibitor is dependent on the inherent instability and functionality of the monomer. Once all the inhibitor is consumed, the polymerization will proceed as usual.

1.1.3. Gelation Theory

The liquid-to-solid transition during the polymerization of monomeric materials is marked by a point of gelation, which in free-radical photopolymerization is the result of chain elongation and the formation of densely cross-linked networks. The transition is often preceded by a rapid increase in viscosity; therefore, gelation can readily be detected with rheological techniques. There are two different types of gelation: chemical gelation, which result from the formation of chemical bonds and physical gelation, which result from the growth of physically connected aggregates. The principal distinction between chemical and physical gelation is the lifetime of the junctions. Chemical bonds are considered permanent while physical junctions due to intermolecular association are finite, constantly being formed and destroyed at such slow rates that the network appears to be permanently connected.

The development of equilibrium mechanical properties during gelation is graphically illustrated in Figure 1.7 [14]. As connectivity builds, the steady shear viscosity of the liquid, η, sample grows quickly in the approach to gelation and diverges to infinity at the point of gelation. At the gel point, the equilibrium modulus, G_∞, remains near zero because the stress in a deformed gel can still relax completely; however, beyond the point of gelation the equilibrium modulus starts to increasingly develop. The

rheological behavior at the point of gelation is unique in that infinite time is required for stress relaxation, which results in a broad distribution of shorter self-similar modes.

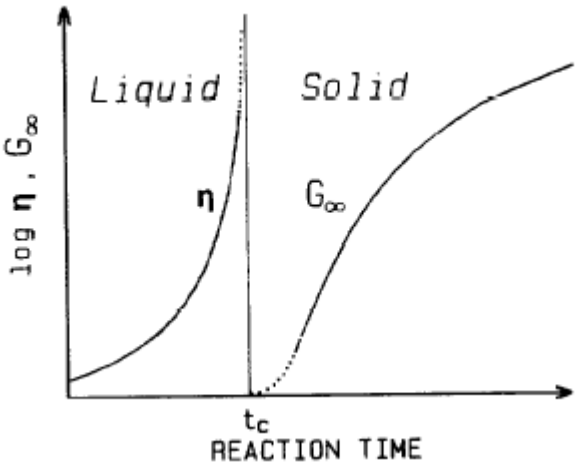

Figure 1.7: Steady shear viscosity and equilibrium modulus of a crossing-linking polymer as a function of reaction time [14].

The photoresin remains a liquid polymer until a critical degree of conversion is reached, which is theoretically equivalent to the gel point [15, 16]. Classical mean-field theories with the ability to predict the critical conversion with reasonable accuracy have been developed [15]. The predictive theories are based on the assumptions that all functional groups of the same type are equally reactive, all groups react independently of one another, and intramolecular condensation does not occur. Flory developed a parameter, α, which can be used to predict the threshold conversion. The Flory parameter depends on the geometry of the network-forming species and is defined as the probability that a given functional group of a branch unit leads, via a chain of bifunctional units, to another branch unit. For homopolymerization, the Flory parameter is defined as [16]:

$$\alpha_c = \frac{1}{1-f} \tag{1.14}$$

where *f* is the functionality of the branching unit, which is defined by Flory as the number of other molecules that can react with the network-forming species. For example a trifunctional monomer has the ability to bond with six other molecules; therefore, according to Flory the monomer would have a functionality *f*=6. The bifunctional acrylate in Figure 1.6 can connect with four molecules, and thus *f*=4. Monomers with higher functionality form infinite cross-linked networks more rapidly than ones with lower functionality. As a result, monomers with higher functionality have to reach a lower critical degree of conversion for gelation to occur. After reaching this threshold conversion, lower functional monomers proceed to higher final conversions as a result of less steric hindrance.

Measurements to determine the instant of gelation can be obtained using several techniques, including rheology and light scattering. Equilibrium rheological techniques, which subject the sample to shear flow, are able to estimate the position of the gel point by extrapolating the appearance of an equilibrium modulus or the divergence of the steady shear viscosity (see Figure 1.7). The major shortcoming of such equilibrium measurements is that the apparent gel point, not the real gel point, is yielded as a result of extrapolation of an experiment that can never really reach equilibrium[17]. Transient rheological techniques, such as dynamic mechanical analysis, apply small amplitude oscillatory shear to the sample. These techniques are better suited for determining the gel point because no extrapolation is required and the instant of gelation can be measured as accurately as the rheometer permits. Dynamic light scattering allows for the nondestructive, real-time determination of both the gel point and the critical dynamics

near the point of gelation [17]. Techniques such as spectroscopy and calorimetry are used to measure the critical degree of conversion at the gel point.

There are several definitions and classifications of gelation in current rheological research; however, nearly all definitions are based on the Winter-Chambon criteria first developed in 1986 [14]. Winter and Chambon used transient rheological techniques to investigate the chemical gelation of polydimethylsiloxane (PDMS). The researchers determined that at the gel point, loss and storage moduli, G'' and G', were congruent and proportional to $\omega^{0.5}$ over several decades of frequency and a wide range of temperatures [14, 17]. The independence of the loss tangent on the frequency of the dynamic experiment was found to be another characteristic of the gel point. Winter and Chambon introduced a general constitutive equation for critical gels that is predictive for all known rheological properties, based on the single material parameter of gel strength [14].

1.1.4. Applications of Photopolymerization

Traditionally, free-radical polymerization has been applied to thin films and coatings where light penetration is generally less of an issue, high production speeds can be achieved, and formulations free from volatile emissions are desirable [2-4]. This type of application allows for the minimization of the disadvantages of free-radical photopolymerization such as shrinkage and poor conversion in thick or strongly absorbing systems. Despite the limitations of free-radical photopolymerization, applications are far-reaching, encompassing the automotive, electronic, medical, optical, graphical arts, flooring, and furniture industries. Research in photopolymerization

continues to fuel the expansion of this list to include areas of rapid prototyping and biomedical implants. A few relevant applications are highlighted below.

1.1.4.1. Films, Coatings, and Adhesives

Photopolymers may be used as coatings for a wide range of substrates, including wood, glass, paper, metals, and plastics. These coatings serve to protect surfaces from scratches and chemical exposure, to provide decoration and color, and to allow modification of surface properties [3, 11]. Currently, most coatings are applied as a liquid monomer formulation and then photopolymerized; however, photocurable powder coatings are being developed and are expected to have a huge impact on the metal, paper, and wood coating industries [2]. Photopolymerized adhesives provide bonding between laminates, such as glass panes or plastic films. In addition, adhesives and release coatings are used to make tapes, labels, and stickers [2, 4]. Photocurable inks are used on packaging materials and magazines [2].

1.1.4.2. Biomaterials

Photopolymerization has become more prominent in biological applications in recent years because it offers rapid reaction rates and superior products. Photopolymerization for biological applications, however, is often more challenging because reactions usually have to occur under visible light and the end product must have zero toxicity [6]. Scaffolding for bone and tissue engineering, bioadhesives for wound closure, and microchips for biochemical analysis are examples of biomaterials produced using free-radical photopolymerizations. Cross-linked hydrophilic polymer networks that are used in applications like contact lenses and drug delivery are also produced using free-radical photopolymerization [18].

1.1.4.3. Stereolithography

Stereolithography is a rapid prototyping technique that translates CAD files into three-dimensional solid objects one layer at a time by tracing a laser beam or ultraviolet light on the surface of a vat of liquid photopolymer. The resin solidifies wherever it is exposed to light, resulting in a solid layer. The process is repeated, layer-by-layer, until the 3-D object is completely built. Figure 1.8 [19] gives a schematic diagram of the process. The ability of stereolithography to produce three-dimensional solids from CAD files within a matter of hours has made it the most widely used rapid prototyping technology. Significant limitations such as the inability to increase part building speeds without loss of accuracy, part size distortions of the final product relative to the CAD design, and spatial resolution limitations that are considerably greater than inherent optical limits are hindering further advancements in the field of stereolithography.

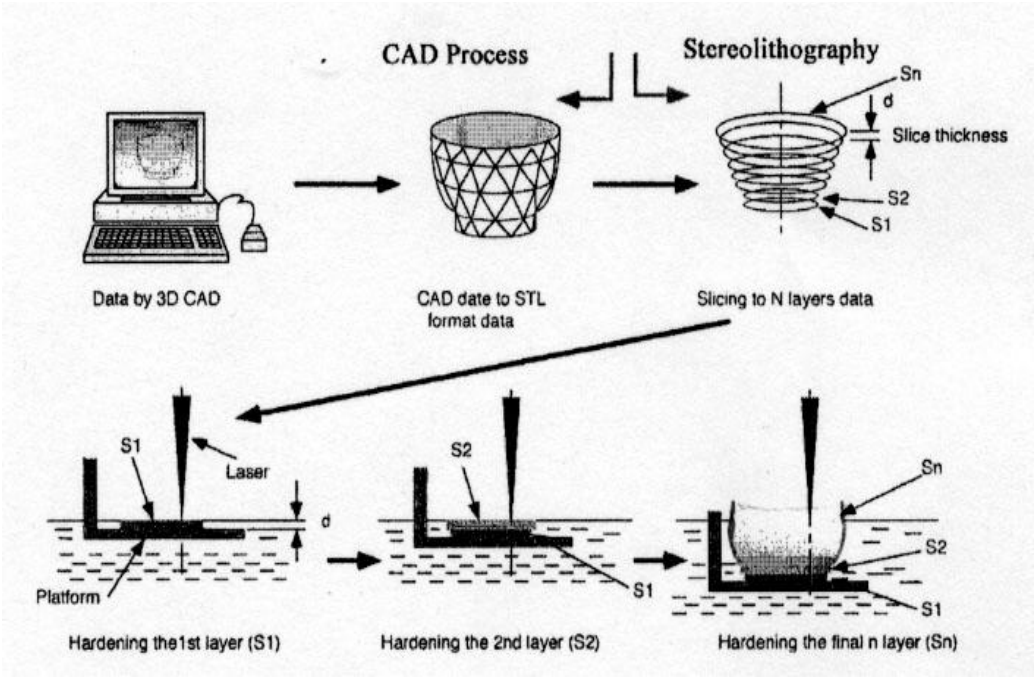

Figure 1.8: Process of stereolithography [19]

1.2. Measurement Techniques

Several techniques are currently used to study photo-induced polymerization. Techniques such as infrared spectroscopy and calorimetry rely on reaction kinetics, while techniques like rheometry rely on changes in mechanical properties to monitor the progress of photopolymerization. The majority of techniques used to study photopolymerization are based on sample volume; therefore, no local spatial information is obtained. In this section the most commonly used techniques will be described.

1.2.1. Spectroscopy

In general, spectroscopy is the subdivision of physics that examines the production, measurement, and interpretation of electromagnetic spectra that arise from both the emission and absorption of radiant energy by matter [20]. Two methods of studying photopolymerization using spectroscopy have been well established: infrared and Raman spectroscopy [10, 11, 20-22]. Infrared (IR) and Raman spectroscopy both measure the vibrational energies of molecules and can be used to obtain both conversion and rate of polymerization the two methods rely on different selection rules for spectral information [20, 22]. Peaks in the spectra correlate to functional groups within a molecule. As monomer is converted to polymer, the height of peaks associated with the monomer specific bonds decreases. The conversion may then be calculated as the ratio of this peak height (or area) at any point in time to the initial peak height (or area). The rate of polymerization is calculated by differentiating the conversion curve with respect to time [21].

Fourier transform infrared (FTIR) is one of the most commonly used IR analysis methods for determining the composition of polymers. FTIR measures the vibrational

energies of atoms or specific groups of atoms within a molecule as well as rotational energies. The FTIR technique identifies components by comparing the spectrum of a sample to reference spectra [22]. FTIR spectroscopy allows rapid multiple scanning of a sample; therefore, the technique has permitted real-time observation of changes in the spectra [20]. As a result, this method is commonly used to follow the cure reaction of photo-induced polymerizations [21].

Raman spectroscopy is based on the Raman effect, which is the inelastic scattering of photons by molecules; therefore, it is an emission phenomenon as opposed to IR absorption, and results from vibrations caused by changes in polarizability [20, 22]. Raman spectroscopy is particularly useful when studying aqueous solutions, wet samples, or where differentiation between polymers with similar structures is necessary [21]. Raman spectroscopy has several advantages compared to FTIR spectroscopy, such as higher quantum efficiency, the ability to study lower frequency vibrations, and higher spatial resolution as a result of shorter excitation wavelengths [11]. The Raman technique has the disadvantages of being slower and more costly. Infrared spectroscopy and Raman spectroscopy are considered complementary techniques, because the selection rules are different [21].

1.2.2. Calorimetry

Calorimetry, which measures heat flow into a material (endothermic) or out of a material (exothermic), is categorized into adiabatic calorimetry, covering the temperature range from 10 to 400 K, and differential scanning calorimetry (DSC), covering the temperature range from 200 to 1000 K [23]. Photodifferential scanning calorimetry (PDSC) is a standard technique for obtaining the rate of polymerization and conversion

[21, 23]. The conversion of monomer carbon double bonds to polymer carbon single bonds is an exothermic reaction. The heat flow from the sample (ΔH in W/g) is directly proportional to the rate of polymerization [21]:

$$R_p = \frac{\rho \Delta H}{\Delta H_p} \tag{1.15}$$

where R_p is the rate of polymerization, ρ is the density of the monomer (g/L) and ΔH_p is the heat of polymerization for the reactive group of the monomer (J/mol). The conversion of the sample is calculated by integrating the area under the rate of polymerization versus time curve [21]. Calorimetry is advantageous because it is not affected by cross-linking reactions and offers direct measurement of the polymerization rate [24]; however, this technique suffers from serious drawbacks such as a long response time of the calorimeter and a low thermal conductivity of most samples which greatly limits temporal resolution [25]. As a result, spectroscopy methods are preferred for performing real-time measurements.

1.2.3. Rheology

Reaction kinetics are traditionally the most common measurement used to monitor the progress of photopolymerization as a function of time; however, it is difficult to extract spatial information about the photopolymerization process from reaction kinetics. Moreover, bond conversion rates measured with calorimetry or spectroscopy are not the most predictive indicator of product quality, which remains the primary focus of the majority of photo-induced polymerization applications. The most relevant parameter in controlling the final product is the transition in mechanical properties from a liquid monomeric resin to a highly cross-linked gel. Analysis of bond conversion rates in

terms of sample rheology requires significant model assumptions, which often leads to inaccurate data and poor ability to control the system. As a result, the direct measurement of mechanical properties during gelation of a photoresin is the preferable approach.

As mentioned at the beginning of this chapter, when exposed to UV irradiation, photoresins react and increase their molecular weight as they form polymer networks. As the network builds, the viscosity increases, which can easily be detected using rheological techniques. In order to study photopolymerization with a rheometer, the sample geometry (mostly parallel plate) must be adapted to accommodate UV irradiation. The general experimental setup, first developed by Khan *et al.* [25], has the top plate holder scooped out to permit the insertion of a 45° mirror, which is used to reflect the UV light onto the sample. The sample is then squeezed between two parallel plates made from quartz glass [25-30, 31-33]. During rheological measurement the sample can then be exposed to UV light. Steady shear rheological methods are good for precisely measuring the viscosity early in the curing and up to the gel point. If viscosity measurements are required over the entire conversion range, then steady shearing rheometry is not the recommended choice since continuous shear would disrupt gelation [21]. In addition, large torques will build up after the gel point and could potentially damage the torque transducers [29].

Dynamic mechanical methods, typically oscillatory parallel plate rheometry, are commonly used to measure the dynamic mechanical properties from the liquid state to the solid state. By using small-amplitude oscillatory deformations, the dynamic storage and loss moduli can be obtained. These quantities can then be used to calculate the

viscosity and gel modulus [34]. Whereas steady shear rheometry can measure the initial stages of cure up to the gel point, dynamic mechanical analysis (DMA) can measure the entire cure process all the way to the completion of cure, although the method is too insensitive to measure low-viscosity liquids. In addition, DMA can be used to measure the properties of final cured samples [34]. Both steady shear rheological methods and DMA are often combined with spectroscopy techniques in order to simultaneous obtain real-time kinetic and mechanical data [26, 30, 33].

The direct measurement of mechanical properties using traditional rheometers adapted to accommodate UV light sources has provided useful insight into photopolymerization. This technique, however, has important drawbacks such as the dimension of the sample, averaging of sample properties, and externally applied stress. Conventional rheometers require large amounts of sample, typically in the range of milliliters, which makes it near impossible to study rare or precious materials [35]. In order for accurate results to be obtained the sample must be at least 25 mm in diameter and 100-500 μm thick. Also, investigating thin samples with a standard rheometer increases the risk of plates grinding against each other when shrinkage occurs [29]. In addition, modeling results have shown that the intensity of UV irradiation can vary significantly due to absorption in the resin by photoinitiator. In view of that, the mechanical properties, represented by G^*, will be a function of both time and location. Conventional rheometers average over the entire sample volume; therefore, detailed spatial information is entirely lost in the complex viscoelastic modulus when measured with a mechanical rheometer. Finally, mechanical rheometers apply an external stress to

deform a sample. Although the deformations are considered small, they can influence the overall photopolymerization process.

1.3. **Microrheology**

Rheology is the study of the deformation and flow of matter; microrheology simply expands this definition to microscopic length scales. Microrheology is predominantly used to experimentally probe the mechanical properties of soft materials. In contrast to traditional rheology methods where bulk properties are measured and the sample is subjected to an externally imposed shear strain, microrheology relies on the Brownian motion of micron-sized particles embedded in the sample to assess the viscoelastic properties of the surrounding medium. The principle advantages of this technique are that it requires only a microscopic amount of material to perform a detailed rheological study and that it can be used to probe the local properties of rheologically inhomogeneous materials. In addition, microrheology is able to probe a much larger frequency range than traditional macrorheology and because microrheology uses only thermally generated forces, it can be used to nondestructively measure even extremely fragile materials[36]. As a result of these strengths, microrheology has lead to advancements in several research areas of complex fluids including living cells, proteins, hydrogels, colloids near the glass transition, and various soft biomaterials [36].

There are two main categories of microrheology techniques: passive, which tracks the random motion of tracer particles due to thermal fluctuations and active, where an external force, usually created with optical tweezers or magnetic fields, is applied to the probe particles in order to measure rheological properties. Passive techniques are useful for measuring low values of predominantly viscous moduli, where active techniques can

be extended to measurable range of samples containing significant amounts of elasticity [35]. Active microrheology methods also allow the option of measuring stress relaxation of a complex fluid under the influence of an external force [36]. Passive particle tracking microrheology, however, is better studied, less invasive to the sample, and more cost effective compared to active microrheology techniques [35-37].

1.3.1. Theory of Particle Tracking Microrheology

The fundamental assumption of passive particle tracking microrheology is that the Brownian dynamics of microscopic particles embedded within a fluid is determined by the mechanical properties of the surrounding environment. Passive techniques rely solely on the thermal energy of the embedded tracer particles, k_BT, to measure rheological properties; therefore, it is essential that measurements be performed on materials that are sufficiently soft in order for the thermal motion of the tracer particles to be detectable. A typical experimental setup employs video-microscopy to track the Brownian motion of micron-sized, inert, fluorescent particles [38]. Information about the local mechanical properties of the sample is then obtained by performing statistical analysis of the tracer particle motion. Figure 1.9 illustrates the principle steps, many of which are explained in detail below, of particle tracking microrheology.

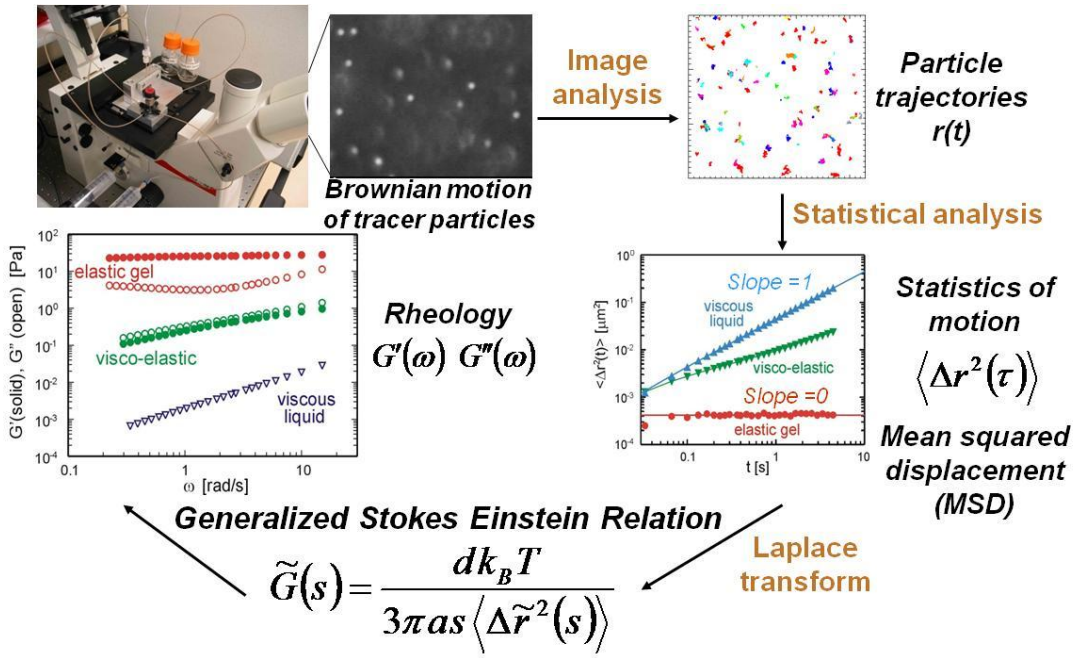

Figure 1.9: Principles of particle tracking microrheology: from particle motion to sample rheology.

The motion of the particles in a Newtonian liquid is diffusive and the diffusion coefficient is given by the Stokes-Einstein relation $D = k_bT/6\pi\eta a$. For diffusive motion, the mean-squared displacement (MSD) is defined as [37]:

$$\left\langle \Delta r^2(\tau) \right\rangle \equiv \left\langle \left| r(t+\tau) - r(t) \right|^2 \right\rangle = 2\,d\,D\tau = \frac{d\,k_b T}{3\pi\eta a}\tau \qquad (1.16)$$

where Δr is the MSD, k_B is Boltzmann's constant, T is the absolute temperature, d is the dimensionality of the system, a is the particle radius, the brackets designate averaging over all starting times t and τ is the lag time. The Stokes-Einstein relation enables viscosity measurements by monitoring the time-dependent MSD of a particle of known size.

Particles implanted in a completely elastic environment will have a maximum displacement that occurs when the thermal energy is equal to the elastic energy of the

deformed cross-linked network [37]. As a result, MSD approaches a plateau for long lag times:

$$\left\langle \Delta r^2 \right\rangle_{\tau \to \infty} = \frac{d\, k_b T}{3\pi G a} \tag{1.17}$$

where G is the storage modulus of the elastic medium [37].

Complex fluids, materials that are neither Newtonian liquid or completely elastic, exhibit much more complex behaviors including a frequency dependent complex viscoelastic response modulus with both viscous and elastic components: $G^*(\omega) = G'(\omega) + iG''(\omega)$ [37]. The fundamental basis of particle tracking microrheology in complex fluids is the application of the generalized Stokes-Einstein relation (GSER) for a sphere in a homogeneous, incompressible fluid, which takes the form (after a Laplace transform) [35-37]:

$$\left\langle \Delta \tilde{r}^2(s) \right\rangle = \frac{d\, k_b T}{3\pi a s \tilde{G}(s)} \tag{1.18}$$

where s is the Laplace frequency, $\Delta \tilde{r}^2(s)$ is the MSD of the particle, and $\tilde{G}(s)$ is a frequency-dependent modulus (the single real function). The GSER is essential to particle tracking microrheology because it translates the microrheological measurement of MSD into the macroscopic measurements of viscosity or elasticity. Both the viscous and elastic response can be determined by calculating the complex viscoelastic modulus from $\tilde{G}(s)$, which is possible since the real and imaginary part are related to each other through the Kramers-Kronig relations [37]. The frequency range where Equation 1.18 remains valid is dependent on both the inertia and compressibility of the system, but includes the typical range of videomicroscopy, 0.1-60 Hz [37]. The mathematical

transformation from the MSD to viscoelasticity tends to amplify experimental noise and does not add fundamental insight. For this study, we have therefore chosen to report transient MSD data rather than viscoelastic moduli in order to emphasize the principles of microrheology when applied to photopolymerization.

1.3.2. Definition of Gelation in Microrheology

The classic Winter—Chambon criteria, which states that the loss tangent becomes independent of frequency at the gel point [14], could not be applied in this research since frequency is unable to be varied in passive microrheology. A theoretically equivalent definition of the point of gelation is the loss and storage modulus being congruent and proportional to the frequency ($G' \sim G'' \sim \omega^{1/2}$). The congruence definition is consistent with the Kramers-Kronig relation; therefore, the loss and storage modulus being equivalent is just as much a rheological property at the gel point as are infinite viscosity and zero equilibrium modulus. A slope of 0.5 in a double-logarithmic plot corresponds to $\langle \Delta r^2(\tau) \rangle \sim \tau^{1/2}$, which can be derived from the congruence definition of $G' \sim G'' \sim \omega^{1/2}$. As a result, the gel point can be determined graphically in microrheology by plotting the slope of the MSD curve as a function of time. The time at which the transient slope profile is equal to a value of 0.5 is determined to be the gel point.

1.4. Project Objectives and Outline

As stated above, photopolymerization is the basis of many industrial applications; however, issues affecting the cure speed and overall quality of the final product (shape, size, and surface finish) are limiting the use of photo-polymerization in certain fields. For example, inhibition by oxygen in free-radical polymerization leads to a significant decrease in cure speed and complicates the overall reaction chemistry. Spatial variations

of photopolymerization impose significant limitations on applications in which a high spatial resolution is required such as rapid prototyping. These limitations are the result of a general lack of understanding and control of the photopolymerization process.

Owning to the great importance of the photopolymerization process, the development of experimental methods capable of monitoring of photopolymerization reactions in real-time and space is necessary. Initially, photo-DSC was used for such investigations; however, this technique suffers from serious drawbacks such as a long response time of the calorimeter and a low thermal conductivity of most of the samples, which greatly limits time resolution of the instrument. Spectroscopic techniques rely solely on chemical changes within the resin and do not provide specific information about the development of mechanical properties. Real-time FTIR spectroscopy has been combined with a rheometer to monitor both conversion and changes in rheological properties of a sample; however, this approach does not account for local spatial variations since a rheometer averages mechanical properties over the entire sample volume.

Intricate applications of photopolymerization in optical, medical and electronic materials demand a thorough understanding of the evolution of mechanical properties during photopolymerization. The experimental ability to examine and quantify spatial variations in photopolymerization systems would be of great benefit to industry. Such experimental information could then ultimately be used to strengthen and validate curing models that are currently used to control and predict photopolymerization processes. Improvements in modeling may result in the higher quality products at a lower cost for consumers.

The goal of this research is to develop a microrheology based technique that can be used to monitor the liquid-to-gel transition in real-time. A proper framework for data analysis will be developed to accurately monitor and quantify changes in the mechanical properties during photopolymerization. Using the constructed technique and analysis, the aim of this study is to experimentally characterize the local structure, mechanical properties, and reaction kinetics of multifunctional acrylate systems with high spatial and temporal resolution. This unique experimental data will then be compared to both internally and externally developed polymerization models.

In the subsequent work, the monitoring of photo-induced free-radical polymerization by microrheology will be discussed in detail. Chapter 2 describes the development of the constructed microrheological setup in detail. Basic experiments were performed to determine if the technique was capable of monitoring the liquid-to-gel transition. This information was used to develop a standard definition of the gel point. Once the technique was verified, the spatial dependence of the gel time was investigated and the experimental data was compared to the Beer-Lambert law.

In Chapter 3, the microrheology based technique was used to study the effect of varying the concentration of photoinitiator on the reaction kinetics of pure acrylate and copolymer systems. The results of this work were compared to an externally developed comprehensive photopolymerization model that incorporated the reaction kinetics, mass transfer, and physical properties of the sample. The effect of inhibitor on the reaction of acrylate resins was investigated by adding controlled amount of a polymerization inhibitor to the system. In addition, the inhibitory effects of oxygen were examined

comparing degassed data to oxygen saturated data. Finally, the agreement between experimental results and classical statistical theory was investigated.

Chapter 4 examines the effects of temporally modulating the illumination delivered to the sample. By delivering multiple pulses of UV illumination separated by varying periods of darkness to the sample, the effectiveness of post UV exposure reactions was studied. The location of the polymerization front as a function of time was determined by varying the location at which data is recorded once the UV light has been extinguished. Heterogeneity of the polymerizing sample was investigated and linked to the gel point via statistical analysis of the data.

In Chapter 5, the impact of oxygen on the photopolymerization of multifunctional acrylate resins was determined using experiments where the UV light delivered to the sample was spatially modulated. The photopolymerization process was modeled as a simple two-step process. Simulation results of the model were directly compared to the experimentally obtained microrheology results. In addition to concluding remarks, the last chapter contains recommended future research and suggested uses for the experimental data obtained through this research.

1.5. References

1. Fouassier, J. P. and J. F. Rabek. Radiation Curing in Polymer Science and Technology Volume III: Polymerizations Mechanisms. London: Elsevier Applied Science, 1993.

2. Drobny, J. G. Radiation Technology for Polymers. London: CRC Press, 2003.

3. Roffey, C. G. Photopolymerization of Surface Coatings. New York: John Wiley & Sons, 1982.

4. Pappas, S. P. UV Curing: Science & Technology Volume II. Norwalk, CT: Technology Marketing Corporation, 1985.

5. Scranton, A., C. Bowman, and R. Peiffer. Photopolymerization : fundamentals and applications. Washington, DC : American Chemical Society, 1997.

6. Odian, George. Principles of polymerization 4th edition Hoboken, N.J. : Wiley-Interscience, 2004

7. Endruweit, A., M. S. Johnson, and A. C. Long. "Curing of composite components by ultraviolet radiation: A review." Polymer Composites 27 (2006): 119-128.

8. Kaur, M. and A. K. Srivastava. "Photopolymerization: A review." Journal of Macromolecular Science-Polymer Reviews C42(2002): 481-512.

9. Decker, C. "Photoinitiated Curing of Multifunctional Monomers." Acta Polymer 43 (1994): 333-347.

10. Kaur, M. and Srivastava, A. K. "Photopolymerization: A Review." Journal of Macromolecule Science- Polymer Reviews 4 (2002): 481-512.

11. Koleske, J. Radiation Curing of Coatings. New York: John Wiley & Sons, 1982.

12. Studer, K., Decker, C., Beck, E., *et al.* "Overcoming Oxygen Inhibition in UV-Curing of Acrylate Coatings by Carbon Dioxide Inerting, Part I." Progress in Organic Coatings 48 (2003): 92-100.

13. Studer, K., Decker, C., Beck, E., *et al.* "Overcoming Oxygen Inhibition in UV-Curing of Acrylate Coatings by Carbon Dioxide Inerting, Part II." Progress in Organic Coatings 48 (2003): 101-111.

14. Winter, H. H. and Chambon, F. "Analysis of Linear Viscoelasticity of a Crosslinking Polymer at the Gel Point." Journal of Rheology 30 (1986): 367-382.

15. Pizzi A. “Extension of Simple Polycondensation Gelation Theories to Simple Radical and Mixed Polycondensation/Radical Gelation.” Journal of Applied Polymer Science 71 (1999) 517-521.

16. Flory, J. P. Principles of Polymer Chemistry. Ithaca, NY: Cornell University Press, 1953.

17. Winter, H. H. and Mours, M. “Rheology of Polymers Near Liquid-Solid Transitions.” Advances in Polymer Science 134 (1997): 1-70.

18. Barachevsky, V. “Applied Aspects of Organic Photochemistry.” High Energy Chemistry 37 (2003): 6-16.

19. Santler, G., Schultes, G., Gaggl A., *et al.* “Stereolithography Versus Milled Three-Dimensional Models: Comparison of Production Method, Indication, and Accuracy.” Computer Aided Surgery 3 (1998): 248-256.

20. Puskas, J. In-situ Spectroscopy of Monomer and Polymer Synthesis. New York: Kluwer Academic/Plenum Publishers, 2003.

21. Alfassi, Z. B. General Aspects of the Chemistry of Radicals. Chichester, New York: Wiley, 1999.

22. Bower, D. L. and W. F. Maddams. The Vibrational Spectroscopy of Polymers. Cambridge, New York: Cambridge University Press, 1989.

23. Gallagher, P. K. Handbook of Thermal Analysis and Calorimetry. New York: Elsevier, 1998.

24. Decker, C. and Moussa, K. “A New Method for Monitoring Ultra-Fast Photopolymerizations By Real-Time Infrared Spectroscopy (RTIR)” Makrol Chem 189 (1988): 2318-2394.

25. Clark, S., Hoyle, C., Jonsson, S., Morel, F., and Decker, C. “Photopolymerization of acrylates using N-aliphaticmaleimides as photoinitiators.” Polymer 40 (1999): 5063-5072.

26. Chiou, B., English, R. and Khan, S. “Rheology and Photo-Cross-Linking of Thiol-ene Polymers.” Macromolecules 29 (1996): 5368-5374.

27. Nakamuchi, T. “Time-Resolved Measurements of Mechanical Properties Using a Rheological Apparatus” Progress in Organic Coatings 14 (1986): 23.

28. Watanbe, K. “Rheological Studies of Ultraviolet Curing with an Oscillating Plate Rheometer.” Journal of Applied Polymer Science 29 (1986): 323-332.

29. Davison, J. and Guthrie, J. "Photochemorheological Studies of UV Curing Processes." JOCCA Surface Coatings International 75 (1992): 315-322.

30. Chiou, B., English, R. and Khan, S. "Real-Time and in-situ Rheological Studies on the UV Curing Kinetics of Thiol-ene Polymers." Macromolecules 30 (1997): 7322-7328.

31. Lange, J. "Viscoelastic Properties and Transitions during Thermal and UV Cure of a Methacrylate Resin." Polymer Engineering and Science 39 (1999): 1651-1660.

32. Naghash, H., Okay, O. and Yagci, Y. "Gel Formation by Chain-Crosslinking Photopolymerization of Methyl Methacrylate and Ethylene Glycol Dimethacrylate." Polymer 38 (1997): 1187-1196.

33. Botella, A., Dupuy, J., Roche, A., *et al.* "Photo-Rheometry/NIR Spectrometry: An in-situ Technique for Monitoring Conversion and Viscoelastic Properties During Photopolymerization." Macromolecule Rapid Communication 25 (2004): 1155-1158.

34. Murayama, T. Dynamic Mechanical Analysis of Polymeric Material. New York: Elsevier Scientific, 1978.

35. Gardel, M. L., *et al.* "Microrheology." Department of Physics and Division of Engineering and Applied Sciences, Harvard University, Cambridge MA: 1-55.

36. Waigh, T. A. "Microrheology of Complex Fluids." Reports on Progress in Physics 68 (2005): 685-742.

37. Breedveld, V. and Pine, D. "Microrheology as a Tool for High-Throughput Screening." Journal of Materials Science 38 (2003): 4461-4470.

38. Mukhopadhyay, A. and Granick, S. "Micro-and Nanorheology." Current Opinion in Colloid & Interface Science 6 (2001): 423-429.

CHAPTER 2

IN-SITU MONITORING OF THE MECHANICAL PROPERTIES DURING PHOTOPOLYMERIZATION WITH PARTICLE TRACKING MICRORHEOLOGY

2.1. Introduction

The UV activated polymerization of multifunctional liquid monomers enhanced with photoinitiator is one of the most effective techniques used to create solid polymeric coatings and objects. The resulting highly cross-linked solid polymer has numerous uses due to the insolubility of the product in organic solvents and the resistance to heat and mechanical strain. Thus, the applications of photopolymerization are wide-ranging, and encompass the automotive, electronic, medical, optical, and coating industries.

Currently, issues affecting the cure speed and overall quality of the final product (shape, size, and surface finish) are limiting the use of photopolymerization in certain applications. For example, inhibition by oxygen in free-radical polymerization leads to a significant decrease in cure speed. Another disadvantage is the inability of many lasers and UV exposure tools to homogeneously cure thick or strongly absorbing samples. Finally, the problem of shrinkage during polymerization negatively impacts applications that require accurate part shape and size. Methods for modifying processes and materials to deal with these issues are traditionally derived in one of two ways: (1) through intuition and trial-and-error experiments or (2) from predictive models to optimize materials and processes for specific applications. In many cases the complexity of light

propagation, photo initiation, and polymerization, in combination with the interdependence of these processes, makes intuitive analysis and design difficult. Although rigorous predictive models for process and material design could save tremendous amounts of time and expense, their use has been limited by difficulties associated with obtaining proper parameterization. As a result, simplified models are often used to describe changes in material properties during photopolymerization.

For example, stereolithography (SL) is a process that utilizes pattern-wise UV exposure to induce polymerization of liquid monomers and thus produces three-dimensional solid objects directly from computer-aided design (CAD) files. The technology heavily relies on the use of models to correctly sequence and control the SL exposure system (i.e. a laser in most systems) to build the part to correct size and shape. Modeling of the energy deposition from the exposure source is quite rigorous using classical optical models. On the other hand, the modeling of the material response to light exposure is generally empirical. The most widely used SL process models employ a simple energy threshold: monomeric liquid is converted to solid polymer instantaneously when the local exposure dose exceeds a critical threshold value. This is a gross oversimplification of the true photopolymerization process, in which the molecular weight and crosslink density change gradually, and the predictivity of these models is generally restricted to the exact experimental conditions for which it was parameterized. In the case of SL, there is significant interest in developing processes and materials that result in higher throughput, better spatial resolution, and improved surface finishes. Making such improvements would be greatly aided by quantitatively accurate models that can capture the behavior of photopolymer resins during polymerization, and during

the last decade several research groups have made significant strides forward [12-19]. One of the main problems with model development is the need for experimental validation and refinement, which is still problematic with existing techniques.

To improve existing theoretical models, experimental methods are needed that are capable of testing the model predictions with high spatial and temporal resolution. In particular, techniques capable of measuring chemical and mechanical changes during the photopolymerization process have recently attracted attention. The first time-resolved techniques for monitoring photopolymerization were molecular spectroscopy (IR [1] and Raman [2]) and calorimetry (photo-DSC [3]). Both approaches detect chemical changes within the resin on the molecular level and do not provide specific information about the evolution of mechanical properties. Calorimetry also has the drawback of long response times due to the relatively low thermal conductivity of the sample, which limits the temporal resolution of the instrument. Real-time FTIR spectroscopy has been combined with a rheometer to simultaneously monitor chemical conversion and changes in sample rheology [4-7]; however, this method does not account for spatial variations across the sample, since rheometers measure average mechanical properties over the entire sample volume. The objective of this study was to develop a set-up in which particle tracking microrheology could be employed to quantitatively monitor the changes in mechanical properties during photopolymerization. The principal advantage that microrheology has over the methods listed above is the ability to achieve excellent spatial and temporal resolution.

2.2. Method and Materials

The samples in this study consisted of three main components: acrylic monomer, photoinitiator, and fluorescent tracer particles for microrheology. Three commercial acrylate monomers with different functionality were used as obtained from Sartomer: ethoxylated pentaerythritol tetraacrylate (E4PETeA, SR®494), trimethylolpropane triacrylate (TMPTA, SR®351), and triethylene glycol diacrylate (TEGDA, SR®272). The structure and molecular weight of all the monomers used in this study are listed in Table 2.1. A general-purpose photoinitiator, 2,2-dimethoxy-1,2-diphenylethan-1-one (DMPA, Irgacure®651, Ciba), was used as received. Silica particles containing red fluorescent dye (rhodamine) with a diameter of 0.5 micron were used as tracers [8].

Table 2.1: The structure and molecular weight of the monomers investigated in this study.

Structure of Monomer	Name of Component	MW (mol/L)
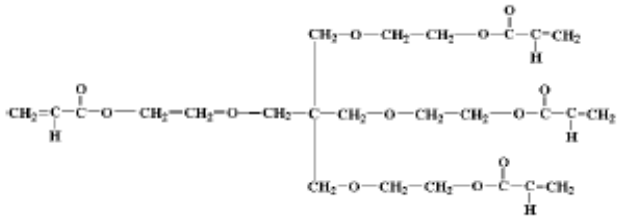	Ethoxylated pentaerythritol tetraacrylate (E4PETeA, SR®494)	528
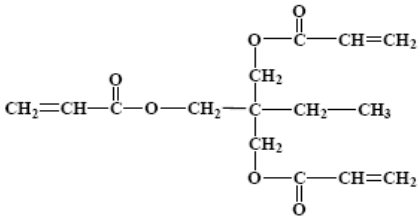	Trimethylolpropane triacrylate (TMPTA, SR®351)	296
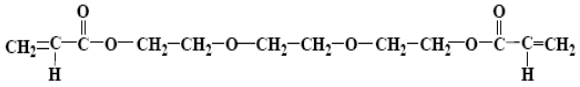	triethylene glycol diacrylate (TEGDA, SR®272)	258

After mixing the components and sonicating the samples briefly to break-up potential tracer particle aggregates, the samples were loaded into a 120 µm deep sample chamber created by placing Parafilm spacers between a microscope slide and cover slip. The samples were sealed with vacuum grease and placed on an inverted microscope. Using a 100x oil-immersion objective, the motion of the fluorescent tracer particles was tracked by capturing images from a CCD camera onto a PC. A detailed diagram of the alignment in the acquisition setup is shown in Figure 2.1. Statistical analysis of the recorded movies was performed with modified versions of image analysis routines originally coded by Crocker and Grier [9] for the software package IDL (Research Systems Inc.). After

obtaining particle positions in subsequent images, particle trajectories were reconstructed and the MSD was calculated as a function of both time and lag time τ [10]. On average, 30 tracer particles were tracked simultaneously during the experiments to obtain statistically meaningful results on the in-plane Brownian motion. Diffusion perpendicular to the focal plane leads to particle loss and terminates trajectories. For highly viscous media like the acrylate monomers, this does not affect experiments; the inset of Figure 2.2 shows that the tracer MSD is less than 0.3 µm for a lag time of 5 seconds for the liquid monomer.

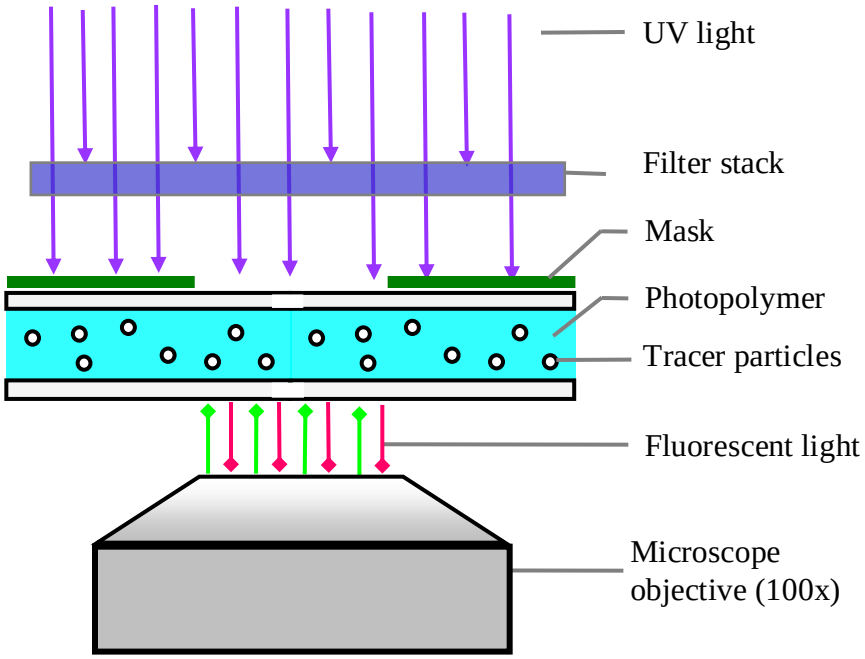

Figure 2.1: Schematic of data acquisition and experimental setup

Exposure of the sample to a 1000W Hg(Xe) UV lamp (Spectra-Physics) was used to induce polymerization; illumination was controlled through a manually operated zero aperture iris diaphragm and optical filters were used to vary intensity and spectral characteristics of the light.

2.3. Results and Discussion

2.3.1. Proof of Concept

Initial experiments were performed on E4PETeA with 5.0 wt.% DMPA to evaluate the ability of microrheology to distinguish between a liquid monomer and photopolymerized gel. The motion of tracer particles in a UV irradiated (100 s) and unexposed sample was tracked and analyzed. The inset of Figure 1 shows that the exposed sample has a slope of zero in the double-logarithmic plot of MSD versus lag time, while the unexposed sample has a slope of one. These slopes are characteristic of an elastic gel (see Eq. (1.17)) and a viscous Newtonian liquid (see Eq. (1.16)), respectively. Next, a sample of the same composition was exposed to UV illumination after 6.6 seconds using a manually controlled shutter. A mask was used to restrict the area of illumination and minimize sample shrinkage, and a 365 nm band-pass filter (center wavelength 356 nm, half-width 15 nm) was inserted in the light path to enhance control of polymerization kinetics for modeling purposes. The transient MSD curves in Figure 2.2 prove that microrheology can accurately monitor changes in sample rheology of UV irradiated photoresins. The point at which the MSD first becomes independent of τ was used to define the gelation point. Before the liquid-to-solid transition, the MSD increases with increasing lag times, characteristic of a viscous liquid. After the transition the MSD is independent of lag time, which is the signature of an elastic gel (see inset). Other definitions of gel point based upon the classic Winter-Chambon gelation theory [11] were examined and yielded comparable gelation point data. Figure 2.2 also illustrates that exposure to UV light initially causes no significant changes in MSD; the sample viscosity apparently does not change significantly during the initial stages of

photopolymerization. After 19.8 seconds (13.2 seconds of UV exposure), a sudden liquid-to-gel transition occurs, which could easily be captured with particle tracking microrheology.

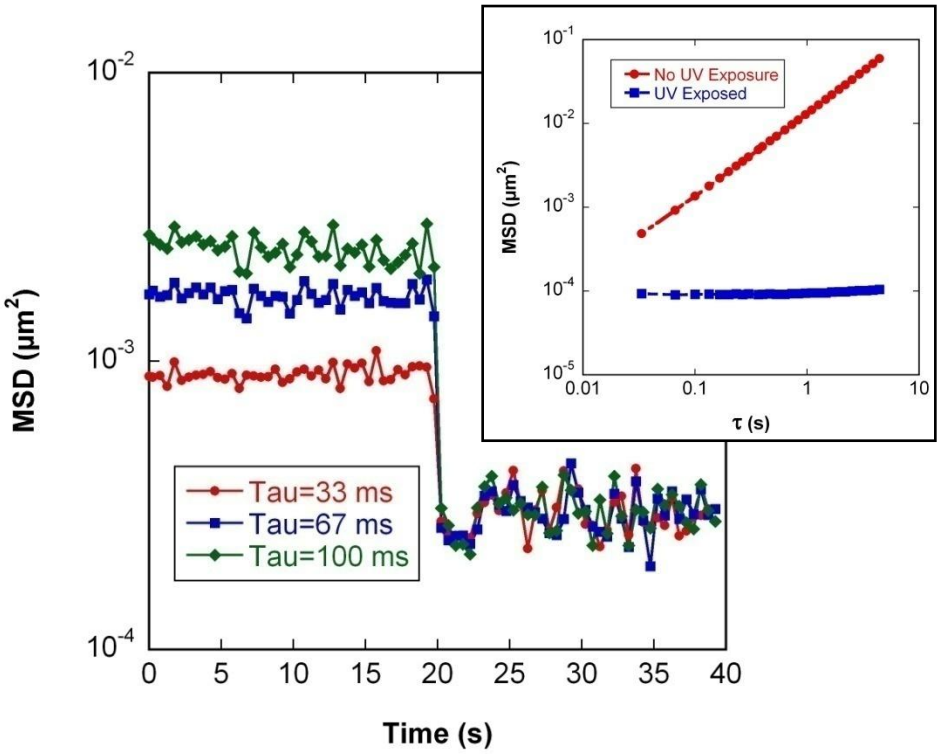

Figure 2.2: Transient MSD for tracer particles in a curing sample of E4PETeA loaded with 5.0 wt% DMPA; gelation occurs at 19.8 seconds. The inset shows steady state results of MSD vs. τ in the liquid and gel regimes.

2.3.2. Depth Profiling

The small depth of focus of the microscope, in combination with accurate manipulation of its location via the fine focus, enabled measurements of polymerization with high spatial resolution. In particular, the gelation transition could be studied as a function of UV penetration depth into the sample (the distance from the illuminated resin surface to the focal plane). For these experiments, samples of E4PETeA were loaded with different concentrations of DMPA initiator and the microscope was focused at the illuminated top surface of the sample chamber (zero penetration depth), before moving

the focal plane to the desired location. Figure 2.3 illustrates that gelation time increases by an approximate factor of two across a sample depth of 120 μm, independent of initiator concentration. To investigate if this depth-dependent gelation was due to oxygen inhibition reactions, E4PETeA with 0.25 wt% DMPA was degassed under vacuum. Comparison of the deoxygenated and oxygenated samples with 0.25 wt% in Figure 2.3 shows that oxygen slows down the photopolymerization process significantly, but that it is not the cause of inhomogeneous cure across 100 μm samples. The error bars in Figure 2 are mainly the result of using a manual shutter to control the UV illumination.

The variations in gel time across the sample cannot be fully explained by absorption either. Beer's law predicts the exponential decay of the amount of photons delivered to the sample with increasing thickness of the absorbing medium, thus limiting the initiation reactions of free-radical photopolymerization at greater penetration depth. For E4PETeA, at 5.0 wt% DMPA 63% of the light penetrates to the bottom of a 100 μm thick sample, while at 0.25 wt% almost 100% of the incident light reaches the bottom; nevertheless, the gelation variations for the 0.25 wt% samples are significant.

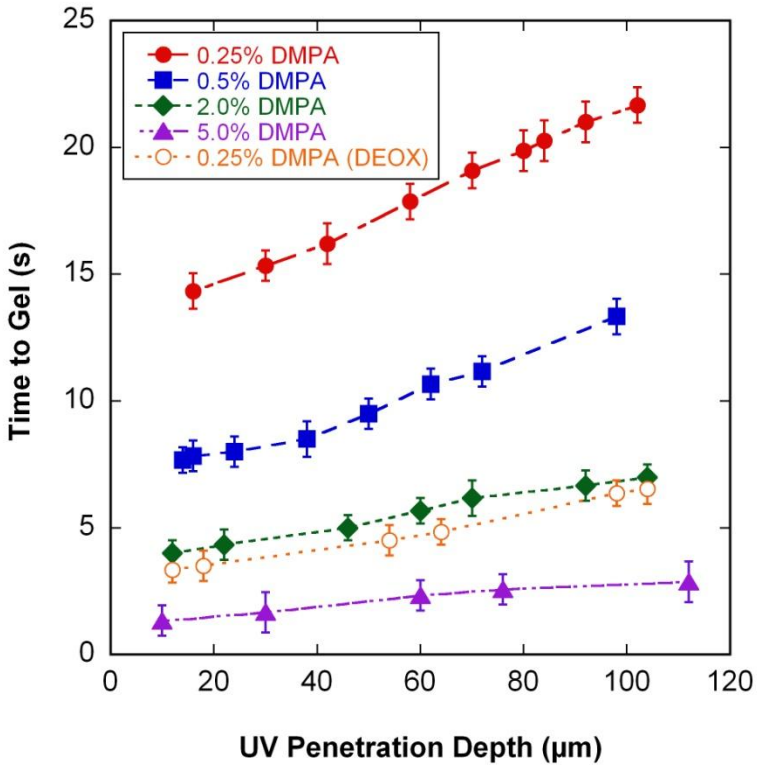

Figure 2.3: Plot of gelation time as a function of UV penetration depth for E4PETeA with 5.0 wt%, 2.0 wt%, 0.5 wt%, and 0.25 wt% (Both oxygenated [•] and degassed [o]) DMPA cured using 365 nm UV irradiation. Lines are to guide the eye.

The measurements were repeated with monomers of different functionality. TEGDA (bifunctional) and TMPTA (trifunctional) with 5.0 wt% DMPA were cured using 365 nm UV irradiance and the results are compared to the data for E4PETeA (tetrafunctional) in Figure 2.4, which confirms that the trend observed for E4PETeA in Figure 2 is independent of functionality. As expected, monomers with higher functionality form cross-linked networks at lower conversions of the polymerizable functional groups; therefore, highly functional monomers require shorter times to reach the point of gelation.

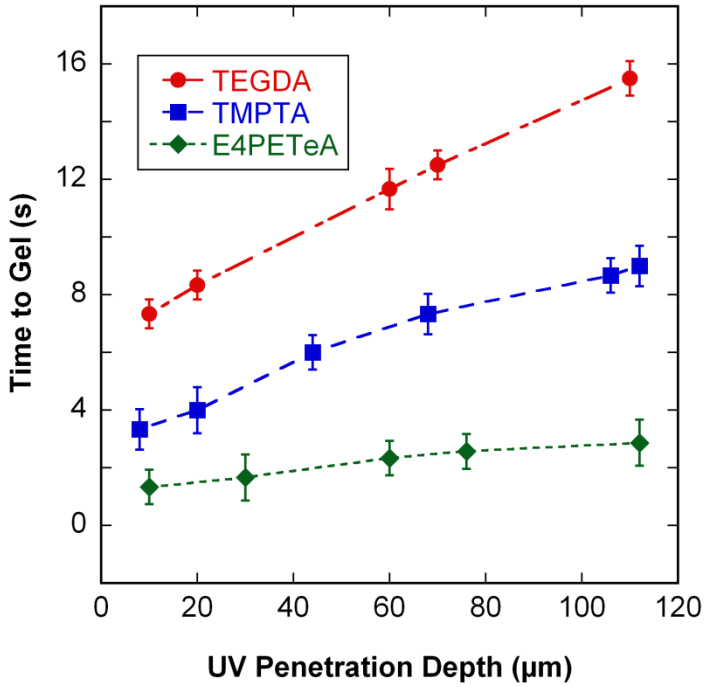

Figure 2.4: Plot of gelation time as a function of UV penetration depth for three different acrylate monomers: TEGDA, TMPTA, and E4PETeA with 5.0 wt% DMPA and cured using 365 nm UV irradiation. Lines are to guide the eye.

2.3.3. Intensity Effects and Beer's Law

As mentioned previously, the energy threshold model, which assumes that gelation occurs once a critical energy dose threshold is reached, is often the starting point for photopolymerization models discussed in the literature [12-14]. For continuous irradiation (i.e. continuous initiation of polymerization) of a sample in which the polymerization reaction time scale for each initiation event is fast compared to the gelation time scale, the critical energy threshold should be the product of gelation time and UV intensity:

$$E_{cr} = I_a t_{gel} \tag{1}$$

where the UV intensity at a given depth, I_a, is defined by Beer's law as:

$$I_a = I_0 \exp(-kx) \tag{2}$$

k being the absorption coefficient, and x the distance below the surface illuminated with intensity I_0. These conditions should be met in the case of the free radical polymerization experiments reported here since at conversions below the gel point the lifetime of active radicals should be much less than one second while the gelation time scales are on the order of seconds at the reported light intensities. According to Eqs. (1) and (2), the gelation time should scale as $t_{gel} \sim \exp(kx)$. The profiles in Figures 2.3 and 2.4 appear to deviate from this exponential prediction. Over the available depth range (working distance of 100x objective), however, it is difficult to differentiate between linear and exponential scaling. To evaluate the accuracy of the threshold model in more detail, the illumination intensity I_0 was varied by inserting various neutral density filters in the light path: ND10 (10% transmission), ND03 (50% transmission), and ND01 (78% transmission). Samples of E4PETeA loaded with 5.0 wt% DMPA were exposed to UV light at 365 nm and, as expected, Figure 2.5A shows that decreasing the UV intensity increases the required gelation time considerably. Given that both the material constant k and location x are controlled between experiments, the gelation time should scale with the inverse of the incident intensity, $t_{gel} \sim 1/I_0$. Therefore, it should be possible to collapse the data in Figure 4A onto a single master curve by normalizing gelation times by the filter transmittance. Deviations between the normalized and unfiltered data in Figure 2.5B illustrate that the critical energy threshold model becomes progressively more inaccurate at low incident light intensity and for thick samples, which was also visible in Figures 2.3 and 2.4. The main reason for failure of the simple threshold model under these conditions is that the model completely neglects reaction kinetics; for slow reactions, the balance between initiation, propagation and termination reactions becomes

increasingly important. These experimental results show that microrheology is capable of capturing previously inaccessible details on photopolymerization and support the need for inclusion of reaction kinetics in photopolymerization models. However, a detailed evaluation of various models is beyond the scope of this communication.

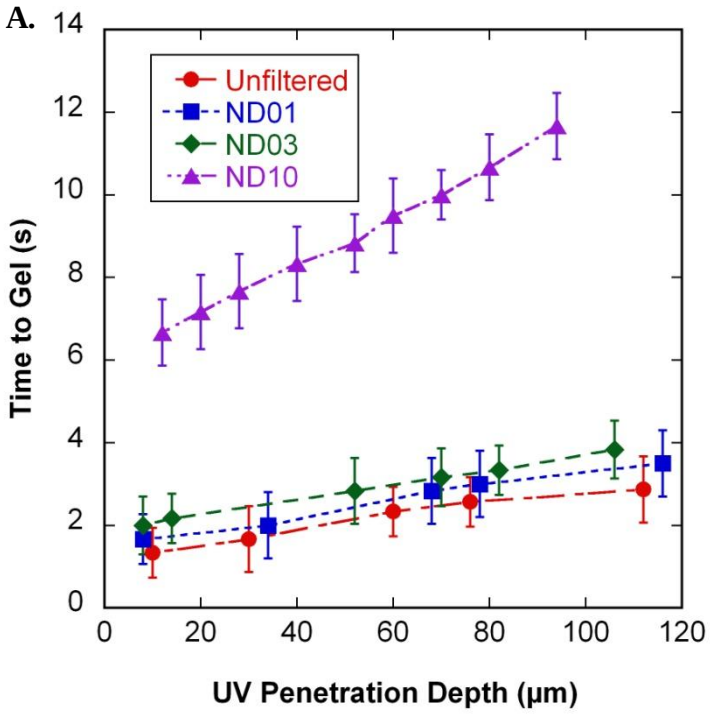

Figure 2.5: (A): Plot of gelation time as a function of UV penetration depth and incident intensity for E4PETeA with 5.0 wt% DMPA, using 365 nm UV irradiance. (B): Plot of same data after normalization with filter transmittance.

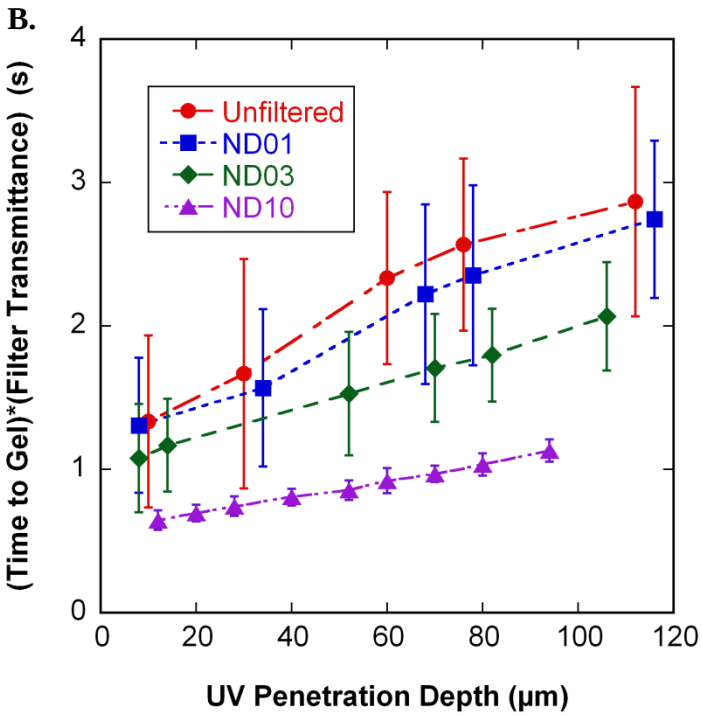

Figure 2.5 continued

2.3.4. Kinetic Effects

To further elucidate the role of reaction kinetics, the effects of initiator concentration and oxygen inhibition were studied. A fraction of the samples was degassed under vacuum and loaded into sample chambers in an oxygen-free environment. All of these samples were cured using 365 nm UV illumination and gelation was determined at a standard depth of 60 μm from the illuminated surface. Figure 2.6 illustrates how the gelation time of E4PETeA depends on the initiator concentration: after a strong decay at low initiator concentrations, the gelation time levels off around 4.0 wt% for the samples with oxygen. Significant impact of oxygen inhibition is also evident, supporting the results in Figure 2.2: the deoxygenated samples undergo gelation much more rapidly than their counterparts with oxygen. For example, at 2.0 wt.% DMPA gelation occurs nearly instantaneously. In the inset, the data are replotted on a double

logarithmic scale to highlight the fact that oxygenated samples follow power-law scaling of gelation time with initiator concentration; the degassed samples show a much stronger decay, which can best be described as exponential. In addition, the inset shows a direct comparison of experimental data to model predictions made using a model developed by Tang and coworkers. [19] This model is a comprehensive photopolymerization model that incorporates both heat and mass transfer and a complete free radical polymerization model including initiation, propagation, and termination. This model was carefully parameterized experimentally for a series of different photopolymer resins including the resin used in this paper. The model was parameterized using experiments conducted in a nitrogen purged environment, and thus an oxygen inhibition model was not directly parameterized for this model. The accuracy of the model was validated by utilizing it to quantitatively predict the results of stereolithography photopolymerization experiments. Utilizing stereolithography experiments, the critical degree of polymerization that results in gelation was determined. Calculations were also performed using the photopolymerization model with an oxygen inhibition model included where oxygen inhibition rate constants for similar resins from the literature were used. [20] However these oxygen inhibited model predictions did not deviate significantly from the predictions without oxygen inhibition and thus are not shown in the graphs. It is obvious that the microrheology experiment is quite sensitive to the presence of oxygen, and thus work is in progress to utilize this data in conjunction with a comprehensive photopolymerization model to extract parameters for oxygen inhibition that can properly capture this behavior. These oxygen inhibition model results will be compared to

differential photocalorimetry experiments conducted in controlled environments containing known concentrations of oxygen.

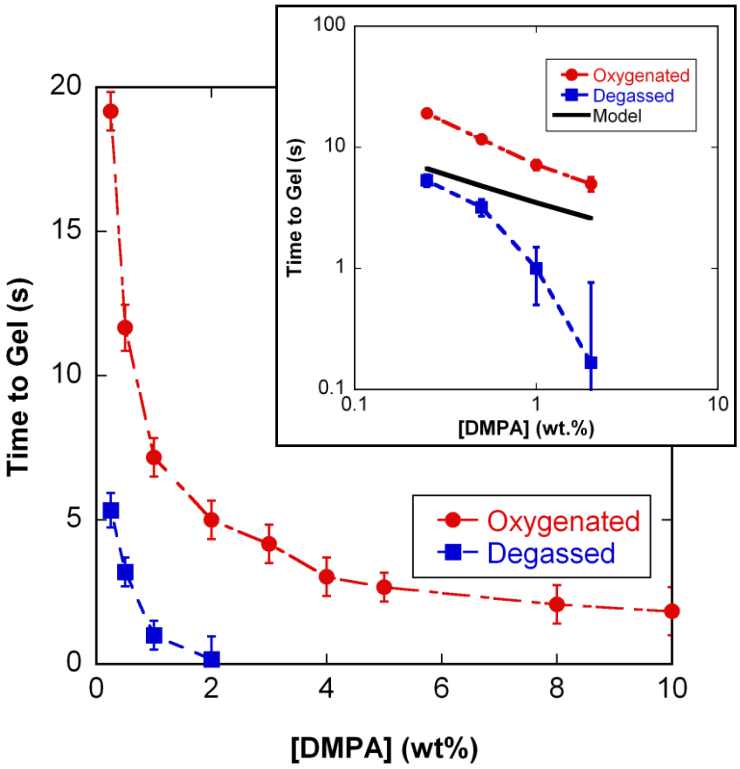

Figure 2.6: Plot of gelation time as a function of DMPA loading concentration for both oxygenated and degassed samples of E4PETEA cured using 365 nm UV irradiance. Lines are to guide the eye, except for the model in the inset.

The experimental results from the microrheological study provide excellent data with high spatial resolution. Such detailed results can be used to optimize and refine photopolymerization models, because of the ability to make detailed comparisons with model predictions. Combining depth profiling experiments with variations of initiator and inhibitor concentrations in the samples will facilitate the determination of model parameters, such as kinetic rate constants for propagation, termination and inhibition. Current techniques are apparently not sensitive enough to accurately determine all rate constants in the reaction pathway, as was shown by the discrepancies between experimental results and model predictions. Although the model parameters used in the

acrylate photopolymerization model have previously been shown to provide reasonable agreement with the differential photocalorimetry (DPC) and stereolithography part shape measurements [19], the more stringent comparison with microrheology data over a wide range of initiator concentrations reveal the limitations of the existing model. Studies are currently underway to understand which model parameters may be relatively insensitive to the methods currently used to parameterize the photopolymerization model and which can be better estimated additional fitting of the model to the microrheology data. Work is also in progress as mentioned previously to model the effect of oxygen quenching observed experimentally in the microrheology experiments by parameterizing the quenching mechanisms in the existing radical photopolymerization model [19].

2.4. Conclusions

The results presented prove that microrheology is an effective tool for monitoring photopolymerization. The important liquid-to-gel transition can be determined with high spatial and temporal accuracy and thus provides unprecedented experimental insight. The results can be used to directly test photopolymerization models and enhance the understanding of photo-induced free-radical polymerization. The role of oxygen inhibition, initiator concentration and UV illumination were investigated for acrylate resins. It was shown that the popular energy threshold model is not sufficient to explain our experimental results. Future optimization of the experimental method will include the use of electronic shutters to minimize experimental errors.

2.5. References

1. Lin, Y. and Stansbury, J. (2001). "Application of FT-NIR spectroscopy for monitoring the kinetics of photoinitiated methacrylate/vinyl ether copolymerizations." Journal of the American Chemical Society **42**: 809.

2. Nelson, E. W. and A. B. Scranton (1996). "In situ Raman spectroscopy for cure monitoring of cationic photopolymerizations of divinyl ethers." Journal of Raman Spectroscopy **27**(2): 137-144.

3. Clark, S. Hoyle C, Jonsson S, Morel F, and Decker C. (1999). "Photopolymerization of acrylates using N-aliphaticmaleimides as photoinitiators." Polymer **40**(18): 5063-5072.

4. Chiou B, English R, and Khan S. (1996). "Rheology and photo-cross-linking of thiol-ene polymers." Macromolecules **29**(16): 5368-5374.

5. Chiou, B., English, R. and Khan, S. (1997) "Real-Time and in-situ Rheological Studies on the UV Curing Kinetics of Thiol-ene Polymers." Macromolecules **30**: 7322-7328.

6. Botella A, Dupuy J, and Roche A. (2004). "Photo-rheometry/NIR spectrometry: An in situ technique for monitoring conversion and viscoelastic properties during photopolymerization." Macromolecular Rapid Communications **25**(12): 1155-1158.

7. Lange, J. "Viscoelastic Properties and Transitions during Thermal and UV Cure of a Methacrylate Resin." Polymer Engineering and Science 39 (1999): 1651-1660.

8. Tolpekin VA, Duits MHG, van den Ende D, and Melema J. (2003). "Stability ratio in binary hard sphere suspensions, measured via time-resolved microscopy." Langmuir **19**(10): 4127-4137.

9. Crocker, J. C. and D. G. Grier (1996). "Methods of digital video microscopy for colloidal studies." Journal of Colloid and Interface Science **179**(1): 298-310.

10. Sato, J. and V. Breedveld (2006). "Transient rheology of solvent-responsive complex fluids by integrating microrheology and microfluidics." Journal of Rheology **50**(1): 1-19.

11. Winter, H. H. and F. Chambon (1986). "Analysis of Linear Viscoelasticity of a Cross-Linking Polymer at the Gel Point." Journal of Rheology **30**(2): 367-382.

12. Brunner, T. A. and R. A. Ferguson (1996). "Simple models for resist processing effects." Solid State Technology **39**(6): 95.

13. Ahn N, Kim B, and Baik H. (1998). “A novel approximate model for resist process.” Optical microlithography XI SPIE Proceedings **3334**: 752-763

14. Cobb N, Zakhor A. (1997). “Experimental Results on Optical Proximity Correction with Variable Threshold Resist Model.” Optical microlithography X SPIE Proceedings **3051**: 458-468.

15. Tang Y, Rosen DW, Muzzy JD, and Henderson CL. (2004). "Stereolithography cure modelling and simulation." International Journal of Materials & Product Technology **21**(4): 255-272.

16. Goodner, M. D. and C. N. Bowman (2002). "Development of a comprehensive free radical photopolymerization model incorporating heat and mass transfer effects in thick films." Chemical Engineering Science **57**(5): 887-900.

17. Dickey MD, Burns RL, Kim EK, Johnson SC, Stacey NA, and Willson CG. (2005). "Study of the kinetics of step and flash imprint lithography photopolymerization." Aiche Journal **51**(9): 2547-2555.

18. Lovestead TM, O'Brien AK, and Bowman CN. (2003). "Models of multivinyl free radical photopolymerization kinetics." Journal of Photochemistry and Photobiology a-Chemistry **159**(2): 135-143.

19. O'Brien, A. K. and C. N. Bowman (2003). "Modeling thermal and optical effects on photopolymerization systems." Macromolecules **36**(20): 7777-7782.

CHAPTER 3

MONITORING OF THE EVOLUTION OF MECHANICAL PROPERTIES DURING THE UV-INITIATED POLYMERIZATIONS IN REAL-TIME

3.1. Introduction

Photopolymerization of multifunctional monomers to produce highly cross-linked polymers is widely used by industries that require ultra-fast processing speeds and high spatial resolution [1-4]. To effectively apply photopolymerization, the fundamentals of the process, such as the reaction kinetics and the mechanical development of the network, need to be well understood. The development of a technique that is capable of rapidly characterizing the local structure, mechanical properties, and reaction kinetics with high spatial and temporal resolution would greatly improve the current understanding of the process, as well as facilitate future advances in photopolymerization.

In order to maximize control of the cross-linking reaction, one must properly understand the how the cure conditions and sample properties are related to the gel point of a cross-linked network. Consequently, techniques capable of measuring the chemical or mechanical changes in real-time are the most commonly used to research photopolymerization. Photodifferential scanning calorimetry, which has been used by numerous researchers to obtain the rate of polymerization and conversion [5-13], was one of the first time-resolved methods developed to monitor photopolymerization. Despite the widespread use of calorimetry, limitations, such as a long response time due to the

thermal resistance of the sample, make it difficult to characterize ultra fast reactions. As a result, time-resolved spectroscopy techniques, such as Fourier transform infrared spectroscopy (FTIR) [14-17] and Raman spectroscopy [18, 19] have been employed to monitor the disappearance of reactive chemical groups during photocuring reactions. However, these techniques focus on chemical change and do not give information directly about the development of mechanical properties.

In view of that dynamic mechanical analysis and UV modified rheometers have been used to measure the real-time evolution of mechanical properties during thermal and UV induced polymerizations [20-26]. More recently, instrumentation that combined FTIR spectroscopy and rheology was developed to simultaneously perform in-situ monitoring of the chemical conversion and changes in sample rheology during photopolymerization [27]. However, these methods do not resolve spatial variations across the sample, since both techniques are based on sample volume, and thus measure average properties of the entire sample. This constraint has lead researchers to employ nuclear magnetic resonance spectroscopy (NMR) [28-31] and magnetic resonance imaging (MRI) [31-35] to study the photopolymerization process. Although these techniques are capable of monitoring chemical and mechanical changes in the system, using NMR and MRI to study photopolymerization is often impractical because these methods are expensive to operate, and thus not easily assessable. Addition limitations, such as limited time resolution and lack of high-throughput capability, have prevented the widespread application of NMR and MRI to study the photopolymerization. To obtain complete understanding of the photopolymerization process, a technique with high spatial resolution, a rapid response time, and flexible application needs to be developed.

Microrheology uses micron-sized tracer particles and a microscope to study the deformation and flow of matter on microscopic length scales [36-38]. The technique has several advantages over traditional techniques and is particularly suitable for monitoring changes in the mechanical properties of a UV exposed sample during photopolymerization. Since the volume over which mechanical properties are averaged in microrheology is the focal volume of a high-magnification microscope objective, the technique can be used to determine the local rheological properties with micrometer precision. In addition, the focal plane of the microscope can be varied to measure polymerization at different locations within the sample, and thus microrheology can be used to probe the properties of rheologically inhomogeneous materials. Additional advantages of microrheology include: small sample volume (on the order of microliters), the application of no external forces, a cost-effective setup, and high-throughput capability. The theory behind particle tracking microrheology and proof that the technique is capable of monitoring photopolymerization with high spatial and temporal resolution are provided in proceeding Chapters [39].

In Chapter 2, microrheology was used to investigate the dependence of the gel time on UV penetration depth for multifunctional acrylates. In addition, the reaction kinetics of a fast-reacting tetrafunctional system was characterized and compared to a comprehensive polymerization model. In this work, we intend to build upon the results of Chapter 2 by characterizing the reaction kinetics of model stereolithography resins that range from monofunctional to tetrafunctional systems. In addition, the reaction kinetics of copolymer systems will be investigated and compared to pure monomer systems. Finally, the effect of inhibitor concentration on reaction of multifunctional acrylates will

be examined. The use of high-speed electronic shutters in this Chapter will improve the accuracy of the method, thus the resulting data will better aid in the development and validation of complex models used to predict UV-initiated polymerization.

3.2. Method and Materials

3.2.1 Formulation of experimental samples

The photo-polymerizable samples investigated in this study were composed of acrylate monomer, photoinitiator, and fluorescent tracer particles. Four acrylate monomers of varying functionality were obtained from Sartomer: ethoxylated pentaerythritol tetraacrylate (E4PETeA, SR494), trimethylolpropane triacrylate (TMPTA, SR351), triethylene glycol diacrylate (TEGDA, SR272), and 2 (2-ethoxyethoxy) ethyl acrylate (EEA, SR256). As received, these monomers contained a small amount of inhibitor, which was removed by running samples through an alumina (grade CG20) filled column obtained from Polysciences Inc. The viscosity of each monomer was measured using an Anton Paar MCR-300 rheometer with a standard cone and plate setup. The number of functional groups and the viscosities of monomer used in this study are given in Table 1. Samples of TEGDA with E4PETeA and TEGDA with EEA were made at various concentrations (86:14 and 67:33 molar percentages) to study cophotopolymerization. A general-purpose photoinitiator, 2,2-dimethoxy-1,2-diphenylethan-1-one (DMPA, Irgacure 651), was obtained from Ciba Specialty Chemicals and used as received. Silica particles containing red fluorescent dye (rhodamine) with a diameter of 1.0 um were used as tracers for microrheololgy [40]. Controlled amounts of MEHQ (Sigma-Aldrich) were added to samples of E4PETeA to study the effect of polymerization inhibitors. After the components were mixed to obtain

a desired concentration of photoinitiator, the samples were briefly sonicated to minimize tracer particle aggregation.

Table 1: Functionality, concentration of double bonds, and viscosities of the monomers used.

Sample	Molar Average Functionality	Concentration of Double Bonds (mol/L)	Viscosity at 25 °C (cP)
E4PETeA	4.00	8.55	126
TMPTA	3.00	11.24	93
TEGDA/E4PETeA (67:33)	2.66	8.58	33
TEGDA/E4PETeA (86:14)	2.28	8.59	18.6
TEGDA	2.00	8.60	13
EEA/TEGDA (67:33)	1.33	8.79	4.8
EEA/TEGDA (86:14)	1.14	8.84	3.6
EEA	1.00	8.89	3

3.2.1. Methods

The mechanical properties of the photoinitiator doped monomers were monitored in real-time using particle tracking microrheology [39]. The samples were loaded into a 120 μm deep sample chamber, created by placing Parafilm spaces between a microscope slide and cover slip. The chamber was sealed using vacuum grease prior to placement on an inverted microscope equipped with a CCD camera. The motion of the tracer particles was tracked using a 63X oil-immersion objective with a spatial resolution of 0.153 μm per pixel. The images were transferred in real-time from the camera to a computer using a precision frame grabber and image acquisition software. Transient MSDs were calculated from the trajectories of the particles [41-44] using modified image analysis routines originally coded by Crocker and Grier [45] for the software package IDL (Research

Systems Inc.). Polymerization was induced by exposing the samples with a 365 nm 1000 W Hg(Xe) UV light source (Spectra-Physics), which was controlled via a high-speed electronic shutter.

To study the effects of oxygen, deoxygenated samples were prepared by loading monomer on a Schlenk line and pulling vacuum for two hours. The line was back filled with argon and the samples were placed in a glove box. The samples were loaded into the sample chamber and sealed with vacuum grease while inside the glove box. Upon removal the microrheology experiments were immediately run in order to prevent reoxygenation of the sample.

3.2.2. Determination of Gel Point via Microrheology

In our previous work [39], the gel point was defined as the point when the transient MSD data first becomes independent of the lag time, τ, which was shown to be a characteristic of an elastic gel. This definition was found to be comparable with methods based upon the classic Winter-Chambon gelation theory [46]**.** In this work, the gel point for multifunctional monomers (E4PETeA, TMPTA, and TEGDA) was determined using the independence of MSD on τ definition. The definition of gel point, however, had to be revised for the monofunctional monomer, EEA, since monomer species containing a single double bond cannot form a true gel network. Upon reaction, monofunctional monomers exhibit a dramatic increase in molecular weight and viscosity. Using the Stokes-Einstein relation, real-time measurements of EEA viscosity during photopolymerization were obtained by monitoring the time-dependent MSD [37]**.** The point at which viscosity diverged by a factor of 30 was used to define the gel point in the monofunctional system.

3.3. Results and Discussion

Microrheology was employed to characterize the local structure, mechanical properties, and reaction kinetics of free-radical photopolymerization with high spatial and temporal resolution. To elucidate the reaction kinetics, we systematically varied key experimental parameters: photoinitiator concentration, functionality of monomer, concentration of inhibitor, and the presence of oxygen. In addition, we examined the applicability of Flory's critical degree of conversion and the change in viscosity of a monofunctional monomer during photopolymerization.

3.3.1. Kinetics of Photopolymerization

3.3.1.1.Homopolymerization

In our previous study, microrheology was used to investigate the effect of initiator concentration the on reaction kinetics of E4PETeA [39]. To further elucidate the role of reaction kinetics, the previously described microrheological measurements were repeated using monomers of different functionality. All samples in this research were cured using 365 nm UV illumination and gelation was determined at a standard depth of 60 μm from the illuminated surface. Figure 3.1 contains the gelation time of oxygen saturated samples of E4PETeA, TMPTA, and TEGDA as a function of the molar ratio of DMPA to functional groups. As expected, increasing the molar ratio of the concentration of DMPA to functional groups leads to an appreciable decrease in the gelation time for all monomers. The observed trend in Figure 3.1 supports prior work, which illustrated that the gelation time of oxygen saturated samples of E4PETeA exhibit power-law scaling with increasing initiator concentration. The highest functional monomer, E4PETeA, requires the least amount of time to reach the point of gelation, followed by TMPTA and

TEGDA. This observation is supported by the critical conditions for the formation of an infinite network proposed by Flory [47], which establishes that monomers with higher functionality form cross-linked networks at lower conversions, thus a shorter amount of time is required to form a gel.

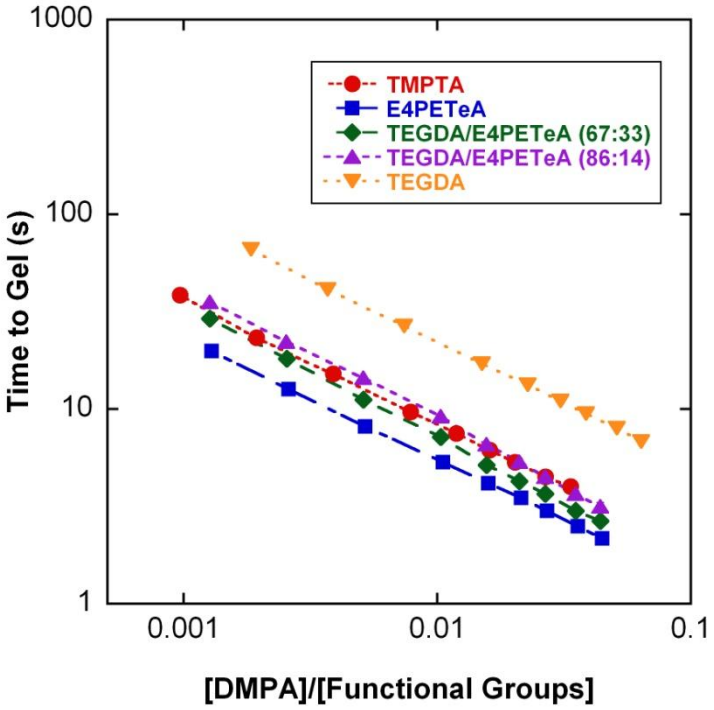

Figure 3.1: Plot of gelation time as a function of mole ratio of DMPA to functional groups for oxygen saturated samples of TMPTA (●), E4PETeA (■), TEGDA/E4PETeA [67:33] (♦), TEGDA/E4PETeA [86:14] (▲), and TEGDA(▼) cured using 365 nm UV irradiance. Lines are to guide the eye.

Although monofunctional EEA cannot develop into a cross-linked gel, microrheology can be used to monitor the marked change in viscosity that occurs upon exposure of DMPA doped EEA to UV light. In order to compare EEA to the multifunctional monomers used in this study, the point when the viscosity of the EEA solution diverged by a factor of 30 was defined as the gelation time. Figure 3.2 shows the gelation time of oxygen saturated samples of EEA and TEGDA as a function of molar

ratio of DMPA to functional groups. The data in Figure 3.2 illustrates that the gelation time for EEA is considerably longer than that of the multifunctional monomers of the same family. This result can be attributed to the fact the EEA cannot cross-link; and therefore, a significantly higher critical degree of conversion (ideally unity) is required to induce gelation. By comparing Figures 3.1 and 3.2, it is apparent that the power law scaling of gelation time with molar ratio of DMPA to function groups is independent of monomer functionality in the presence of oxygen. This finding was surprising since one would expect the scaling to depend on network formation; however, the data clearly show that a cross-linking and non cross-linking system have the same scaling.

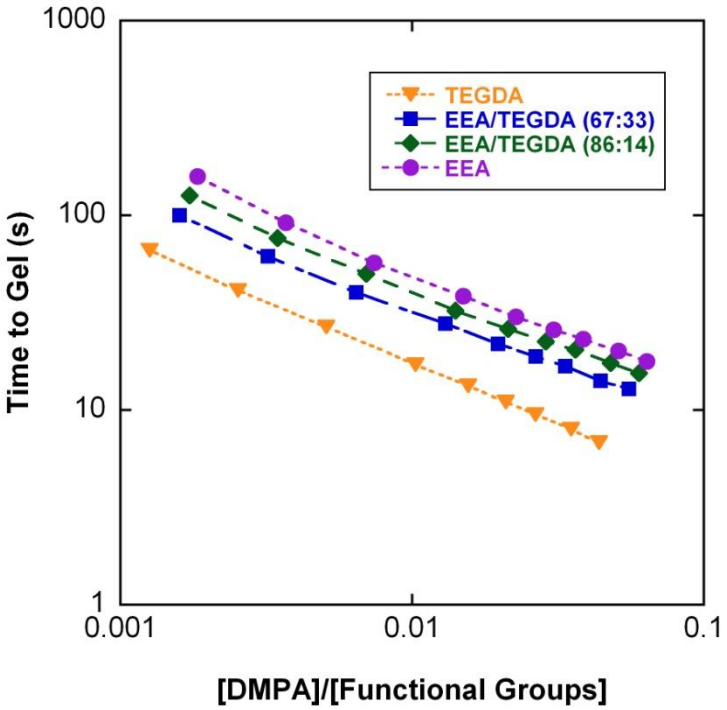

Figure 3.2: Plot of gelation time as a function of mole ratio of DMPA to functional groups for oxygen saturated samples of TEGDA (▼), EEA/TEGDA [67:33] (■), EEA/TEGDA [86:14] (♦), and EEA [86:14] (●) cured using 365 nm UV irradiance. Lines are to guide the eye.

In addition to studying the effect of initiator concentration on reaction kinetics, one can utilize microrheology to dissect the effects of oxygen inhibition. Previous work

establishes that oxygen has a significant impact on the reaction kinetics of E4PETeA. To better understand the role of oxygen inhibition, samples of varying functionality and initiator concentration were degassed under vacuum and loaded into sample chambers in an oxygen free environment. The gelation times of degassed samples of E4PETeA, TMPTA, and TEGDA as a function of the molar ratio of DMPA to functional groups are shown in Figure 3.3, while the same data for EEA is shown in Figure 3.4. Comparing the oxygen saturated data to the degassed data in Figures 3.3 and 3.4 clearly indicates that oxygen has a strong inhibitory effect on all of the monomers. Unlike the oxygen saturated data, which exhibits power law scaling of gel time with molar ratio of DMPA to function groups, the degassed data of Figures 3.3 and 3.4 follow a stronger decay that can best be described as exponential. As illustrated in Figures 3.3 and 3.4, this decay appears to strengthen with increasing functionality. The higher functional monomers form a more densely cross-linked network at lower critical degrees of conversion; therefore, in the absence of oxygen the gelation time is dependent on network formation.

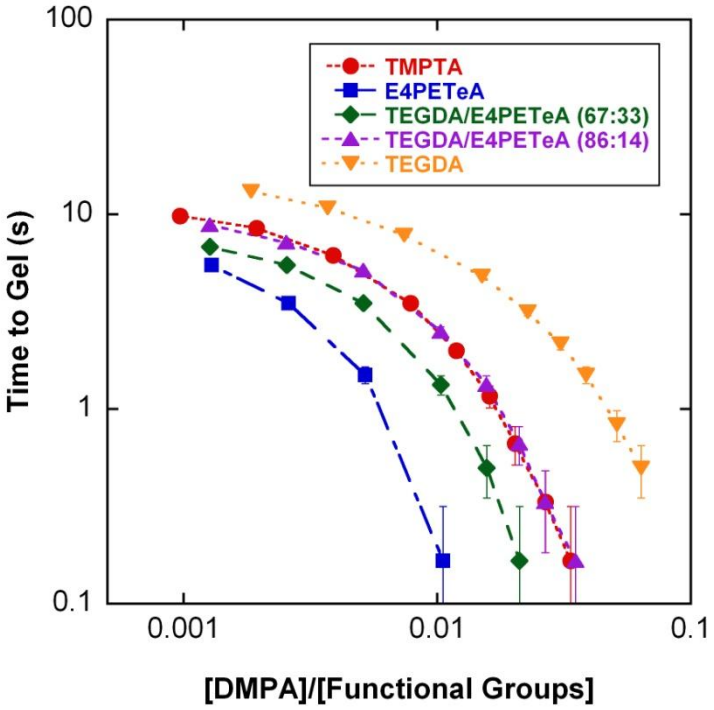

Figure 3.3: Plot of gelation time as a function of mole ratio of DMPA to functional groups for degassed samples of TMPTA (●), E4PETeA (■), TEGDA/E4PETeA [67:33] (♦), TEGDA/E4PETeA [86:14] (▲), and TEGDA(▼) cured using 365 nm UV irradiance. Lines are to guide the eye.

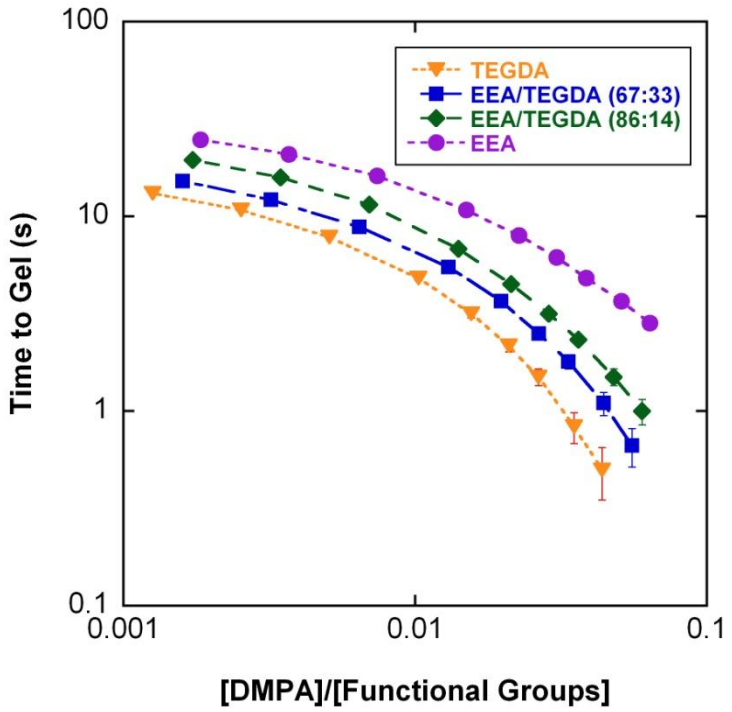

Figure 3.4: Plot of gelation time as a function of mole ratio of DMPA to functional groups for oxygen saturated samples of TEGDA (▼), EEA/TEGDA [67:33] (■), EEA/TEGDA [86:14] (♦), and EEA [86:14] (●) cured using 365 nm UV irradiance. Lines are to guide the eye.

3.3.1.2.Copolymerization

In addition to probing the effects of initiator concentration and oxygen inhibition on the full cure behavior of homopolymer systems, microrheology can be used to investigate the copolymerization of acrylate systems. Monomers of lower functionality and viscosity are often used as reactive diluents to improve the reactivity, viscosity and final conversion of more viscous monomers. In addition, diluting a multifunctional monomer with a monomer of lower functionality enables the systematic control of the cross-linked network formed during UV initiated polymerizations. Figures 3.1 and 3.3 contain the oxygen saturated and degassed results for mixtures of TEGDA with 14 and 33 mole percent of E4PETeA. E4PETeA and TEGDA have the same general backbone

structure; however, E4PETeA has two additional branched vinyl chains, thus E4PETeA has a total of four functional groups, while TEGDA only has two. In addition to having a higher functionality, the viscosity of E4PETeA is ten times greater than that of TEGDA.

Figure 3.1 graphically illustrates the effect of adding increasing amounts of a higher functional monomer to one of lower functionality. Increasing the amount of E4PETeA added to samples of TEGDA increases the reaction rate by increasing the rate of cross-linking reactions, and thus decreases the time required to reach gelation. As revealed in Figure 3.1, in the presence of oxygen the 67:33 mole percent mixture of TEGDA/E4PETeA reaches the gel point faster than pure TMPTA, while the 86:14 mole percent mixture gels at nearly the same time as pure TMPTA. At higher initiator loadings, the 86:14 mixture of TEGDA/E4PETeA actually forms a gel faster than TMPTA cured under the same conditions. The degassed data in Figure 3.3 show that the two mixtures of TEGDA/E4PETeA consistently form a gel faster than TMPTA in the absence of oxygen. Considering the molar average functionalities listed for all systems in Table 3.1, these results may seem counterintuitive; however, the viscosities of the systems must also be taken into consideration. The viscosity controls the diffusion of the reacting species, which influences the termination step from the beginning of the polymerization and determines when the propagation becomes diffusion controlled.

Although TMPTA has a higher molar average functionality than both mixtures of TEGDA/E4PETeA, the viscosities of the TEGDA/E4PETeA mixtures are significantly lower then that of pure TMPTA. The reduced viscosity of the TEGDA/E4PETeA mixtures allows for greater mobility of free-radicals and monomer molecules, thus the reaction is less limited by diffusion. In addition to having a higher initial viscosity, the

trifuctional TMPTA forms a highly cross linked network, which further reduces the mobility of system. Previous work has shown that the reactivity of a viscous methacrylate monomer can be improved by adding a low-viscosity diluent methacrylate monomer [8, 48-52].

To better understand the process of photocopolymerization, mixtures of the monofunctional EEA and the difunctional TEGDA we prepared at the same molar ratios as the TEGDA/E4PETeA mixtures. The oxygen saturated and degassed data for the EEA/TEGDA mixtures, along with the homopolymerization data for EEA and TEGDA, can be found in Figures 3.2 and 3.4. The data in Figures 3.2 and 3.4 clearly demonstrate that increasing the amount of TEGDA added to a monofunctional system decreases the observed gel time. This behavior was not unexpected given that as the amount of cross-linking agent, TEGDA in this case, is increased, the formation of an infinite network will occur more rapidly since the number of molecules that can act as crosslinks is significantly increased. Litvinov *et al.* recently reported that the presence of a mono-acrylate, slows down the cure rate of a difunctional acrylate [30]. This behavior has been successfully modeled by Bowman *et al.* using a kinetic gelation model [53]. In the presence of oxygen, Figure 3.2, the gel time data of the EEA/TEGDA mixtures is closer to the pure EEA data; however, degassing the mixtures shifts the EEA/TEGDA data closer to that of pure TEGDA as shown in Figure 3.4.

Another important observation is that the power law scaling of gelation time with molar ratio of DMPA to function groups, originally reported for oxygen saturated homopolymerization in Figures 3.1 and 3.2, is applicable to the all copolymer systems studied here as well. Additionally, the stronger exponential-like scaling observed for

degassed homopolymer systems in Figures 3.3 and 3.4 also holds for all of the copolymer systems. However, the original observation that the observed scaling of degassed data strengthens with increasing functionality in homopolymer systems is not applicable to the copolymer mixtures of TEGDA/E4PETeA, which appear to have a higher reactivity due to the reduced viscosity of the mixtures when compared to pure TMPTA. The microrheological data presented above clearly indicated that the copolymerization of acrylate systems is dependent on monomer viscosity and functionality.

3.3.2. Effect of Inhibitor

Polymerization inhibitors, such as hydroquinone (HQ) and hydroquinone monomethyl ether (MEHQ), are used to promote process and shelf stability of highly reactive acrylate monomer formulations. Inhibitors are able to scavenge free-radicals that form during manufacturing or storage of the photoresin formulation. Since the majority of commercially used monomers contain only minute amounts, the effects of inhibitors on cure rate are considered negligible. To better understand the effects of inhibition, samples of E4PETeA and TMPTA loaded with 0.5 wt.% and 5.0 wt.% of photoinitiator were prepared with various concentrations of MEHQ. The gelation times of oxygen saturated and degassed systems at a fixed UV penetration depth of 60 μm are shown in Figure 3.5.

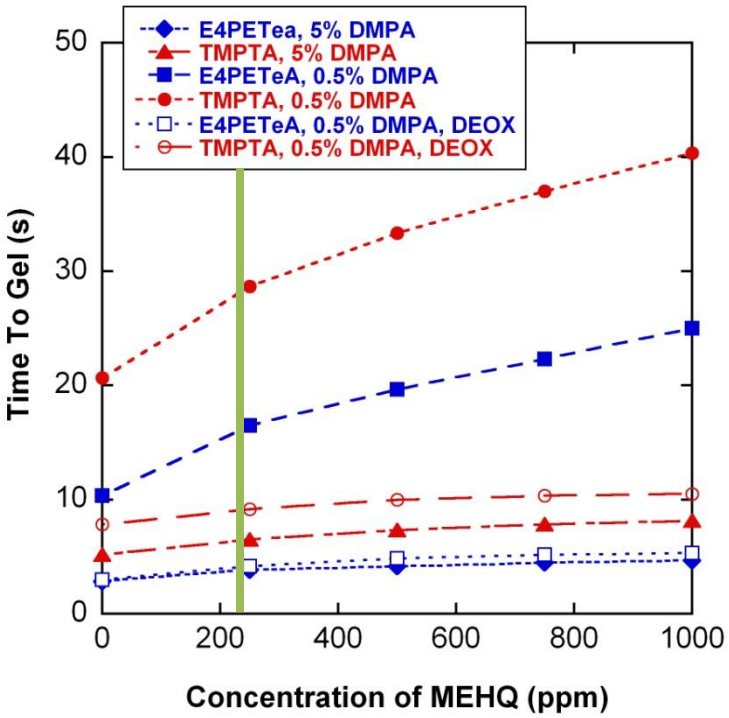

Figure 3.5: Plot of gelation time as a function of inhibitor (MEHQ) concentration for E4PETeA and TMPTA loaded with 5.0 wt% and 0.5 wt% DMPA (both degassed and oxygenated saturated) cured using 365 nm UV irradiance. The closed data points are oxygen saturated and the open data points are deoxygenated. The vertical line indicates the concentration of inhibitor in the samples as received (240 ppm MEHQ). Lines are to guide the eye.

As can be seen in Figure 3.5, increasing the concentration of MEHQ lengthens the overall cure time. The addition of MEHQ mainly affects the initiation and propagation steps of the reaction kinetics, by quenching both free and chain radicals before they have a chance to react with other unsaturated sites. MEHQ reacts with chain radicals by hydride abstraction to form a hydroquinone radical that is considered stable and unable to initiate further polymerization. Although the stabilized MEHQ radical cannot initiate polymerization, it can react with additional chain radicals and terminate propagation. Eventually, once all the MEHQ is consumed, the photopolymerization will proceed to gelation.

As revealed in Figure 3.5, the inhibitory effect of MEHQ is greater at lower concentrations of photoinitiator. The gelation time for a sample of E4PETeA loaded with 0.5 wt.% DMPA increases by a factor of 2.4 for a 1000 ppm increase in MEHQ concentration, while a sample containing 5.0 wt.% DMPA exhibits an increase of 1.65 times under the same conditions. Similar results are observed for TMPTA loaded with 0.5 wt.% and 5.0 wt.% DMPA. These findings are likely the result of the efficiency of MEHQ consumption being reduced by an increase in radical concentration. Under identical illumination conditions, samples loaded with 5.0 wt.% DMPA will generate a higher radical concentration than samples loaded with 0.5 wt.% DMPA. Thus, the monomer samples containing 5.0 wt.% DMPA will be less effected by the presence of MEHQ compared to 0.5 wt.% DMPA loaded samples.

In addition, the data in Figure 3.5 demonstrates that the effect of inhibitor on cure time begins to level off around a MEHQ concentration of 750 ppm in samples with 5.0 wt.% DMPA. Increasing the concentration of inhibitor beyond this point has a less significant effect on the gelation time compared to initial increases in inhibitor concentration. This trend is not observed in E4PETeA and TMPTA samples containing 0.5 wt.% DMPA. These results indicate that increasing the concentration of MEHQ is essentially ineffective at prolonging the shelf-life of monomers containing relatively high amounts of photoinitiator.

Studies performed to determine the optimal inhibitor concentration necessary to protect commercial formulations from early gelation support the results obtained in this research. In one such investigation [54], Sartomer Inc. used a UV equipped rheometer to determine the effects of varying the concentration of MEHQ in samples of TMPTA

loaded with 2.0 wt.% photoinitiator on cure time. In the Sartomer study, a 50% increase in gelation time was observed between the 0 ppm and 1000 ppm samples of TMPTA, while our data show gelation time increases by 58% when TMPTA was loaded with 5.0 wt.% DMPA. In addition, the Sartomer results indicate a plateau in cure time was reached around a concentration of 500 ppm MEHQ [54].

To better understand the effect of polymerization inhibitors, samples of E4PETeA and TMPTA loaded with 0.5 wt.% photoinitiator and MEHQ were deoxygenated before exposure to UV irradiance. Figure 3.5 illustrates the effect of MEHQ on the gelation time for oxygenated saturated and degassed samples at a fixed UV penetration depth of 60 μm. The degassed data in Figure 3.5 exhibit the same trends observed for oxygen saturated samples loaded with 5.0 wt.% DMPA. When MEHQ concentration was raised from 0 ppm to 1000 ppm the gel time for degassed E4PETeA with 0.5 wt.% DMPA was increased by a factor of 1.77, which is less significant then the factor of 2.4 increase observed for oxygen saturated E4PETeA with 0.5 wt.% DMPA cured under identical conditions. Oxygen, like MEHQ, is known to inhibit polymerization by consuming free-radicals, thus at a constant photoinitiator concentration, a degassed sample will have a higher concentration of radicals when compared to an oxygen saturated sample under the same illumination conditions. As a result, deoxygenating a sample reduces the effectiveness of inhibition by MEHQ. The inhibitory efficiency of MEHQ on free-radical polymerizations being strongly dependent on the presence of oxygen has been widely reported in literature [55-58]. Leon found that oxygen is needed for MEHQ to work effectively in acrylic monomers, but is not necessary for vinyl acetate monomer, and actually destabilizes it at elevated temperatures[57].

3.3.3. Kinetic Applications of Microrheology Data

The need to understand the relationship between the mechanical properties and the reactivity of the monomer functional groups has fueled the development of models capable of describing network formation during cross-linking photopolymerization. The modeling approaches can be divided into three main catigories, each having their advantages and limitations. Flory and Stockmayer [47, 59, 60] first proposed statistical theory some 50 years ago; since then the statistical approach has been elaborated by Gordon [61], Miller-Marcosko [62], and Durand-Bruneau [63]. Tobita-Hamielec [64-68], Oaky [69-72], and Mikos [73] have developed non-mean-field kinetic based approaches to explore network formation. Finally, percolation type models of network formation have been developed and extensively studied by Boots [9] and Bowman [53, 74, 75]. Here, we exploit the ability of microrheology to monitor the mechanical properties in real-time to examine the simple statistical theory on network formation originally proposed by Flory [47].

Multifunctional monomers form a polymer network via cross-linking reactions in which two or more chains are joined together by a covalent bond to form a branch point. Cross-linking is distinguished by the formation of an insoluble polymer at a specific time in the polymerization known as the gel point. The gel point corresponds to the formation of an infinite network in which polymer molecules have been cross-linked to each other to form a macroscopic molecule. Flory and also Stockmayer developed a statistical approach to determine the critical conditions for the formation of an infinite network. In its simplest form, statistical theory of network formation assumes that the reactivity of all functional groups of the same type is equal and independent of molecular size. An

additional assumption is that there are no intramolecular reactions (e.g., cyclization) between functional groups on the same molecule.

The Flory approach to statistical theory is developed around the branching coefficient α, which is defined as the probability that a given functional group of a branch unit at the end of a polymer chain segment leads to another branch unit. According to Flory, the criterion for the formation of an infinite network in a system containing a reactant of functionality f is that at least one of the (f - 1) chain segments radiating from a branch unit will in turn be connected to another branch unit. Thus, the critical value of α for gel formation is

$$\alpha = \frac{1}{(f-1)} \tag{3.1}$$

where f is the functionality of the branching unit, which is defined by Flory as the number of other molecules that can react with the network-forming species. For example a tetrafunctional monomer has the ability to bond with eight other molecules; therefore, according to Flory the monomer would have a functionality of f = 8. If more than one type of multifunctional branching unit is present an average f value of all the monomer molecules is used in Equation 3.1. Monomers with higher functionality form infinite cross-linked networks more rapidly than ones with lower functionality. As a result, monomers with higher functionality have to reach a lower critical branching coefficient for gelation to occur.

The critical branching parameter predicted by Flory was calculated for each monomer and comonomer system. To approximate the agreement between the gel time data ascertained with microrheology and statistical theory, the data in Figures 3.3 and 3.4 was normalized to its respective critical branching parameter. For example, the gel time

data for a degassed sample of TMPTA loaded with 2.0 wt.% DMPA was multiplied by the inverse of the branching coefficient calculated for a trifunctional monomer. Only the degassed gel time data was considered for comparison because the statistical theory originally proposed by Flory does not take into account inhibition of oxygen. The renormalization results for 0.25, 1.0, 2.0, 3.0 and 8.0 wt.% DMPA as a function of the molar average functionality are shown below in Figure 3.6.

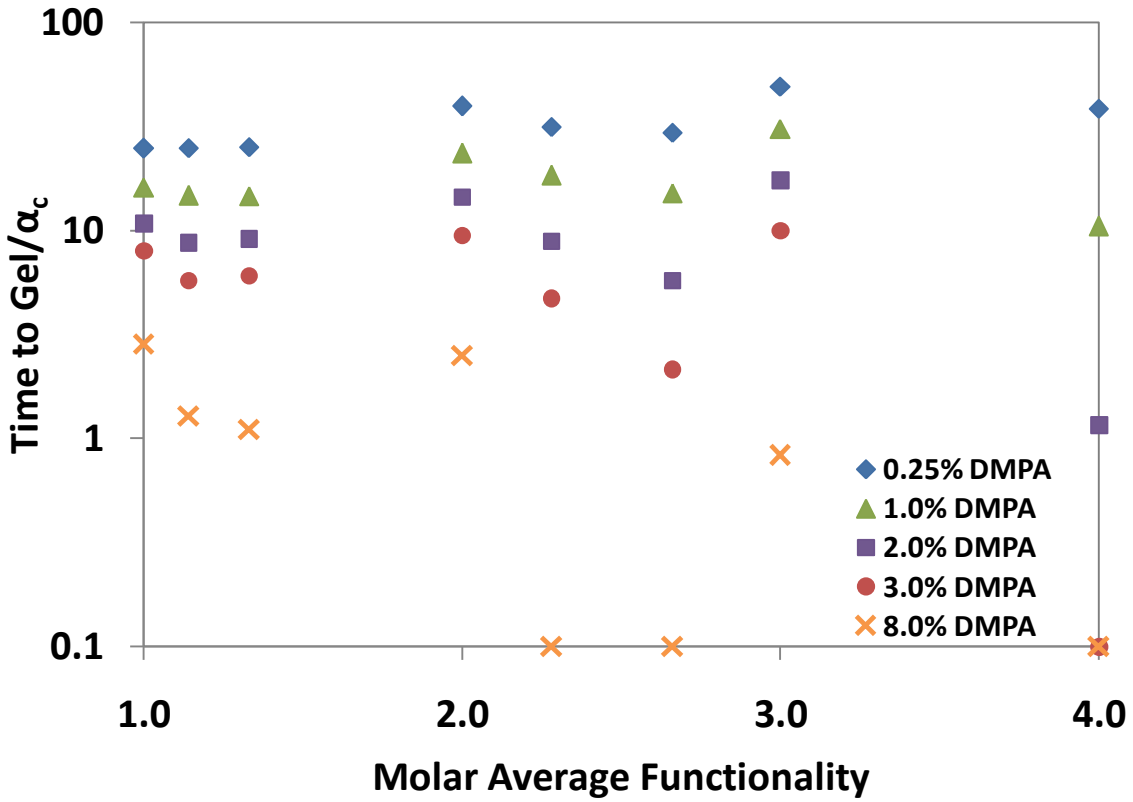

Figure 3.6: Plot of gelation time divided by the critical degree of conversion predicted by Flory as a function of the molar average functionality for pure monomers and monomer mixtures loaded with varying concentrations (weight percent) of DMPA.

In Figure 3.6, ideal agreement between the experimental data and statistical theory would result in normalized time being independent of the molar average functionality for each initiator concentration. At low concentrations of DMPA, Figure 3.6 shows that the experimental data exhibits reasonable agreement with the statistical theory

proposed by Flory; however, at the high concentrations of DMPA, the statistical theory and microrheology display poor agreement. According to Figure 3.6, the Flory theory over predicts the point at which an infinite network is formed in copolymer systems. The primary reason for the discrepancies between statistical theory and experimental data is that Flory assumes equal reactivity of functional groups and no intramolecular reactions. Countless studies, however, have proven these assumptions to be invalid for multifunctional monomers. Bowman *et al.* has shown that increasing the reaction rate, via initiator concentration or functionality, results in a larger amount of intramolecular reactions, such as primary and secondary cyclization [76-78]. Figure 3.6, ultimately shows that statistical theory, in its simplest form, does a reasonable job predicting the formation of an infinite network in systems with a low rate of polymerization.

3.4. Conclusions

In this work, particle tracking microrheology was employed to monitor the mechanical properties of multifunctional acrylate resins during UV-initiated homo and copolymerizations in real-time. Using microrheology, information critical to understanding of the structural evolution and reaction kinetics of cross-linking photopolymerization was obtained with high spatial and temporal resolution. Although it was show that both oxygen and MEHQ retard the polymerization reaction, the inhibitory effect of oxygen was significantly greater than that of MEHQ. It was determined that the presence of oxygen effectively alters the scaling of the reaction kinetics for the multifunctional acrylates investigated in this work. Through modeling it was concluded that oxygen diffusion is responsible for the previously reported linear scaling of gelation

time with UV penetration depth in E4PETeA samples loaded with high concentrations of photoinitiator.

In addition, it was found that the dilution of multifunctional monomers with a monomer of lower functionality increases the measured gel time. From this work it is suggested that the copolymerization of multifunctional acrylate resins is strongly dependant on the monomer viscosity and functionality. It was also illustrated that Flory's critical branching coefficient for network formation is closely correlated to the gel time of multifunctional acrylate systems at low photoinitiator concentrations. Ultimately, microrheology provides unique information that is unattainable with other photopolymerization characterization methods and this knowledge can be used to develop a more quantitative understanding of the complex process.

3.5. References

1. Drobny, J.G., *Radiation Technology for Polymers*. 2003, London: CRC Press.

2. Fouassier, J.P. and J.F. Rabek, *Radition Curing in Polymer Science and Technology Volume III: Polymerization Mechanisms*. 1993, London: Elsevier Applied Science.

3. Pappas, S.P., *UV Curing: Science & Technology Volume II*. 1985, Norwalk, CT: Technology Marketing Corporation.

4. Decker, C., (1994). "Photoinitiated Curing of Multifunctional Monomers." Acta Polymer, **43**: 333-347.

5. Maffezzoli, A. and R. Terzi, (1998). "Effect of irradiation intensity on the isothermal photopolymerization kinetics of acrylic resins for stereolithography." Thermochimica Acta, **321**(1-2): 111-121.

6. Sandner, B., N. Kotzian, J. Tubke, S. Wartewig, and O. Lange, (1997). "Photocalorimetric monitoring of the polymerization of an oligo(ethylene glycol) dimethacrylate in oligo(ethylene glycol) dimethyl ethers." Macromolecular Chemistry and Physics, **198**(9): 2715-2727.

7. Clark, S.C., C.E. Hoyle, S. Jonsson, F. Morel, and C. Decker, (1999). "Photopolymerization of acrylates using N-aliphaticmaleimides as photoinitiators." Polymer, **40**(18): 5063-5072.

8. Dickens, S.H., J.W. Stansbury, K.M. Choi, and C.J.E. Floyd, (2003). "Photopolymerization kinetics of methacrylate dental resins." Macromolecules, **36**(16): 6043-6053.

9. Boots, H.M.J., J.G. Kloosterboer, G.M.M. Vandehei, and R.B. Pandey, (1985). "Inhomogenity during the Bulk-Polymerization of Divinyl Compounds-Differential Scanning Calorimetry Experiments and Percolation Theory." British Polymer Journal, **17**(2): 219-223.

10. Tryson, G.R. and A.R. Shultz, (1979). "Calorimetric Study of Acrylate Photopolymerization." Journal of Polymer Science Part B-Polymer Physics, **17**(12): 2059-2075.

11. Corcione, C.E., A. Greco, and A. Maffezzoli, (2004). "Photopolymerization kinetics of an epoxy-based resin for stereolithography." Journal of Applied Polymer Science, **92**(6): 3484-3491.

12. Kim, W.S., R. Houbertz, T.H. Lee, and Y.S. Bae, (2004). "Effect of photoinitiator on photopolymerization of inorganic-organic hybrid polymers (ORMOCER (R))." Journal of Polymer Science Part B-Polymer Physics, **42**(10): 1979-1986.

13. Chiu, H.T., M.F. Cheng, and H.Y. Liu, (2007). "The analysis of photocuring behavior of polyester acrylate by means of differential photo calorimeter (DPC) and rigid-body pendulum rheometer (RPT)." Polymer-Plastics Technology and Engineering, **46**(3): 199-205.

14. He, L., S.F. Zhang, S.Z. Jin, and Z.N. Qi, (1995). "Study of In-situ Photopolymerization of Chiral Liquid-Crystal Acrylate." Polymer International, **38**(2): 211-214.

15. Wang, J.Z.Y. and R.H. Bogner, (1995). "Techniques to Monitor the UV Curing of Potential Solvent-Free Film Coating Polymers." International Journal of Pharmaceutics, **113**(1): 113-122.

16. McGettrick, B.P., J.K. Vij, and C.B. McArdle, (1994). "Characterization of Model Anaerobic Adhesive Cure using Real-time Fourier-Transform IR Spectroscopy and Dielectric Spectroscopy." Journal of Applied Polymer Science, **52**(6): 737-746.

17. Priola, A., G. Gozzelino, F. Ferrero, and G. Malucelli, (1993). "Investigation on the Structure-Property Relationships for Films Obtained from UV Curable Coatings." Progress in Organic Coatings, **22**(1-4): 301-314.

18. Nelson, E.W. and A.B. Scranton, (1996). "In situ Raman spectroscopy for cure monitoring of cationic photopolymerizations of divinyl ethers." Journal of Raman Spectroscopy, **27**(2): 137-144.

19. Mailhot, G., J.L. Philippart, and M. Bolte, (1991). "Raman Spectroscopy: An Original and Nondestructive Method to Determine the Rate of Polymerization Photoinitiated by Laser Beam." Polymer Communications, **32**(8): 229-231.

20. Nakamuchi, T., (1986). "Time-Resolved Measurements of Mechanical Properties Using a Rheological Apparatus." Progress in Organic Coatings, **14**: 23-32.

21. Watanbe, K., (1996). "Rheological Studies of Ultraviolet Curing with an Oscillating Plate Rheometer." Journal of Applied Polymer Science, **29**: 323-332.

22. Davison, J.W. and J.T. Guthrie, (1992). "Photochemorheological Studies of UV Curing Processes." Jocca-Surface Coatings International, **75**(8): 315-322.

23. Chiou, B.S., R.J. English, and S.A. Khan, (1996). "Rheology and photo-cross-linking of thiol-ene polymers." Macromolecules, **29**(16): 5368-5374.

24. Lange, J., (1999). "Viscoelastic properties and transitions during thermal and UV cure of a methacrylate resin." Polymer Engineering and Science, **39**(9): 1651-1660.

25. Naghash, H.J., O. Okay, and Y. Yagci, (1997). "Gel formation by chain-crosslinking photopolymerization of methyl methacrylate and ethylene glycol dimethacrylate." Polymer, **38**(5): 1187-1196.

26. Chiou, B.S. and S.A. Kham, (1997). "Real-time FTIR and in situ rheological studies on the UV curing kinetics of thiol-ene polymers." Macromolecules, **30**(23): 7322-7328.

27. Botella, A., J. Dupuy, A.A. Roche, H. Sautereau, and V. Verney, (2004). "Photo-rheometry/NIR spectrometry: An in situ technique for monitoring conversion and viscoelastic properties during photopolymerization." Macromolecular Rapid Communications, **25**(12): 1155-1158.

28. Litvinov, V.M. and A.A. Dias, (2001). "Analysis of network structure of UV-cured acrylates by H-1 NMR relaxation, C-13 NMR spectroscopy, and dynamic mechanical experiments." Macromolecules, **34**(12): 4051-4060.

29. Jager, W.F., A. Lungu, D.Y. Chen, and D.C. Neckers, (1997). "Photopolymerization of polyfunctional acrylates and methacrylate mixtures: Characterization of polymeric networks by a combination of fluorescence spectroscopy and solid state nuclear magnetic resonance." Macromolecules, **30**(4): 780-791.

30. Litvinov, V.M. and A.A. Dias, (2005). "Real-time NMR. How fast can we do it?" Macromolecular Symposia, **230**: 20-25.

31. Nunes, T.G., F.C.P. Garcia, R. Osorio, R. Carvalho, and M. Toledano, (2006). "Polymerization efficacy of simplified adhesive systems studied by NMR and MRI techniques." Dental Materials, **22**(10): 963-972.

32. Pereira, S.G., N. Reis, and T.G. Nunes, (2005). "Spatially resolved studies on the photopolymerization of dimethacrylate monomers." Polymer, **46**(19): 8034-8044.

33. Nunes, T.G., L. Ceballos, R. Osorio, and M. Toledano, (2005). "Spatially resolved photopolymerization kinetics and oxygen inhibition in dental adhesives." Biomaterials, **26**(14): 1809-1817.

34. Guillot, G., T.G. Nunes, J.P. Ruaud, and W. Polido, (2004). "Aspects of the photopolymerization of a commercial dental resin studied by H-1 magnetic resonance imaging." Polymer, **45**(16): 5525-5532.

35. Pereira, S.G., T.G. Nunes, and S. Kalachandra, (2002). "Low viscosity dimethacrylate comonomer compositions [Bis-GMA and CH(3)Bis-GMA] for novel dental composites; analysis of the network by stray-field MRI, solid-state NMR and DSC & FTIR." Biomaterials, **23**(18): 3799-3806.

36. Mukhopadhyay, A. and S. Granick, (2001). "Micro- and nanorheology." Current Opinion in Colloid & Interface Science, **6**(5-6): 423-429.

37. Waigh, T.A., (2005). "Microrheology of complex fluids." Reports on Progress in Physics, **68**(3): 685-742.

38. Breedveld, V. and D.J. Pine, (2003). "Microrheology as a tool for high-throughput screening." Journal of Materials Science, **38**(22): 4461-4470.

39. Slopek, R.P., H.K. McKinley, C.L. Henderson, and V. Breedveld, (2006). "In situ monitoring of mechanical properties during photopolymerization with particle tracking microrheology." Polymer, **47**(7): 2263-2268.

40. Tolpekin, V.A., M.H.G. Duits, D. van den Ende, and J. Mellema, (2003). "Stability ratio in binary hard sphere suspensions, measured via time-resolved microscopy." Langmuir, **19**(10): 4127-4137.

41. Sato, J. and V. Breedveld, (2006). "Transient rheology of solvent-responsive complex fluids by integrating microrheology and microfluidics." Journal of Rheology, **50**(1): 1-19.

42. Breedveld, V., A.P. Nowak, J. Sato, T.J. Deming, and D.J. Pine, (2004). "Rheology of block copolypeptide solutions: Hydrogels with tunable properties." Macromolecules, **37**(10): 3943-3953.

43. Mason, T.G., H. Gang, and D.A. Weitz, (1996). "Rheology of complex fluids measured by dynamic light scattering." Journal of Molecular Structure, **383**(1-3): 81-90.

44. Mason, T.G., J. Bibette, and D.A. Weitz, (1995). "Elasticity of Compressed Emulsions." Physical Review Letters, **75**(10): 2051-2054.

45. Crocker, J.C. and D.G. Grier, (1996). "Methods of digital video microscopy for colloidal studies." Journal of Colloid and Interface Science, **179**(1): 298-310.

46. Winter, H.H. and F. Chambon, (1986). "Analysis of Linear Viscoelasticity of a Cross-Linking Polymer at the Gel Point." Journal of Rheology, **30**(2): 367-382.

47. Flory, P.J., *Principles of Polymer Chemistry*. 1953, Ithaca, NY: Cornell University Press.

48. Socha, E., E. Andrzejewska, M. Andrzejewski, M.B. Bogacki, and K. Bielicka-Daszkiewicz, (2004). "Copolymerization of dodecyl methacrylate with oxyethylene glycol dimethacrylates determination of reactivity ratios." Polimery, **49**(5): 356-358.

49. Andrzejewska, E., (2001). "Photopolymerization kinetics of multifunctional monomers." Progress in Polymer Science, **26**(4): 605-665.

50. Andrzejewska, E., E. Socha, M. Bogacki, and M. Andrzejewski, (2005). "Chain length dependent termination in radical cross-linking polymerization." Polymer, **46**(15): 5437-5446.

51. Kilambi, H., S.K. Reddy, L. Schneidewind, J.W. Stansbury, and C.N. Bowman, (2007). "Copolymerization and dark polymerization studies for photopolymerization of novel acrylic monomers." Polymer, **48**(7): 2014-2021.

52. Goodner, M.D., S.M. Newman, and C.N. Bowman, (1995). "Effects of Comonomer composition on Photopolymerizations of Multiethylene Glycol Dimethacrylates." Journal of Dental Research, **74**: 229-229.

53. Anseth, K.S. and C.N. Bowman, (1994). "Kinetic Gelation Model Predictions of Cross-inked Polymer Network Microstructure." Chemical Engineering Science, **49**(14): 2207-2217.

54. Sartomer, *Inhibitionn of Acrylate UV-Curing Systems*. 1990, Exton, PA: Sartomer Company Literature.

55. Becker, H. and H. Vogel, (2004). "Stabilization of acrylic esters." Chemical Engineering & Technology, **27**(10): 1122-1126.

56. Becker, H. and H. Vogel, (2006). "The role of hydroquinone monomethyl ether in the stabilization of acrylic acid." Chemical Engineering & Technology, **29**(10): 1227-1231.

57. Leon, B.L., (1993). "The effect of oxygen on vinyl acetate and acrylic monomer stabilization." Process Safety Progress, **12**(1): 47-48.

58. Li, R.J. and F.J. Schork, (2006). "Modeling of the inhibition mechanism of acrylic acid polymerization." Industrial & Engineering Chemistry Research, **45**(9): 3001-3008.

59. Stockmayer, W.H., (1943). "Theory of molecular size distribution and gel formation in branched-chain polymers." Journal of Chemical Physics, **11**(2): 45-55.

60. Stockmayer, W.H., (1944). "Theory of molecular size distribution and gel formation in branched polymers II General cross linking." Journal of Chemical Physics, **12**(4): 125-131.

61. Gordon, M., (1962). "Goods Theory of Cascade Processes Applied to Statistics of Polymer Distributions." Proceedings of the Royal Society of London Series a-Mathematical and Physical Sciences, **268**(1333): 240-&.

62. Miller, D.R. and C.W. Macosko, (1976). "New Derivation of Post Gel Properties of Network Polymers." Macromolecules, **9**(2): 206-211.

63. Durand, D. and C.M. Bruneau, (1985). "Statistics of Random Macromolecular Networks Made by Chainwise Polymerization of Polyfunctional Monomers 1. Characterization of the Pre-gel Region." European Polymer Journal, **21**(6): 527-535.

64. Tobita, H. and A.E. Hamielec, (1988). "A Kinetic Model for Network Formation in Free-radical Polymerization." Makromolekulare Chemie-Macromolecular Symposia, **20-1**: 501-543

65. Tobita, H. and A.E. Hamielec, (1989). "Network Formation in Free-radical Copoymerization-Pseudo Kinetic Rate-constant Method for Copolymers with Long Branches." Acs Symposium Series, **404**: 242-255.

66. Tobita, H. and A.E. Hamielec, (1989). "Modeling of Network formation in Free-radical Polymerization." Macromolecules, **22**(7): 3098-3105.

67. Tobita, H. and A.E. Hamielec, (1991). "Kinetics of Free-radical Copolymeration-The Pseudo-Kinetic Rate constant Method." Polymer, **32**(14): 2641-2647.

68. Tobita, H. and A.E. Hamielec, (1992). "Control of Network Structure in Free-radical Cross-linking Copolymerizatioin." Polymer, **33**(17): 3647-3657.

69. Okay, O., (1994). "Kinetics of Gelation in Free-radical Cross-linking Copolymerization." Polymer, **35**(12): 2613-2618.

70. Okay, O., (1994). "Kinetic Modeling of Network Formation and Properties in Free-radical Cross-linking Copolymerization." Polymer, **35**(4): 796-807.

71. Okay, O., H.J. Naghash, and I. Capek, (1995). "Free-radical Cross-linking Copolymeriation- Effect of Cycliation on Diffusion-controlled Termination at Low Conversion." Polymer, **36**(12): 2413-2419.

72. Okay, O., H.J. Naghash, and O. Pekcan, (1995). "Critical Properties for Gelation in Free-radical Cross-linking Copolymerization." Macromolecular Theory and Simulations, **4**(5): 967-981.

73. Mikos, A.G., C.G. Takoudis, and N.A. Peppas, (1986). "Kinetic Modeling of Copolymerization Cross-linking Reactions." Macromolecules, **19**(8): 2174-2182.

74. Goodner, M.D. and C.N. Bowman, (2002). "Development of a comprehensive free radical photopolymerization model incorporating heat and mass transfer effects in thick films." Chemical Engineering Science, **57**(5): 887-900.

75. Lovestead, T.M., A.K. O'Brien, and C.N. Bowman, (2003). "Models of multivinyl free radical photopolymerization kinetics." Journal of Photochemistry and Photobiology a-Chemistry, **159**(2): 135-143.

76. Elliott, J.E., J. Nie, and C.N. Bowman, (2003). "The effect of primary cyclization on free radical polymerization kinetics: experimental characterization." Polymer, **44**(2): 327-332.

77. Elliott, J.E. and C.N. Bowman, (2002). "Effect of primary cyclization on free radical polymerization kinetics: Modeling approach." Macromolecules, **35**(18): 7125-7131.

78. Anseth, K.S. and C.N. Bowman, (1993). "Kinetic Gelation Model Predictions of Gel Point Conversions, Cyclization Rates, and Heterogeneity during Polymerization of Tetrafunctional Monomers." Abstracts of Papers of the American Chemical Society, **206**: 88-PMSE.

CHAPTER 4

PHOTOPOLYMERIZATION IN ACRYLATE MONOMER FILMS: HETEROGENEITY AND DARK REACTION STUDIED WITH MICRORHEOLOGY

4.1. Introduction

Cross-linked solid polymers produced by UV-curing multifunctional monomers are being used in a wide variety of applications ranging from protective coatings to dental composites [1-6]. Adapting these materials for specific applications presents a significant challenge and requires a fundamental understanding of the relationship between the formation of the highly cross-linked network and the properties of the final product. One of the primary limitations of the photopolymerization process is that the network structure formed by the UV-induced polymerization of multifunctional monomers is extremely heterogeneous [3, 5, 7]. Heterogeneity in the network structure formed during photopolymerization is a function of volume, thus inhomogeneities occur in the plane of the initiating light and as a function of penetration depth. As the heterogeneity of the network increases, the probability that the final material will contain regions with significantly weaker structures also increases. Heterogeneous regions generally act as defects and reduce the overall strength of the material, which could result in premature mechanical failure of the final product [7, 8].

Inhomogeneities in the final material are mainly the result of post UV exposure polymerization reactions, the formation of microgel regions via cyclization reactions, and

the attenuation of UV light by the reacting medium. The polymerization of branched photo-reactive resins exhibits a marked post curing effect after illumination is stopped [9-12]. A significant dark conversion is essential for the performance of printing inks and protective coatings; in these applications, polymerization is only initiated by light and then continues to completion in the dark. On the other hand, for applications that require high spatial resolution, substantial dark reactions can lead to undesirable product heterogeneity [13]. Although cationic systems, which have a slow rate of consumption of active centers, have a significantly greater post-curing effect than highly reactive free-radical systems [14-18], research has shown that after termination of irradiation, free-radical photo-induced reactions continue to proceed over a time scale of seconds, minutes, and even hours [10-12, 19]. In addition, post UV exposure reactions have been shown to produce byproducts which lead to yellowing and polymer degradation during, thereby reducing long-term stability [20]. The extent of dark reaction depends on several factors, including the amount of initiating radicals generated during the UV irradiation step, the reactivity of the branched functional group, and the degree of monomer conversion. Studies have shown that mobility restrictions of the radicals due to the conversion of monomer into polymer tend to slow down the termination kinetics, increase the radical lifetimes and enhance the extend of dark conversion [10-12, 19, 21-23].

Post UV Exposure polymerization reactions are most commonly investigated by employing Fourier transform infrared spectroscopy (FTIR) and electron spin resonance spectroscopy (ESRS). Using FTIR, Garcia *et al.* monitored the concentration of methacrylic monomers in the dark period after exposure to a variety of UV illumination

conditions. Important postpolymerization processes were found in all the examined cases, indicating that even at low monomer conversion a non-negligible radical concentration remains after production is switched off [12]. Bowman *et al*. used ESRS to monitor the concentration and mobility of free-radicals in multiethylene glycol dimethacrylates as a function of polymerization time. Their research shows that highly crosslinked and fast reacting systems have the highest concentration of radicals trapped in the polymer network after exposure to UV light [10]. Numerous studies have shown that such highly reactive, trapped free-radicals can influence the long-term chemical and physical durability of the cross-linked polymer [9, 11, 13, 20, 22, 24].

Multifunctional monomers have more than one functional group and each group may possess a different reactivity, which can also change with time. Unequal reactivity commonly results in an undesirable side reaction known as cyclization, where a growing polymer radical loops back onto itself and polymerizes through a pendant double bond on the same chain [25-28]. Cyclization does not contribute to the formation of a sample-spanning network, but results in the formation of microgels early in the polymerization reaction that greatly increase the heterogeneity of the final network, thus significantly impacting the mechanical properties of the manufactured product. Microgels are regions in the polymerizing system, localized around a center of initiation, with a higher average cross-linking density than the overall network [7, 29, 30]. Macroscopic gelation requires the formation of a sample-spanning, infinite network; the polymerizing system does not gel until the microgel regions are connected macroscopically through a network of cross-links [31-33].

Bowman *et al.* used dynamic mechanical analysis, [7] dielectric analysis, [29] and differential scanning calorimetry (DSC) [34] to investigate the heterogeneity of the polymer product obtained from the homopolymeriation and copolymerization of multifunctional methacrylates. These studies revealed that the photopolymerization of higher functionality monomers results in stronger heterogeneity. In addition, the researchers found that increasing the concentration of crosslinking agent in copolymer systems increases the overall heterogeneity. To better understand the resulting polymer structure, Bowman *et al.* modified a previously developed kinetic gelation model to incorporate unequal reactivity of the functional groups on multifunctional monomers. The simulations indicated that heterogeneity is most significant in systems with small monomer molecules at low double-bond conversion in the presence of a large amount of solvent and without diluting monofunctional monomer [21, 25]. FTIR and dynamic light scattering techniques were used by Soucek and Nebioglu to examine the reaction kinetics and microgel particle size of unsaturated polyesters acrylates during UV-curing. The researchers found that internal (maleic) double bonds were involved in microgel formation at a rate similar to that or the more reactive terminal (acrylic) double bonds. The introduction of internal double bonds caused smaller microgels, whereas terminal acrylate double bonds resulted in larger microgel particle sizes [30].

The ultimate thickness of polymer films and coatings is typically less than 1000 μm since the attenuation of the curing light strongly increases with sample depth [35]. The attenuation of UV light by the polymerizing medium is caused by the absorption of light by the initiator and changes in the refractive index of the medium as liquid monomer is converted to solid polymer. In general, the intensity of the incident UV light

decreases exponentially with sample depth and the local intensity of the initiating light is described by the well-defined Beer-Lambert law. Attenuation of the curing light results in the development of spatially heterogeneous monomer-to-polymer conversion profiles perpendicular to the illuminated surface. These conversion profiles propagate as traveling waves known as polymerization fronts and continue to invade unpolymerized regions until the energy required for polymerization exceeds the local energy at a given depth [36-38]. To polymerize thick samples via UV curing, photobleaching initiators have been developed that become less absorbing once cleaved by UV light, thereby allowing light to penetrate deeper into the sample [3, 6, 39, 40]. Although the heterogeneous nature of the polymerization fronts is considered a drawback in some applications, researchers have exploited this phenomenon to fabricate microfluidic devices [41-43], dental composites [44-46], printing inks and microcircuits via photolithography [47, 48].

The simplest, most commonly used method to study frontal photopolymerization employs a thermally insulated tube filled with a mixture of monomer and initiator. Upon initiation of the reaction via UV light at one end of the tube, a self-sustained wave of chemical conversion propagates through the tube. The velocity of the front, temperature, and conversion are usually measured as a function of time and location [36, 49-58]. Lee and co-workers used a stereolithography apparatus to examine cure depth as a function of photoinitiator concentration and laser dosage in the photopolymerization of dental composite Bis-GMA. The researchers determined that the optimal concentration of photoinitiator to maximize cure depth strongly depends on the photonic energy delivered to the sample [44]. The techniques that are currently being used to study frontal photopolymerization have large sample dimensions, which makes it nearly impossible to

ascertain high-resolution local spatial information on the polymerization front. The lengthscales of the techniques described above range from a few millimeters in the stereolithography apparatus to several centimeters in the tube experiments. In Chapter 2, our own research has shown that a factor of two difference in gel time can be observed between the top and bottom of a 100 μm thick acrylate sample [59].

The desire to control the polymerization reaction and predict the cure optimal cure depth of a photosensitive sample has fueled the development of frontal photopolymerization models. Frontal photopolymerization using photobleaching initiators has been extensively modeled by Scranton *et al.*, Douglas *et al.*, Bowman and O'Brien, Miller *et al.*, Ivanov and Decker, and Terrones and Pearlstein [35, 38-40, 60-62]. These models predict the heterogeneous initiator concentration distribution and the resulting initiation rate. The resulting simulations show the importance in choice of photoinitiator and initiator concentration based on the desired sample thickness and application.

Although recent research in the formation of polymer networks has provided considerable insight into the heterogeneous nature of UV induced free-radical polymerization, several applications of photopolymerization continue to be limited by the inhomogeneity of the polymerized product. It is clear that the ability to predict and control spatial variations of properties in photopolymerized materials will require progress in the understanding of spatiotemporal variations of the polymerization process. However, most of the current measurement techniques for investigating the heterogeneity of photopolymerization average over larger sample volumes and do not provides high-resolution spatial information. Our previous research has shown that particle tracking

microrheology microrheology can successfully be used to characterize the local structure, mechanical properties, and reaction kinetics during the photopolymerization of multifunctional acrylate monomers. In this work, we expand the use of particle tracking microrheology to examine the heterogeneity and dark reactions that take place during the free-radical polymerization of multifunction acrylate monomers with high spatial and temporal resolution.

4.2. Methods and Materials

4.2.1. Sample preparation and Experimental Method

In order to study heterogeneity during photopolymerization, UV sensitive samples containing a mixture of multifunctional acrylate monomer, photoinitiator, and fluorescent tracer particles were prepared. Multifunctional monomers of varying functionality were obtained from Sartomer: ethoxylated pentaerythritol tetraacrylate (E4PETeA, SR494), trimethylolpropane triacrylate (TMPTA, SR351), and triethylene glycol diacrylate (TEGDA, SR272). As received, these monomers contained a small amount of inhibitor, which was removed by running samples through an alumina (grade CG20) filled column obtained from Polysciences Inc. To study the homogeneity of copolymer systems, samples of TEGDA with E4PETeA were combined to obtain a final molar ratio of 67:33 percent TEGDA to E4PETeA. The general-purpose photoinitiator used in previous work, 2,2-dimethoxy-1,2-diphenylethan-1-one (DMPA, Irgacure 651), was employed again as received from Ciba Specialty Chemicals. Silica particles containing red fluorescent dye (rhodamine) with a diameter of 1.0 um were used as tracers for microrheology [63]. The tracer particles were loaded into a sample of each monomer containing a small amount of MEHQ to prevent premature polymerization of the particle stock solution. The inhibitory

effects of MEHQ on the photopolymerization were studied in detail in Chapter 3. After the components were mixed to obtain a desired concentration of photoinitiator, the samples were briefly sonicated to minimize tracer particle aggregation. As described in detail in previous chapters, the samples were then loaded into a sample chamber and microrheology was performed on the sample.

4.2.2. Shuttering of UV Light

Ultraviolet light from a Spectral-Physics UV flood light source (model 66923) equipped with a 1000 W high-pressure Hg(Xe) bulb was directed through an attached liquid IR filter fitted with a zero aperture high-speed electronic shutter. Before reaching the sample chamber, the UV light is reflected from an aluminum coated mirror placed at a 45° angle above the sample through a 365 nm bandpass filter. The UV illumination profile delivered to the sample was varied as a function of time using a LabView computer program to control the electronic high-speed shutter. Another LabView-controlled shutter was used to control illumination of the sample for fluorescence microscopy; tracking the motion of the tracer particles via video microscopy began once this shutter was opened. Since it is not possible to detect from the movie of tracer particles when the UV shutter is opened, a well-defined delay (generally 4 seconds) was introduced between the opening times of both shutters. The delay time is used to synchronize the timelines of particle tracking and illumination, so that gelation times can be determined accurately.

To study the extent of the post- exposure reaction, the high-speed shutter in the the UV light path was used to expose the samples with a sequence of pulses instead of continuos illumination. The length of the pulses of UV light was either 1.0 or 0.5 second.

The dark interval separating the UV pulses was varied from 0.125 to 2 seconds in different experimental runs. By exposing the monomer samples to multiple pulses of UV illumination, followed by darkness, the effects of the post exposure reaction are enhanced, because a sample experiences post exposure reaction multiple times during a single polymerization experiment. As a result, we are able to more accurately analyze the contribution of dark reactions to the overall polymerization. For examining frontal photopolymerization and heterogeneity of the curing system, the sample was illuminated continuously, but the polymerization reaction was stopped at various times before and immediately after the experimentally determined gel time by closing the UV shutter. The high-speed shutter provides a temporal resolution of ca. 20 ms.

4.2.3. Heterogeneity Parameter and Data Analysis

In a perfectly homogenous medium, all tracer particles will experience the same local rheology and their motion will be equally restricted. In a heterogeneous medium, on the other hand, the motion of certain particles may be more restricted than others. To quantify the heterogeneity of a polymerizing sample perpendicular to the plane of UV irradiance, a non-Gaussian parameter has been introduced [64, 65]:

$$\alpha(\tau) = \frac{\left\langle \Delta x^4(\tau) \right\rangle}{3\left\langle \Delta x^2(\tau) \right\rangle^2} - 1 \qquad (4.1)$$

This distribution parameter uses the trajectories of all tracer particles in the field of view to determine the displacement distribution (van Hove correlation function) and then quantifies the deviations relative to a Gaussian distribution. The van Hove correlation function in a homogenous medium is Gaussian, whereas in heterogeneous media the same correlation function exhibits large deviations from a Gaussian distribution. As a

result, values of α close to 0 imply a homogeneous sample, while values greater than 0 indicate that a sample is heterogeneous. Data analysis similar to that described in Chapter 2 was used to determine the liquid-to-gel transition for all monomers examined in this work.

4.3. Results and Discussion

4.3.1. Extent of Post UV Exposure Reactions

To study the effect of post UV exposure reaction, monomer samples loaded with varying amounts of photoinitiator were exposed to successive pulses of UV illumination separated by variety of dark intervals ranging from 125 to 2000 milliseconds using the high-speed electronic shutter controlling the UV light. Repeatedly exposing a sample to alternating light and dark pulses allows us to probe the contribution of the dark reaction to the process of gelation. After every UV pulse, dark reactions can occur during the time that the shutter is closed; by having multiple pulses, the relative importance of these contributions to the gelation process are emphasized. For each gelation event of a shuttered sample, the total amount of UV exposure time was determined by summing the durations of the UV pulses to achieve gelation. This UV dosage was then compared to the gel time of a sample exposed to continuous UV illumination. Although shuttering the UV light always increases the overall cure time of a sample due to the dark periods between pulses, post UV exposure reactions in the shuttered samples may reduce the amount of UV light required to form a polymerized gel. The normalized UV dosage was defined as the ration of UV exposure time until gelation with shuttering to the value for the continuously exposed sample. A normalized value less than one therefore indicates the presence of significant post UV exposure reactions, because less UV light is needed

with shuttering; values greater than one would suggest that introducing dark periods actually increases the energy required to achieve gelation. Figure 4.1 presents the normalized exposure as a function of the duration of the dark intervals between pulses, for samples of E4PETeA at different initiator concentration. The duration of the UV pulse was also varied.

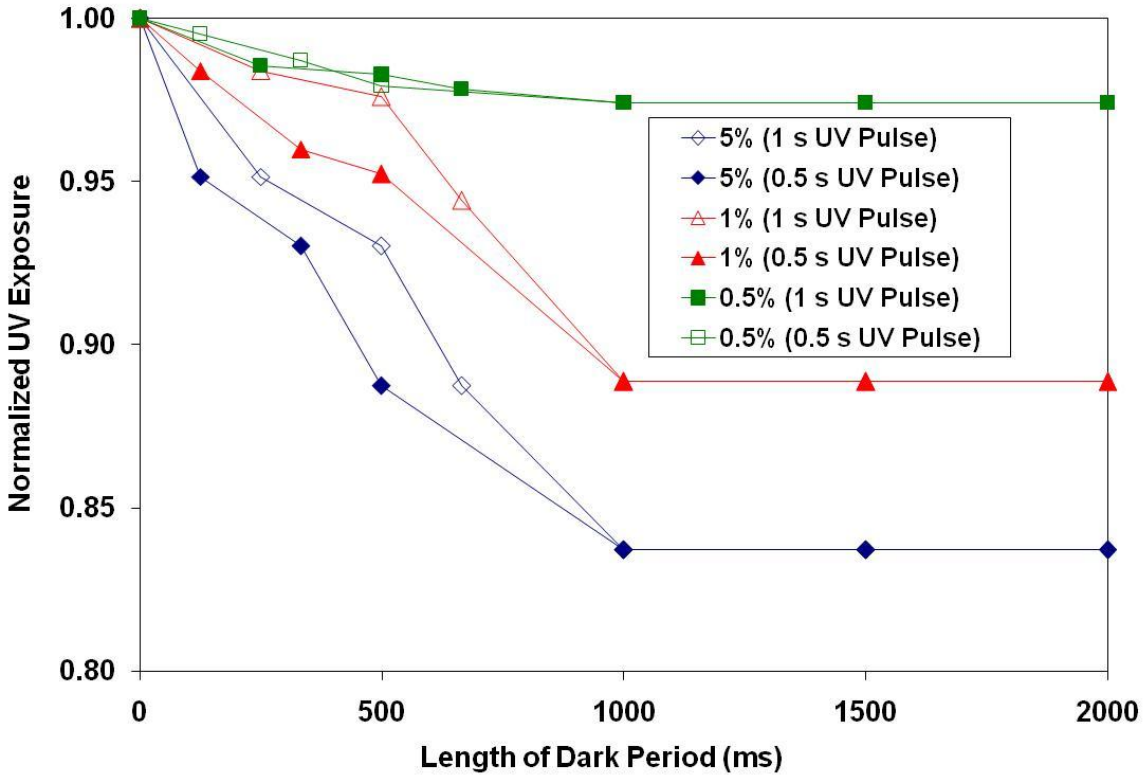

Figure 4.1: Normalized UV exposure time as a function of the length of the dark period for samples of E4PETeA loaded with 0.5 wt.% (■), 1.0 wt.% (▲), and 5.0 wt.% (♦) DMPA. Open symbols represent 1 second pulses of UV illumination at 365 nm, while closed symbols represent 0.5 second pulses.

All results in Figure 4.1 show normalized exposures of less than 1, which indicates that dark reactions have a significant contribution towards gelation. According to the graph, increasing the concentration of photoinitiator increases the contribution of the post UV exposure reaction to the gelation process. This result can most likely be attributed to the fact that more free-radicals are generated at higher photoinitiator

concentrations, which can continue the reaction during the dark intervals. Figure 4.1 also suggests that post-UV exposure reactions are insignificant after one second; increasing the dark interval beyond one second does not increase the effectiveness of the dark reaction in any of the photosensitive systems. In light of the fact that free-radical lifetimes of much less than one second have been reported in literature for difunctional acrylates [22], this observation may be surprising. Research has shown that the lifetime of a free-radical ultimately depends on the surrounding environment. At higher conversions, the lifetime of free-radicals increases; simultaneously, however, the reactivity of these free-radicals decreases since they become diffusion-limited [10, 19, 21, 23]. Garcia and co-workers have reported radical lifetimes of over 20 minutes in samples of methacrylic monomers [12].

In addition, the data in Figure 4.1 clearly show that the energy-threshold model, which assumes that a critical dose of energy is required to achieve gelation, is not applicable to our acrylate systems. For the energy-threshold model to hold, all data in Figure 4.1 would have had to collapse at normalized exposure values of 1, with a slope of zero. Instead, the experiments show that the energy dose required to reach gelation can be reduced by pulsing the sample with alternating light and dark periods. Although Figure 4.1 proves that post UV exposure reactions effectively contribute to network formation, the data do not specify how this effectiveness changes with time and monomer conversion.

An interesting detail in Figure 4.1 is that for all samples the use of 0.5 second UV pulses increases the effectiveness of the dark reactions in comparison to the 1.0 second UV pulses for short dark intervals, while the maximum effect at long dark intervals

remains the same. Each one-second pulse must be replaced by two half-second pulses to deliver the same amount of UV. Because the 0.5 second pulses are separated by a dark interval, during which dark reactions can occur, one might expect that dark reactions play a larger role in the experiments with the shorter UV pulses. Although this is indeed true for the short dark intervals, the effect disappears for intervals that exceed the radical lifetime. In addition, the concentration of free-radicals generated by a 0.5 second pulse of UV light is significantly lower than that generated by a 1.0 seconds pulse. Once the UV light has been extinguished, primary radicals may be consumed via reaction with another primary radical, monomer, or a growing polymer chain. Since primary radicals have a larger diffusion coefficient than monomer or growing polymer chains, the probability that a radical will be terminated via radical-radical recombination is significantly greater than consumption of a radical by a monomer or growing polymer chain. The reaction of primary radicals via radical-radical recombination does not contribute to the formation of a polymer network. In addition, the probability of primary radical recombination increases with increasing free-radical concentration, thus the probability of radical-radical recombination occurring during a dark interval that is preceded by a 1.0 second pulse of UV illumination is nearly twice that of one proceeded by a 0.5 second pulse of illumination. As a result, the free-radicals generated by a 0.5 second pulse of UV irradiance may be more effective at contributing to the formation polymer network during the dark interval.

To investigate the effect of monomer functionality on post UV exposure reactions, samples of TEGDA and TMPTA loaded with 5.0 wt.% DMPA were also polymerized under shuttered UV illumination. The resulting data is compared to the

E4PETeA sample loaded with 5.0 wt.% DMPA in Figure 4.2, which illustrates that the effect of post UV exposure reactions is more pronounced in higher functional monomers.

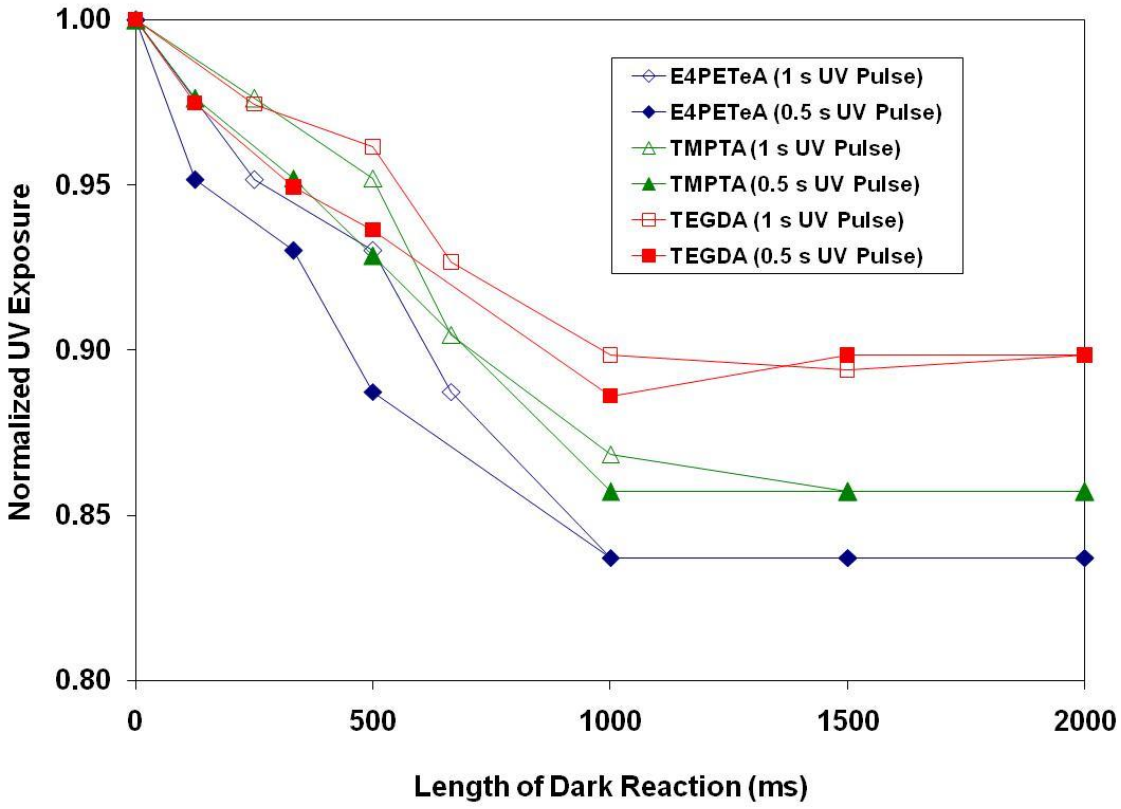

Figure 4.2: Normalized UV exposure time as a function of the length of the dark period for samples of E4PETeA (♦), TMPTA (▲), and TEGDA (■) loaded with 5.0 wt.% DMPA. Open symbols represent 1 second pulses of UV illumination at 365 nm, while closed symbols represent 0.5 second pulses.

The tetrafunctional monomer, E4PETeA, exhibited the largest contribution of post UV exposure reaction, followed by the trifunctional TMPTA and the difunctional TEGDA, when cured under identical conditions. Figure 4.2 also illustrates that for dark intervals less than 500 ms, there is a significant overlap in the data for TMPTA and TEGDA. These results can be explained by taking into consideration the reactivity and viscosity of the monomers. E4PETeA is considerably more viscous than TEGDA, which lowers the mobility of radicals and their ability to recombine. In addition, due to the higher functionality of the E4PETeA monomer, the sample requires a lower monomer

conversion to achieve gelation. As a result, reactions which contribute to the formation of a cross-linked network are more likely to occur in E4PETeA once the UV light has been extinguished. Research by Bowman *et al.* has shown that increasing the functionality of the monomer increases the number of trapped radicals in the polymerizing system. These trapped radicals can continue to contribute to network formation long after the UV light has been switched off [12]. In another study, Bowman and co-workers found that highly reactive acrylate monomers exhibited more extensive polymerization in the dark compared to lower functional, less reactive acrylates [19]. Using FTIR, the researchers found that the highly reactive monomer was observed to attain 35% additional conversion in the dark after the UV light was extinguished at 35% conversion, whereas the less reactive acrylates attained only 3% additional conversion under similar conditions.

Chapters 2 and 3 have shown that oxygen plays a significant role in photopolymerization of acrylate resins. To elucidate the effects of oxygen on post UV exposure reactions, samples of E4PETeA loaded with 0.5 wt.% DMPA were degassed as described in pervious chapters. The degassed samples were exposed to shuttered UV illumination and compared to oxygen saturated data collected under similar conditions. Figure 4.3 shows that removing the oxygen from the photosensitive monomer greatly increases the effectiveness of the dark reaction. In addition, Figure 4.3 illustrates that even in the absence of oxygen, extending the dark interval beyond 1.0 second does not increase the effectiveness of the post UV exposure reactions. By comparing the data in Figure 4.3 to Figures 4.1 and 4.2, it is clear that the dark reaction approaches the level of maximum effectiveness more rapidly in the degassed samples. Since oxygen acts as an

inhibitor in free-radical polymerization systems by reacting with active radicals, an oxygen saturated system will initially have lower concentrations of active free-radicals that are needed to maintain reactivity during the dark intervals. An extensive literature search has revealed that little research has been performed to determine the effects of oxygen on the extent of post UV exposure reactions. Although microrheology cannot be used to ascertain information about the radical concentration, the novel data obtained from the above described shuttering experiments clearly provides insights that lead to a more complete understanding of the photopolymerization of acrylate resins. It is expected that this unique data can be used to parameterize and validate models used to predict the effects of post UV exposure reactions.

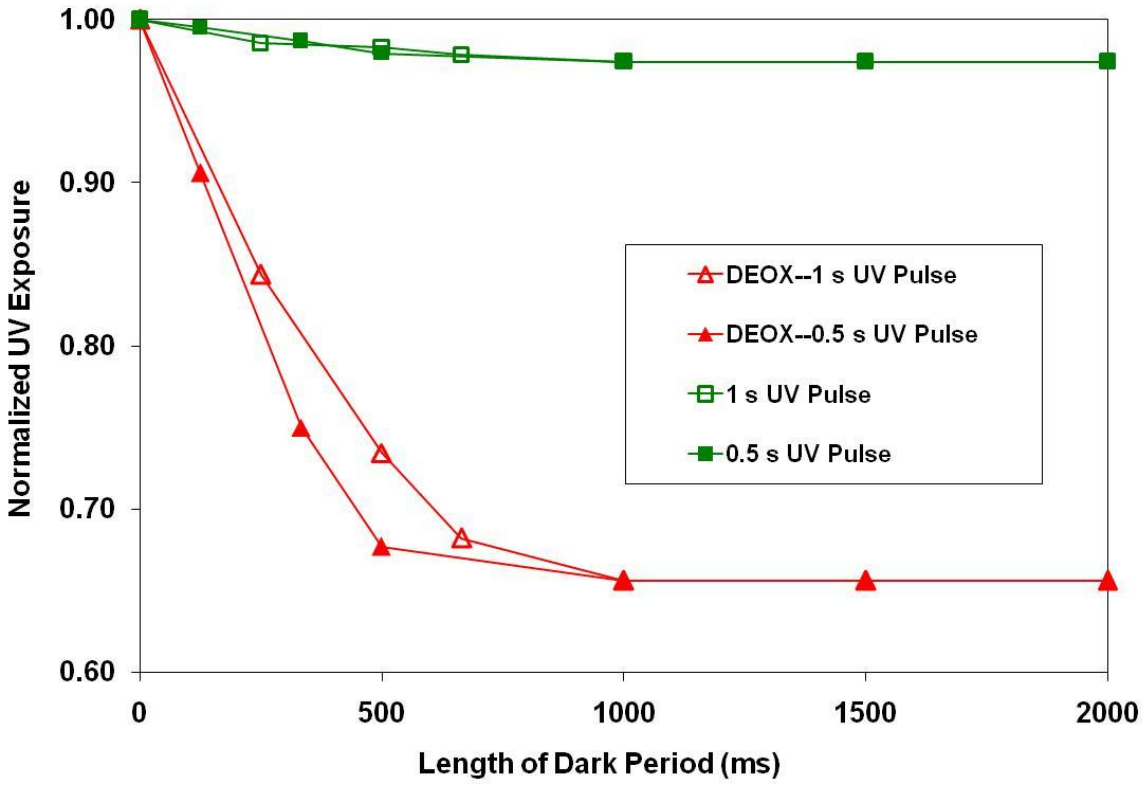

Figure 4.3: Normalized UV exposure time as a function of the length of the dark period for oxygen saturated (■) and degassed (▲) samples of E4PETeA loaded with 5.0 wt.%. Open symbols represent 1 second pulses of UV illumination at 365 nm, while closed symbols represent 0.5 second pulses.

4.3.2. Frontal Photopolymerization

Previous work in Chapter 2 has already shown that for a 100 μm thick sample of E4PETeA, the UV exposed side of the sample forms a gel significantly faster than the unexposed sample side. The dependence of gel time on UV penetration depth can be attributed to the attenuation of UV light via absorbance by the initiator and the presence of oxygen in the sample, as will be discussed in more detail in Chapter 5.

The attenuation of UV light with increasing sample depth through absorption by the photoinitiator as a function of sample depth has been well documented in literature and is described by Beer's law [35]. However, most experimental work on frontal polymerization has been limited to thick samples because of the inability to detect the polymerization with high spatial and temporal resolution in thin samples. By using particle tracking microrheology, we were able to monitor the evolution of mechanical properties during polymerization by tracking the mobility of tracer particles (MSD as a function of correlation time, τ) in real-time. By repeating the experiment at different depths, depth profiles could be constructed, as shown in Chapter 2. For example, it was found that E4PETeA with 5.0 wt.% DMPA formed a gel after ca. 2.6 seconds at 60 μm from the illuminated surface (illumination at 365 nm and 10 W/m^2). In order to examine the spatial variations during photopolymerization in more detail, we decided to change our tactics, making use of the high-speed electronic shutter in the UV path. Instead of monitoring the evolution of tracer mobility at a fixed depth under continuous illumination until fully cured, we exposed samples to a single pulse of UV light of a well-defined duration, ranging from 1.50 to 3.00 seconds (in increments of 0.10 seconds).

Figure 4.4 presents the evolution of the MSD of tracer particles as a function of time for different correlation times at the various illumination times. All data were recorded at a depth of 60 μm from the illuminated surface. To facilitate data analysis, a 4 second delay in UV illumination was introduced at the start of each experimental run in order to create a baseline; in Figure 4.4, $t = 0$ is defined as the moment when the UV shutter is opened. As can be seen, exposing samples of E4PETeA to UV pulses of up to 2.4 seconds did not result in any significant changes in the measured MSD; the tracer mobility remainsis equal to the initial values even long after the illumination is ended. A characteristic peak shows up for 2.4 seconds of illumination, which is not observed in Figure 4.4a for the 1.5 s pulse. When the sample is exposed to 2.5 seconds of UV, a slight drop can be observed in the MSD values at all correlation times (Figure 4.4c). However, this sample does not undergo gelation; after the UV light has been switched off, the MSD values still increase as a function of correlation time, characteristic of a viscous sample. As seen in Figure 4.4d, exposing the E4PETeA sample to 2.6 seconds of UV illumination results in a more extensive decline in MSD, but gelation by our definition does not occur gelation 2.7 seconds of continuous UV (Figure 4.4e), when the MSD values become independent of correlation time. Exposures beyond 2.7 seconds did not result in further changes in MSD and are therefore not shown.

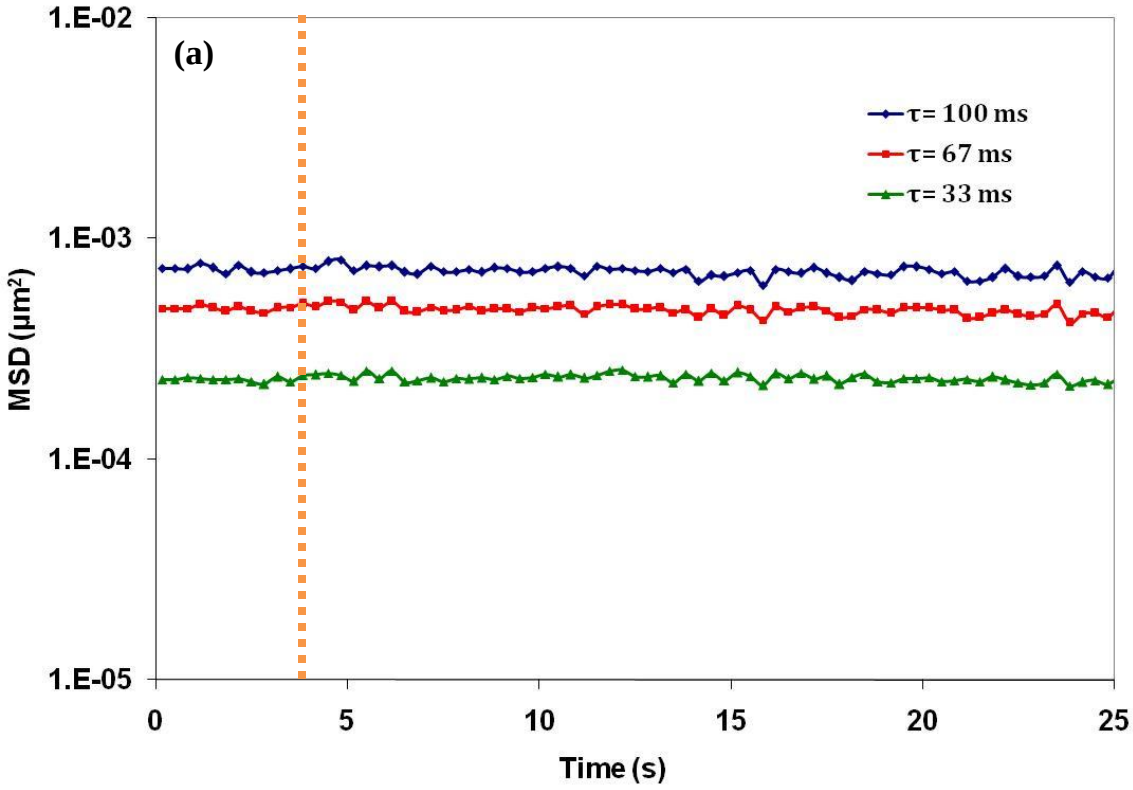

Figure 4.4: Transient MSD for tracer particles in a curing sample of E4PETeA loaded with 5.0 wt.% DMPA exposed to (a) 1.5 s, (b) 2.4 s, (c) 2.5 s, (d) 2.6, and (e) 2.7 s of continuous UV irradiance at a wavelength of 365 nm. The dashed line represents the start of UV illunination.

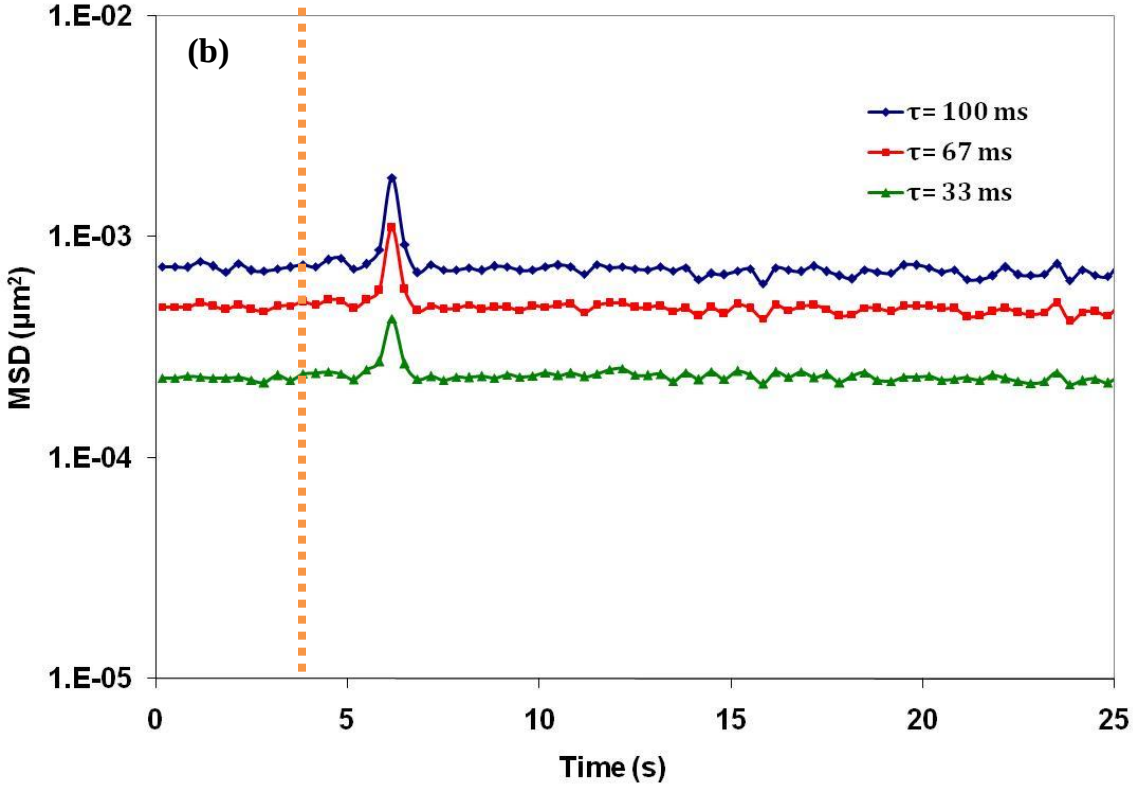

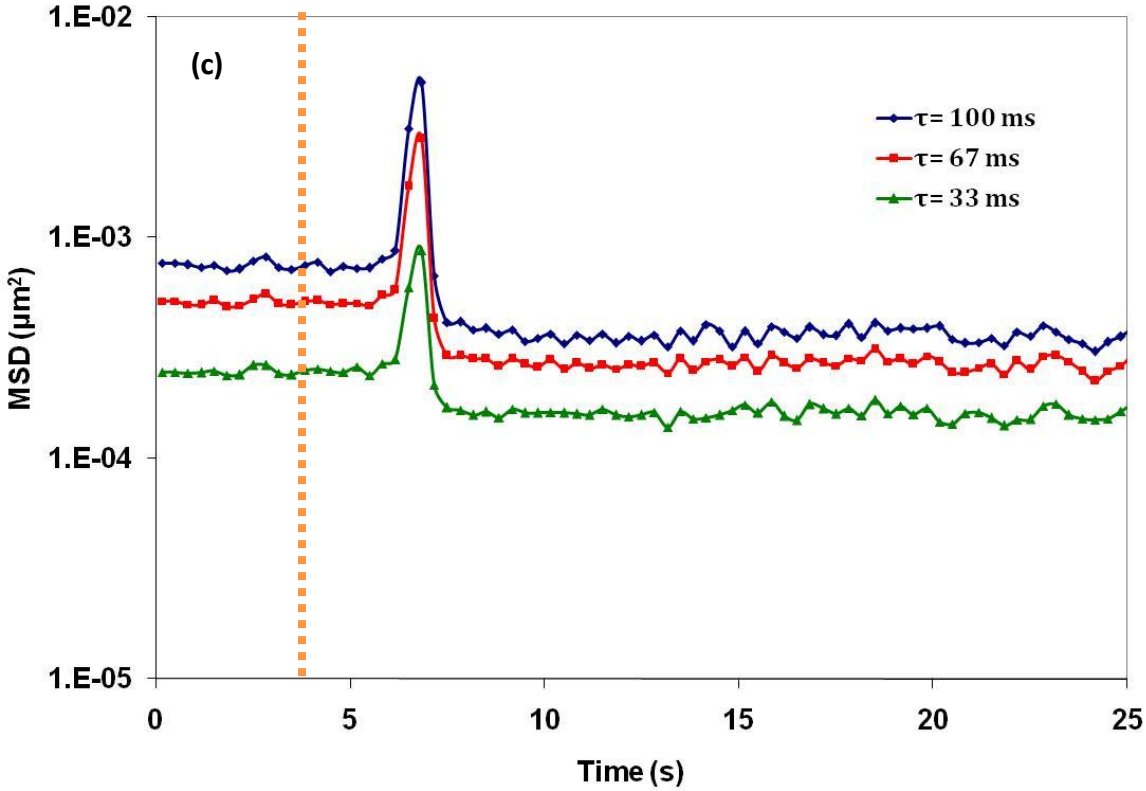

Figure 4.4 continued

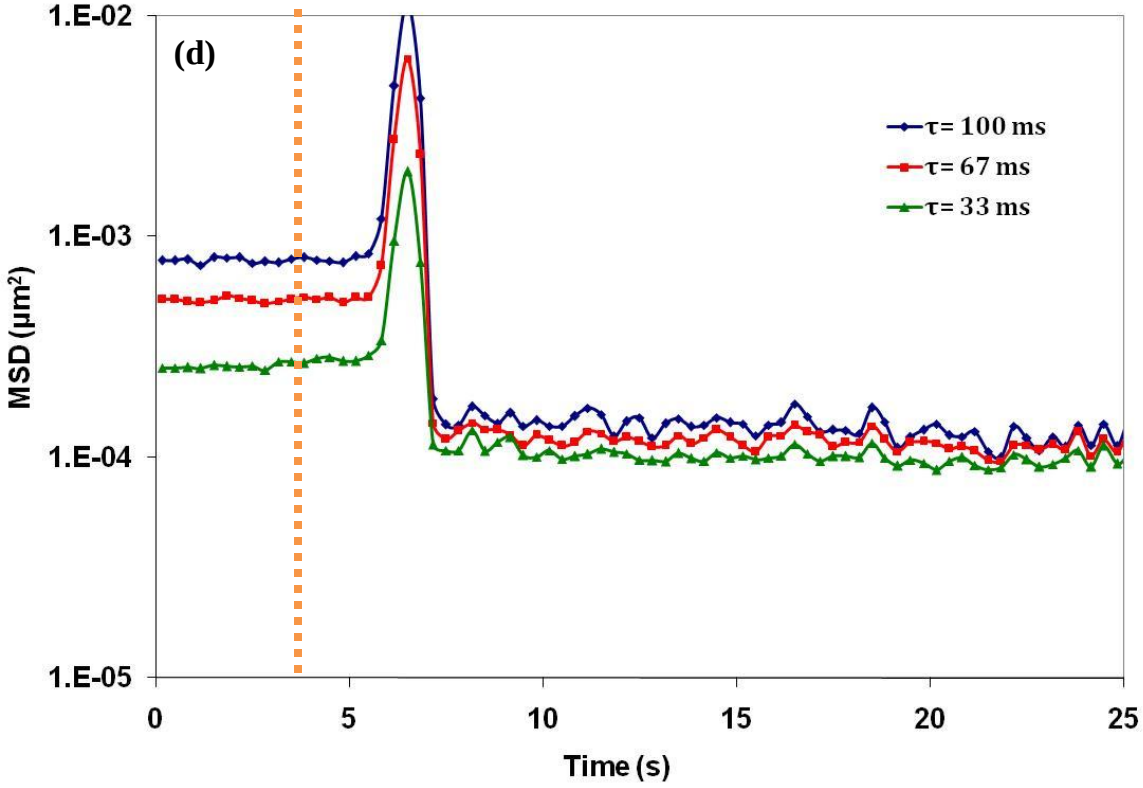

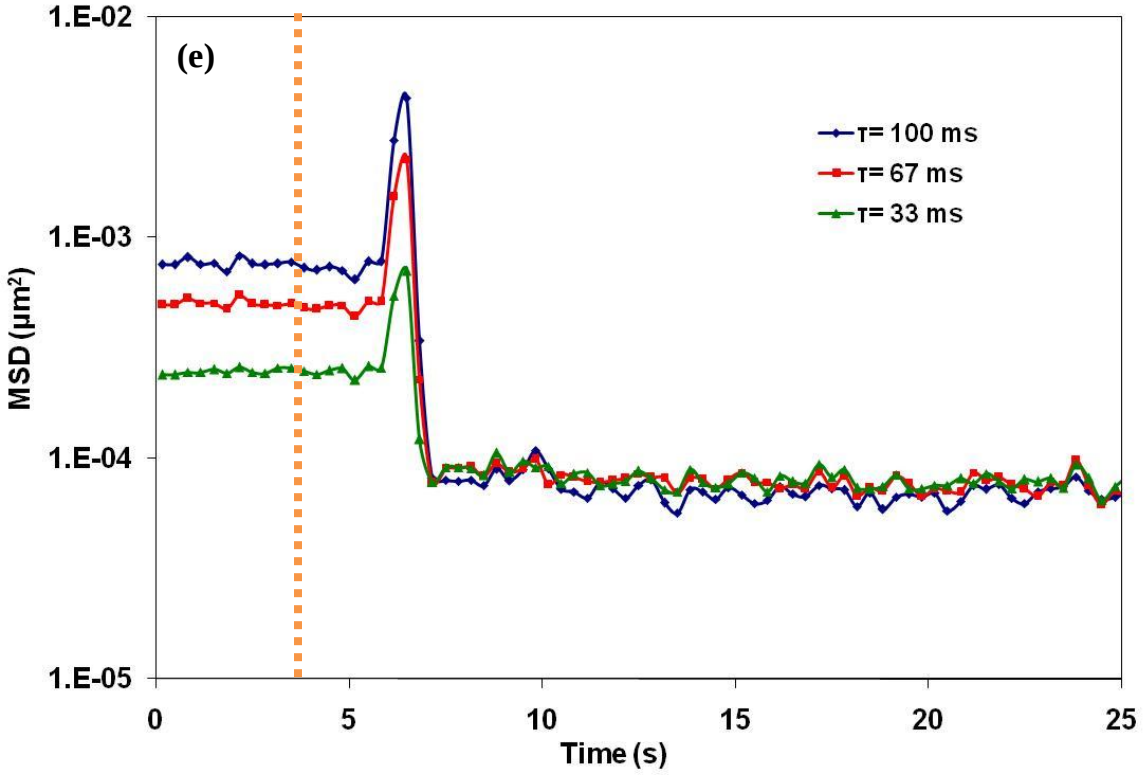

Figure 4.4 continued

All samples except the one illuminated for 1.5 s show the characteristic peak already pointed out for Figures 4.4b. These peaks are the result of slight bulk motion of the tracer particles, caused by sample shrinkage due to gelation in the upper regions of the sample, closer to the illuminated surface. Previous research (Figure 2.2) has shown that at a location of 20 microns from the surface, E4PETeA with 5 wt.% DMPA gels after 1.7 seconds, while approximately 2.6 seconds was required for gelation to occur at a sample depth of 60 μm. Indeed, for 1.5 seconds of UV exposure no peak in the MSD is observed (Figure 4.1a), since nowhere in the sample gelation has taken place yet under these conditions.

These high-temporal resolution experiments illustrate that the liquid-to-gel transition occurs over 300 ms in a sample of E4PETeA with 5.0 wt.% DMPA at 60 μm from the illuminated surface. It is important to point out the difference between these experiments and the shuttering experiments that showed that post UV exposure reactions can contribute to network formation up to one second after switching off the UV light. In Figure 4.4, no changes are observed in the plots of transient MSD after the UV pulse. The explanation is that multiple short pulses were delivered in the shuttering experiments, followed by multiple dark intervals. Under those conditions, dark reactions play a more important role.

Another advantage of the experiments presented in Figure 4.4 is that they enable post-illumination inspection of the mechanical properties at various locations in the sample. Since the setup is mounted on an inverted microscope, it is trivial to obtain local spatial information about the polymerization front by varying the focal plane. Once the experiments in Figure 4.4 were completed, additional measurements of tracer mobility

were carried out between 20 and 100 μm from the illuminated surface, using the fine focus knob of the microscope to quantitatively change location. Data analysis of the MSD as a function of correlation time at each depth provided a detailed measure of the location of the polymerization front. Figure 4.5 illustrates how microrheological data can be used to determine the location of the polymerization front with high-spatial resolution. The graph shows the MSD as a function of correlation time for a sample of E4PETeA with 5.0 wt.% DMPA that was exposed to UV for 2.5 and 2.6 seconds of continuous UV irradiation (see also Fig. 4.4c).

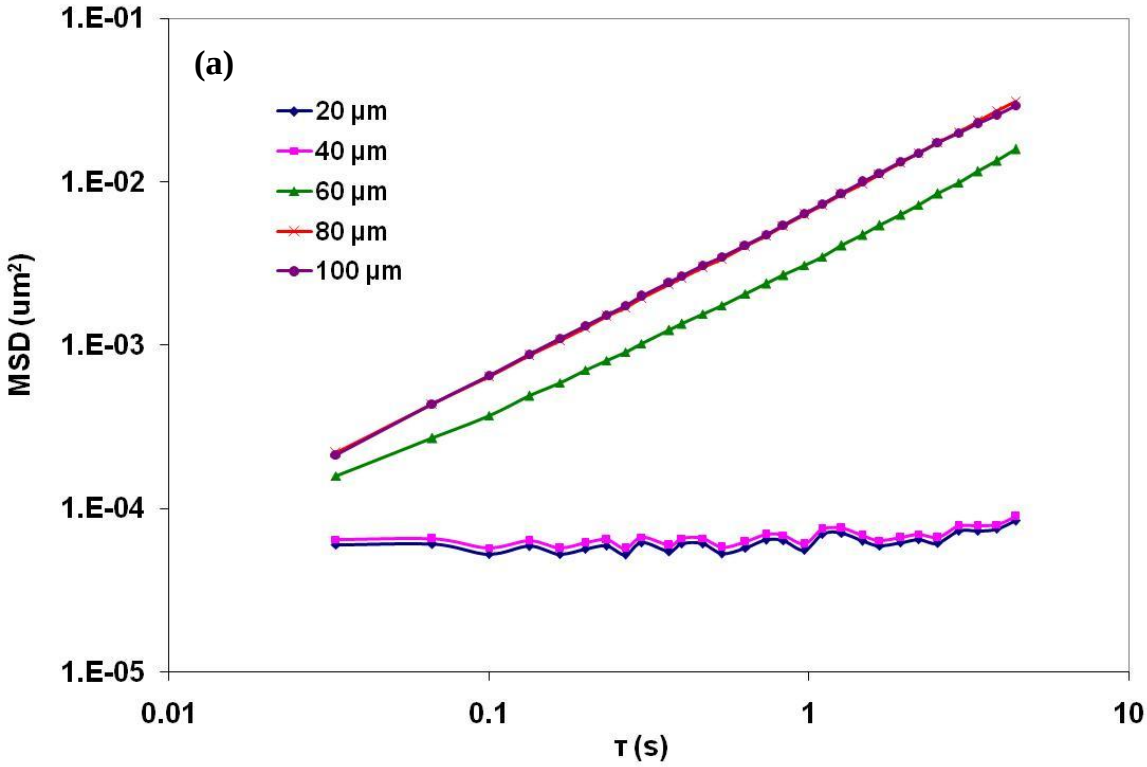

Figure 4.5: MSD of tracer particles as a function of correlation time for E4PETeA loaded with 5.0 wt.% DMPA after (a) 2.5 seconds and (b) 2.6 seconds of UV irradiance at 365 nm.

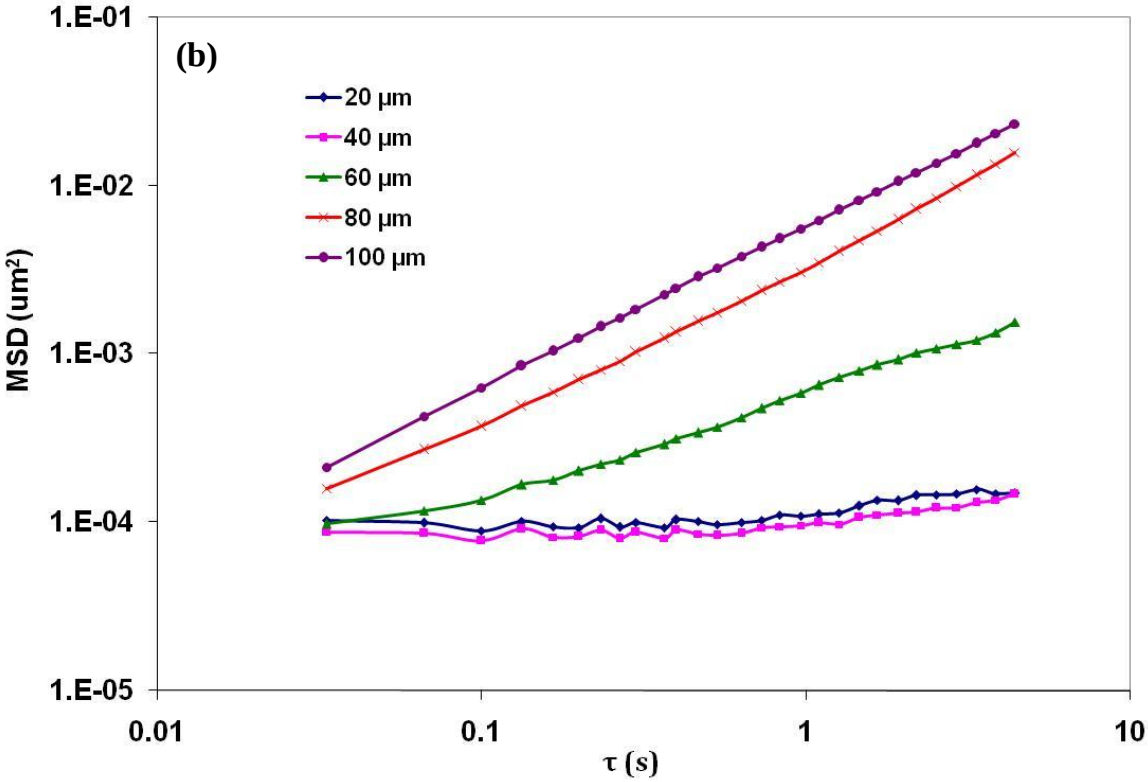

Figure 4.5 continued

In a double-logarithmic plot of MSD versus correlation time, a slope of one is indicative of a Newtonian liquid, while a plateau (slope zero) is characteristic for a gel. This can easily be understood, because tracer particles are able to move freely in a liquid environment, so that MSD increases with correlation time, while particles in a densely cross-linked network are trapped and cannot move even on long timescales, resulting in constant MSD values. We can thus conclude from Figure 4.5a that after 2.5 seconds of UV irradiance the liquid-to-gel polymerization front has propagated through 40 µm of the photosensitive resin. Deeper into the sample clearly remains liquid-like with constant viscosity, as shown by the overlap of the data at 80 and 100 µm. At 60 µm, the sample is in the beginning stages of polymerization and tracers are slightly mobile than at 80 µm, but it has not reached gelation yet. When the experiment was repeated with 2.6 s

illumination (Figure 4.5b), the evolution of the viscoelastic network can clearly be observed at 60 μm. During this interval, the front has also reached 80 μm. To present the data from Figure 4.5 in a more compact way for a variation of illumination times, it is necessary to point out that the microrheological data from the MSD vs. τ plots can be summarized by two parameters, the slope and the offset of the lines. As explained above, the slope represents the viscoelastic nature of the sample, ranging from zero for purely viscous to 1 for fully elastic. In Chapter 2, the slope of log(MSD) versus log(τ) was plotted as a function of time and used to determine the point of gelation. In addition, the offset, represented by the of the MSD value at τ = 1.33 s, quantifies the magnitude of the rheological properties (viscosity or elasticity). Stronger gels and more viscous liquids both lead to lower tracer mobility and lower MSD values.

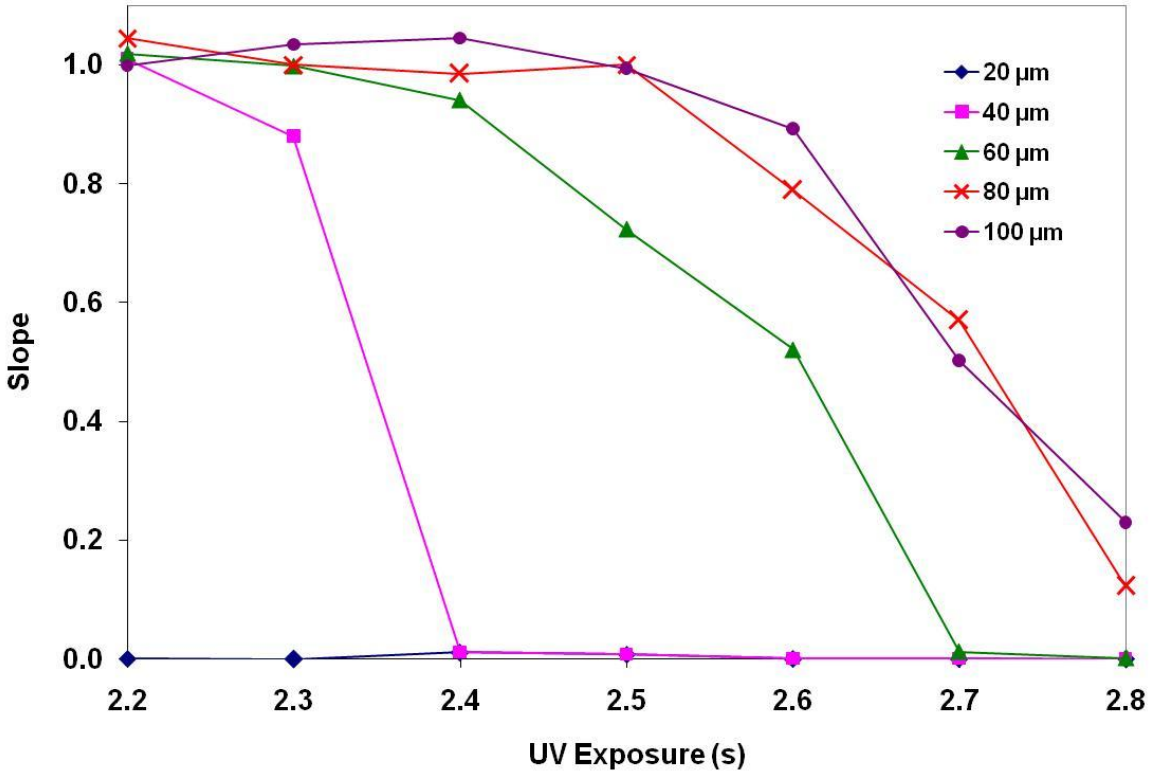

Figure 4.6: The slope of the MSD data at varying UV penetration depths as a function of continuous UV irradiance time for samples of E4PETeA loaded with 5.0 wt.% DMPA.

Figures 4.6 and 4.7 summarize the development of the mechanical properties of the network as a function of UV exposure for samples of E4PETeA loaded with 5.0 wt.% DMPA. time is clearly illustrated in, which plots the slope of the MSD as a function of UV exposure time. It is apparent from Figure 4.6 that the liquid-to-gel transitions in the sample, evidenced by the slope changing from 1 to 0, occurs at different times for different depths. For comparison, the depth profiles in Chapter 2 only presented the times at which gelation occurred (slope equal to 0), without the detailed evolution of mechanical properties of E4PETeA as a function of UV exposure time. The process is further illustrated by Figure 4.7, which plots the value of MSD at a constant correlation time of 1.33 seconds as a function of UV penetration depth and UV illumination.

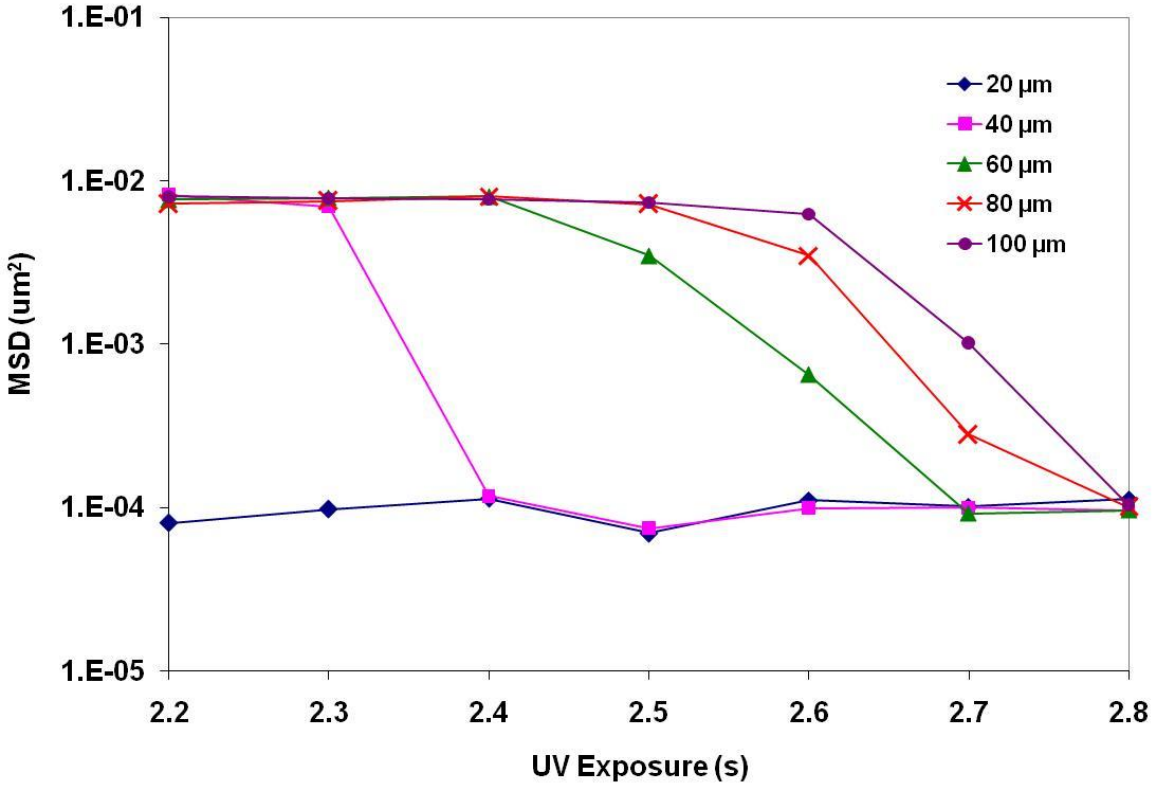

Figure 4.7: MSD of tracer particles at a constant value of correlation time, τ = 1.33 seconds, as a function of UV penetration depth and continuous UV irradiance time for samples of E4PETeA loaded with 5.0 wt.% DMPA.

In Figure 4.7 a the maximum MSD value of approximately 0.01 μm^2 is only found in the liquid states, while MSD values around 0.0001 μm^2 are typical after the sample has undergone polymerization. Although the top of the sample reaches the gel point in less than two seconds, the bottom of the sample does not gel until the entire sample has been exposed to 2.8 seconds of UV irradiance. Figures 4.6 and 4.7 also show that the liquid-to-gel transition occurs more rapidly near the illuminated surface. For example, at a depth of 40 µm the transition from monomer liquid to polymerized gel occurs within 100 ms, while at a depth of 80 µm the transition takes 300 ms. This observed decrease in the rate of polymerization with sample depth has been well-documented in literature and is attributed to the attenuation of UV light. These data

supports the Chapter 2 observation that gel time is a strong function of UV penetration depth for a 100 micron thick sample. The information obtained here about the development of the polymerization front with high spatial and temporal resolution could not have been obtained using volume based techniques that are commonly used to study photopolymerization such as FTIR, calormetry, and macrorheology.

4.3.3. Heterogeneity during Photopolymerization

Thus far, we have only discussed spatial heterogeneity of a polymerizing sample in terms of distance from the illuminated surface. However, microrheology can also be used to study spatial inhomogeneities that occur within the focal plane of the microscope, i.e. within the polymerizing front, during photopolymerization. The length scale over which particle tracking microrheology can resolve spatial heterogeneities within the focal plane of the microscope is dependent on the particle concentration and the distance between neighboring particles. In this study, real-time images of the focal plane were captured using a standard CCD camera and a 63X oil immersion objective, so that the field of view was approximately 98 by 74 microns. The particle concentration used in this study was low, less than 0.03 % by volume, and resulted in a typical separation distance between particles of 1 to 10 microns. Thus, the maximum resolution of the experimental setup used to study homogeneity within the focal plane is approximately 1 μm. In a perfectly homogeneous medium, all tracer particles within this field of view should experience the same mechanical properties; in a mechanically heterogeneous medium, the motion of certain tracer particles will be more restricted than others. Equation 4.1 can be used to characterize the distribution of displacements of all tracer particles within the field of view via the distribution parameter α and thus quantify structural heterogeneity.

As mentioned above, $\alpha = 0$, indicates a perfectly homogeneous sample, while values greater than zero suggest increasing heterogeneity. Figure 4.8 presents the distribution parameter as a function of sample depth and UV exposure time for samples of E4PETeA loaded with 5.0 wt.% DMPA, analogous to Figures 4.6 and 4.7.

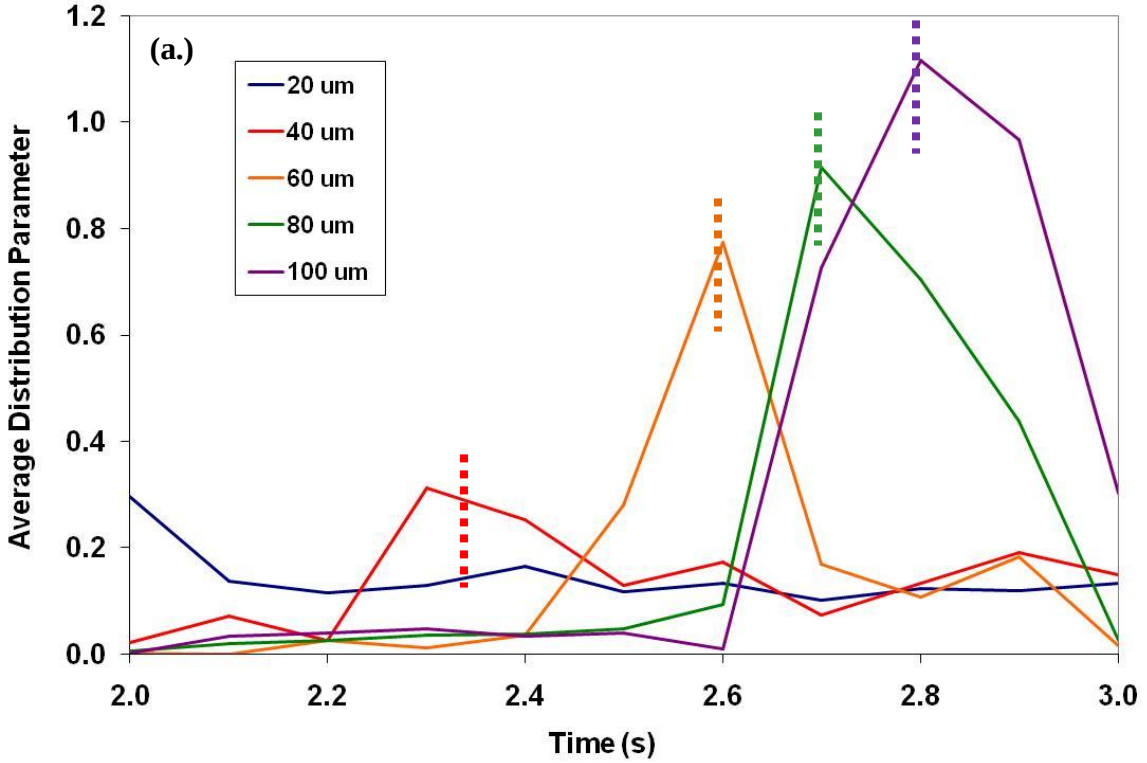

Figure 4.8: The average distribution parameter, α, at varying sample depths as a function of UV exposure time in samples of E4PETeA loaded with 5.0 wt.% DMPA. The dashed vertical lines denote the time for gelation at a given depth.

A maximum in the distribution parameter is clearly observed at each depth. The peak directly corresponds to the experimentally measured point of gelation, which is denoted by the dashed line for each sample depth. The structural heterogeneity reaches a maximum during the liquid-to-gel transition. Both before and after gelation, the samples have low values, indicating that the material is relatively homogeneous in both the liquid and gel phases. These experimental observations are supported by models in literature

that were originally developed to predict the formation of microgel regions during the polymerization of multifunctional methacrylates [21, 25, 28, 66]. The models show that early reactions do not greatly contribute to the formation of microgels; however; as the polymerization reaction progresses, regions of microgelation rapidly develop and due to mobility restrictions, a maximum in the number of microgel occurs at high conversions. Eventally, the microgels connect with each other, forming a complete more homogeneous polymer network. The formation of microgels via cyclization reactions results in increased heterogeneity of highly cross-linked networks. Research has shown that the development of microgels strongly depends on the type and functionality of the monomer.

To investigate the effect of monomer functionality on heterogeneity during photopolymerization, the above data analysis was repeated for pure TEGDA and for a mixture of TEGDA with E4PETeA (2:1 molar ratio), both loaded with 5.0 wt.% DMPA. Spikes in structural heterogeneity, similar to those reported in Figure 4.8 for E4PETeA, were observed for both pure TEGDA and the monomer mixture. The magnitude of the maximum distribution parameter that was recorded, varied with monomer functionality and UV penetration depth, as shown in Figure 4.9. It is important to note that for a given depth the various monomer samples reach gelation at different times. Figure 4.9 does not show the effect of UV exposure time; it plots the maximum recorded value of the distribution parameter at each depth, which has been shown by Figure 4.8 to coincide with the gel point.

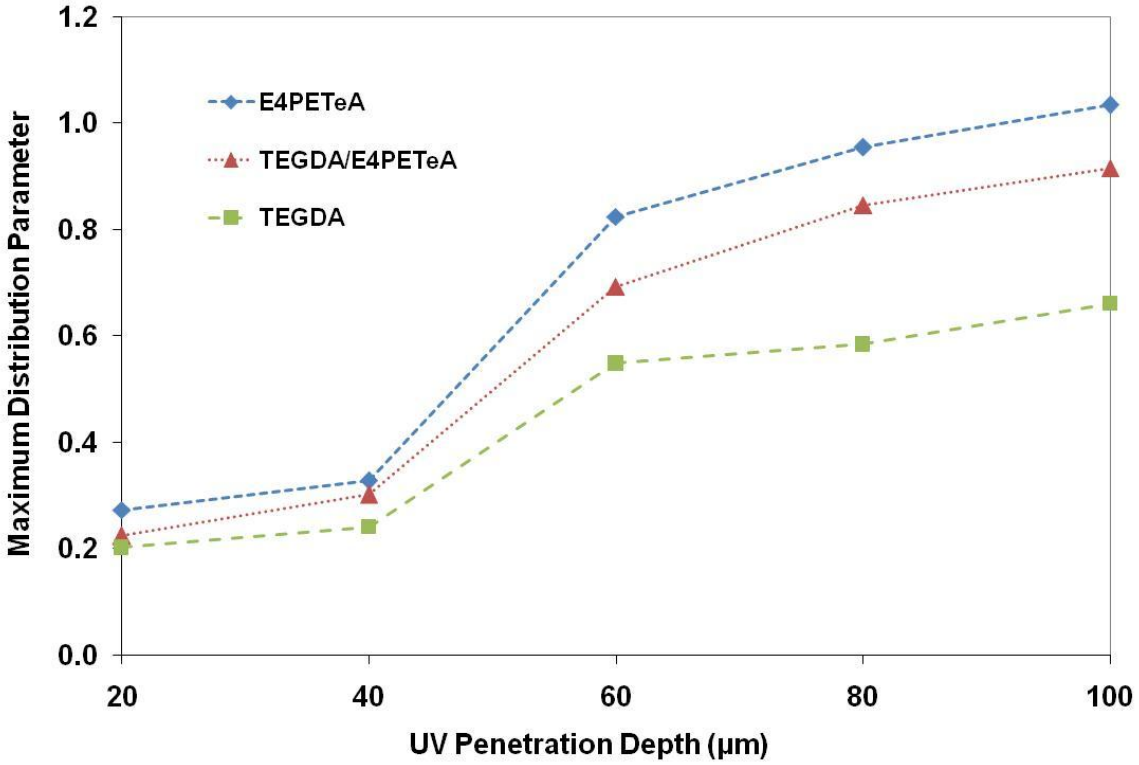

Figure 4.9: Plot of the maximum distribution parameter measured at each depth for samples of E4PETeA (♦), TEGDA (■), and a 67:33 mole % mixture of TEGDA with E4PETeA (▲) all loaded with 5.0 wt.% DMPA. The lines are to guide the eye.

E4PETeA exhibits the highest degree of heterogeneity at all UV penetrations depths, followed by the copolymer sample of TEGDA with E4PETeA, and pure TEGDA. The observation that higher functional monomers yield a greater amount of heterogeneity during photopolymerization has been widely reported. Using DMA [7], DSC [34], and DEA [29] techniques, Bowman and co-workers studied monofunctional and multifunctional methacrylate. The researchers found that trimethacrylate has significantly more extensive structural heterogeneity than comparable difunctional systems, in spite of the higher glass transition temperature, larger storage moduli, and smaller molecular weights between cross-links of the trifunctional monomer. In addition, the researchers found that adding trimethacrylate to a monomethacrylate system greatly increased the

measured heterogeneity of the monofunctional system [7, 29]. Bowman *et al.* attributed these results to the increased reactivity of the pendant double bonds in higher functional methacrylate systems. Bowman *et al.* [31, 67] and Hamielec *et al.* [68-71] independently developed comprehensive polymerization models which predict an increased occurrence of cyclization reactions with increasing concentrations of cross-linking agent in copolymerization systems, and thus more heterogeneous samples.

Figure 4.9 not only confirms the effect of monomer functionality; it also illustrates that the maximum heterogeneity increases as a function of UV penetration depth. The dependence of heterogeneity on the UV penetration depth has not been widely reported in literature, largely because no experimental methods have been able to capture this effect. At first, this observed trend may seem counterintuitive since several studies have shown that slower reacting systems, such as those further away from the illuminated surface, exhibit less structural heterogeneity than faster reacting systems with a higher rate of polymerization [31, 71-73]. However, one must take into consideration that the uniformity of the UV irradiance in the focal plane decreases as a function of sample depth due to attenuation of the UV light by the polymerizing sample. Studies of the homogeneity of UV irradiance have shown that the intensity and uniformity of the polymerizing light are affected by several factors including sample thickness [39, 40, 60-62]. Non-uniform UV illumination permits some areas of the sample to form a gel faster than other areas. As a result, structural inhomogeneities become more pronounced the further you are from the illuminated surface.

It is important to note that the distribution parameter is not an absolute measure of structural heterogeneity, but rather a quantitative measure of the statistical deviations

from a perfectly homogeneous system. Previous research has shown that distribution parameter obtained via microrheology can accurately be used to quantify the real-time heterogeneity of salt responsive block copolypeptide hydrogels [74]. The analysis identifies heterogeneities within the field of view, with a spatial resolution of roughly 10 μm, but the distribution parameter cannot be used to characterize the size and location of the microgels within the polymerizing sample. To examine the size scale of the microgels and the structural features, microscopy techniques such as TEM are necessary. Nevertheless, we believe that the unique data reported in this section provide considerable insight into the heterogeneous nature of UV-induced free-radial polymerizations.

4.4. Conclusions

The results presented above clearly show that particle tracking microrheology can accurately be used to examine the local spatial variations that develop during free-radical photopolymerization. Free-radicals were found to continue to contribute to network formation for up to 1 s after UV illumination was discontinued in all monomer samples, at low and high initiator concentration, and independent of monomer functionality. The post UV exposure reaction was found to be more significant when 0.5 second pulses of UV light were delivered to the sample. The removal of oxygen maximized the effect of post UV exposure reactions.

Using microrheology, the propoagation of the polymerization front was monitored as a function of time. It was found that at our standard depth of 60 μm the liquid-to-gel transition of E4PETeA occurred over 300 milliseconds and that heterogeneity perpendicular to the plane of UV illumination strongly depends on monomer

functionality and depth of UV penetration. Polymerization of the tetrafunctional monomer, E4PETeA, was found to be significantly more heterogeneous than the bifunctional monomer, TEDGA. Data on the copolymerization of TEGDA with E4PETeA shows that the addition of a higher functional cross-linking agent greatly increases heterogeneity. The in-plane heterogeneity was found to increase with UV penetration depth for all monomers examined in this work. This observation was attributed to the fact that the uniformity of the UV decreases with sample depth.

4.5. References

1. Decker, C., (1994). "Photoinitiated Curing of Multifunctional Monomers." Acta Polymer, **43**: 333-347.

2. Drobny, J.G., *Radiation Technology for Polymers*. 2003, London: CRC Press.

3. Fouassier, J.P. and J.F. Rabek, *Radition Curing in Polymer Science and Technology Volume III: Polymerization Mechanisms*. 1993, London: Elsevier Applied Science.

4. Kaur, M. and A.K. Srivastava, (2002). "Photopolymerization: A review." Journal of Macromolecular Science-Polymer Reviews, **C42**(4): 481-512.

5. Pappas, S.P., *UV Curing: Science & Technology Volume II*. 1985, Norwalk, CT: Technology Marketing Corporation.

6. Roffey, J.G., *Photopolymerization of Surface Coatings*. 1982, New York: John Wiley & Sons.

7. Young, J.S., A.R. Kannurpatti, and C.N. Bowman, (1998). "Effect of comonomer concentration and functionality on photopolymerization rates, mechanical properties and heterogeneity of the polymer." Macromolecular Chemistry and Physics, **199**(6): 1043-1049.

8. Feng, L. and B.I. Suh, (2006). "A mechanism on why slower polymerization of a dental composite produces lower contraction stress." Journal of Biomedical Materials Research Part B-Applied Biomaterials, **78B**(1): 63-69.

9. Andrzejewska, E., (2001). "Photopolymerization kinetics of multifunctional monomers." Progress in Polymer Science, **26**(4): 605-665.

10. Anseth, K.S., K.J. Anderson, and C.N. Bowman, (1996). "Radical concentrations, environments, and reactivities during crosslinking polymerizations." Macromolecular Chemistry and Physics, **197**(3): 833-848.

11. Pavlinec, J. and N. Moszner, (2003). "Dark reactions of free radicals crosslinked polymer networks trapped in densely after photopolymerization." Journal of Applied Polymer Science, **89**(3): 579-588.

12. Garcia, N., P. Tiemblo, L. Hermosilla, C. Sieiro, and J. Guzman, (2005). "Long-lived radicals in the postpolymerization of methacrylic monomers at low conversions." Macromolecules, **38**(18): 7601-7609.

13. Tanabe, M., G.W.M. Vandermeulen, W.Y. Chan, P.W. Cyr, L. Vanderark, D.A. Rider, and I. Manners, (2006). "Photocontrolled living polymerizations." Nature Materials, **5**(6): 467-470.

14. Corcione, C.E., A. Greco, and A. Maffezzoli, (2004). "Photopolymerization kinetics of an epoxy-based resin for stereolithography." Journal of Applied Polymer Science, **92**(6): 3484-3491.

15. Kwon, S., Y. Lee, H. Jeon, K. Han, and S. Mah, (2006). "Living cationic polymerization of isobutyl vinyl ether (II): Photoinduced living cationic polymerization in a mixed solvent of toluene and diethyl ether." Journal of Applied Polymer Science, **101**(6): 3581-3586.

16. Sipani, V., A. Kirsch, and A.B. Scranton, (2004). "Dark cure studies of cationic photopolymerizations of epoxides: Characterization of kinetic rate constants at high conversions." Journal of Polymer Science Part a-Polymer Chemistry, **42**(17): 4409-4416.

17. Sipani, V. and A.B. Scranton, (2003). "Kinetic studies of cationic photopolymerizations of phenyl glycidyl ether: termination/trapping rate constants for iodonium photoinitiators." Journal of Photochemistry and Photobiology a-Chemistry, **159**(2): 189-195.

18. Sipani, V. and A.B. Scranton, (2003). "Dark-cure studies of cationic photopolymerizations of epoxides: Characterization of the active center lifetime and kinetic rate constants." Journal of Polymer Science Part a-Polymer Chemistry, **41**(13): 2064-2072.

19. Kilambi, H., S.K. Reddy, L. Schneidewind, J.W. Stansbury, and C.N. Bowman, (2007). "Copolymerization and dark polymerization studies for photopolymerization of novel acrylic monomers." Polymer, **48**(7): 2014-2021.

20. Lee, T.Y., C.A. Guymon, E.S. Jonsson, S. Hait, and C.E. Hoyle, (2005). "Synthesis, initiation, and polymerization of photoinitiating monomers." Macromolecules, **38**(18): 7529-7531.

21. Goodner, M.D. and C.N. Bowman, (1999). "Modeling primary radical termination and its effects on autoacceleration in photopolymerization kinetics." Macromolecules, **32**(20): 6552-6559.

22. P. Bosch, J.S.J.L.M.J.G.P.C.C.S., (1998). "Kinetic investigations on the photopolymerization of di- and tetrafunctional methacrylic monomers in polymeric matrices. ESR and calorimetric studies. II. Postpolymerization reactions." Journal of Polymer Science Part A: Polymer Chemistry, **36**(15): 2785-2791.

23. Wen, M. and A.V. McCormick, (2000). "A kinetic model for radical trapping in photopolymerization of multifunctional monomers." Macromolecules, **33**(25): 9247-9254.

24. Veksli, Z., M. Andreis, and B. Rakvin, (2000). "ESR spectroscopy for the study of polymer heterogeneity." Progress in Polymer Science, **25**(7): 949-986.

25. Elliott, J.E. and C.N. Bowman, (2002). "Effect of primary cyclization on free radical polymerization kinetics: Modeling approach." Macromolecules, **35**(18): 7125-7131.

26. Elliott, J.E., J. Nie, and C.N. Bowman, (2003). "The effect of primary cyclization on free radical polymerization kinetics: experimental characterization." Polymer, **44**(2): 327-332.

27. Ikeda, J., Y. Hasei, Y. Yasuda, H. Aota, and A. Matsumoto, (2004). "Effect of primary polymer chain rigidity on intramolecular cyclization and intramolecular crosslinking in free-radical crosslinking monomethacrylate/dimethacrylate copolymerizations." Journal of Applied Polymer Science, **94**(3): 1086-1093.

28. Lovestead, T.M., A.K. O'Brien, and C.N. Bowman, (2003). "Models of multivinyl free radical photopolymerization kinetics." Journal of Photochemistry and Photobiology a-Chemistry, **159**(2): 135-143.

29. Kannurpatti, A.R. and C.N. Bowman, (1998). "Structural evolution of dimethacrylate networks studied by dielectric spectroscopy." Macromolecules, **31**(10): 3311-3316.

30. Nebioglu, A. and M.D. Soucek, (2006). "Reaction kinetics and microgel particle size characterization of ultraviolet-curing unsaturated polyester acrylates." Journal of Polymer Science Part a-Polymer Chemistry, **44**(22): 6544-6557.

31. Anseth, K.S. and C.N. Bowman, (1994). "Kinetic Gelation Model Predictions of Cross-linked Polymer Network Microstructure," Chemical Engineering Science, **49**(14): 2207-2217.

32. Bowman, C.N. and K.S. Anseth, (1995). "Microstructural Evolution in Polymerizations of Tetrafunctional Monomers." Macromolecular Symposia, **93**: 269-276.

33. Kannurpatti, A.R., K.J. Anderson, J.W. Anseth, and C.N. Bowman, (1997). "Use of "living" radical polymerizations to study the structural evolution and properties of highly crosslinked polymer networks." Journal of Polymer Science Part B-Polymer Physics, **35**(14): 2297-2307.

34. Anseth, K.S., L.M. Kline, T.A. Walker, K.J. Anderson, and C.N. Bowman, (1995). "Reaction-kinetics and Volume Relaxation during Polymerizations of Multiethylene Glycol Dimethacrylates." Macromolecules, **28**(7): 2491-2499.

35. Kenning, N.S., D. Kriks, M. El-Maazawi, and A. Scranton, (2006). "Spatial and temporal evolution of the photoinitiation rate for thick polymer systems illuminated with polychromatic light." Polymer International, **55**(9): 994-1006.

36. Goldfeder, P.M. and V.A. Volpert, (1998). "A model of frontal polymerization including the gel effect." Mathematical Problems in Engineering, **4**(5): 377-391.

37. Goldfeder, P.M., V.A. Volpert, V.M. Ilyashenko, A.M. Khan, J.A. Pojman, and S.E. Solovyov, (1997). "Mathematical modeling of free-radical polymerization fronts." Journal of Physical Chemistry B, **101**(18): 3474-3482.

38. Warren, J.A., J.T. Cabral, and J.F. Douglas, (2005). "Solution of a field theory model of frontal photopolymerization." Physical Review E, **72**(2).

39. Ivanov, V.V. and C. Decker, (2001). "Kinetic study of photoinitiated frontal polymerization." Polymer International, **50**(1): 113-118.

40. Terrones, G. and A.J. Pearlstein, (2001). "Effects of optical attenuation and consumption of a photobleaching initiator on local initiation rates in photopolymerizations." Macromolecules, **34**(10): 3195-3204.

41. Cabral, J.T., S.D. Hudson, C. Harrison, and J.F. Douglas, (2004). "Frontal photopolymerization for microfluidic applications." Langmuir, **20**(23): 10020-10029.

42. Wu, T., Y. Mei, J.T. Cabral, C. Xu, and K.L. Beers, (2004). "A New Synthetic Method for Controlled Polymerization Using a Microfluidic System." J. Am. Chem. Soc., **126**(32): 9880-9881.

43. Cygan, Z.T., J.T. Cabral, K.L. Beers, and E.J. Amis, (2005). "Microfluidic Platform for the Generation of Organic-Phase Microreactors." Langmuir, **21**(8): 3629-3634.

44. Lee, J.H., R.K. Prud'homme, and I.A. Aksay, (2001). "Cure depth in photopolymerization: Experiments and theory." Journal of Materials Research, **16**(12): 3536-3544.

45. Pereira, S.G., N. Reis, and T.G. Nunes, (2005). "Spatially resolved studies on the photopolymerization of dimethacrylate monomers." Polymer, **46**(19): 8034-8044.

46. Apicella, A., M. Simeone, R. Aversa, A. Lanza, and D. Apicella, (2005). "Light shielding effect of overlaying resin composite on the photopolymerization cure kinetics of a resin composite and a dentin adhesive." Dental Materials, **21**(10): 954-961.

47. Christian, D., (1998). "The use of UV irradiation in polymerization." Polymer International, **45**(2): 133-141.

48. Christian, D., (2002). "Light-induced crosslinking polymerization." Polymer International, **51**(11): 1141-1150.

49. Briskman, V., K. Kostarev, V. Levtov, T. Lyubimova, A. Mashinsky, G. Nechitailo, and V. Romanov, (1996). "Polymerization under different gravity conditions." Acta Astronautica, **39**(5): 395-402.

50. Ohtsuka, Y. and Y. Koike, (1984). "Studies on the Light-focusing Plastic Rod. 16. Mechanism of Gradient Index Formation in Photocopolymerization of Multiple Monomer Systems," Applied Optics, **23**(11): 1774-1778.

51. Ohtsuka, Y. and Y. Koike, (1985). "Studies on the Light-focusing Plastic Rod. 18. control of Refractive Index Distribution of Plastic Radial Gradient Index Rod by Photocopolymerization." Applied Optics, **24**(24): 4316-4320.

52. Koike, Y., H. Hatanaka, and Y. Ohtsuka, (1984). "Studies on the Light-focusing Plastic Rod. 17. Plastic Grin Rod Lens Prepared by Photocopolymerization of Ternary Monomer System." Applied Optics, **23**(11): 1779-1783.

53. Ohtsuka, Y. and T. Sugano, (1983). "Studies on the Light-focusing Plastic Rod. 14. Grin Rod of CR-39 Trifluoroethyl Methacrylate Copolymer by a Vapor Phase Transfer Process." Applied Optics, **22**(3): 413-417.

54. Koike, Y. and Y. Ohtsuka, (1983). "Studies on the Light-focusing Plastic Rod. 15. Grin Rod Prepared by Photocopolymerization of a Ternary Monomer system." Applied Optics, **22**(3): 418-423.

55. Koike, Y., Y. Kimoto, and Y. Ohtsuka, (1982). "Studies of the Light-focusing Plastic Rod. 13. Photocopolymerization of Methyl-Methacrylate Vinyl Esters of Aromatic Carboxylic Acid." Journal of Applied Polymer Science, **27**(9): 3253-3264.

56. Koike, Y., Y. Kimoto, and Y. Ohtsuka, (1982). "Studies of the Light-Focusing Plastic Rod 12. The Grin Fiber Lens of Methyl mehtacrylate-Vinyl Phenylacetate Copolymer." Applied Optics, **21**(6): 1057-1062.

57. Ohtsuka, Y. and K. Maeda, (1981). "Studies on the light-focusing Plastic Rod. 11. Preperation of a Light-Defocusing Plastic Rod." Applied Optics, **20**(20): 3562-3565.

58. Ohtsuka, Y. and Y. Terao, (1981). "Studies on the Light-focusing Plastic Rod. 9. Chemical Composition of the Copolymer Rod Diethylene Glycol Bis(Allyl Carbonate) with 2,2,3,3- Tetrafluoropropyl Methacrylate." Journal of Applied Polymer Science, **26**(9): 2907-2915.

59. Slopek, R.P., H.K. McKinley, C.L. Henderson, and V. Breedveld, (2006). "In situ monitoring of mechanical properties during photopolymerization with particle tracking microrheology." Polymer, **47**(7): 2263-2268.

60. Ivanov, V.V., V.P. Begishev, L.R. Guseva, and K.G. Kostarev, (1995). "Front Photopolymerization at Constant Extinction and Limited Mass-Transfer." Vysokomolekulyarnye Soedineniya Seriya a & Seriya B, **37**(6): 1064-1067.

61. O'Brien, A.K. and C.N. Bowman, (2003). "Modeling thermal and optical effects on photopolymerization systems." Macromolecules, **36**(20): 7777-7782.

62. Terrones, G. and A.J. Pearlstein, (2001). "Effects of kinetics and optical attenuation on the completeness, uniformity, and dynamics of monomer conversion in free-radical photopolymerizations." Macromolecules, **34**(26): 8894-8906.

63. Tolpekin, V.A., M.H.G. Duits, D. van den Ende, and J. Mellema, (2003). "Stability ratio in binary hard sphere suspensions, measured via time-resolved microscopy." Langmuir, **19**(10): 4127-4137.

64. Weeks, E.R., J.C. Crocker, A.C. Levitt, A. Schofield, and D.A. Weitz, (2000). "Three-dimensional direct imaging of structural relaxation near the colloidal glass transition." Science, **287**(5453): 627-631.

65. Kegel, W.K. and A. van Blaaderen, (2000). "Direct observation of dynamical heterogeneities in colloidal hard-sphere suspensions." Science, **287**(5451): 290-293.

66. Kurdikar, D.L. and N.A. Peppas, (1994). "A Kinetic Study of Diacrylate Photopolymerizations." Polymer, **35**(5): 1004-1011.

67. Anseth, K.S., M.D. Goodner, M.A. Reill, A.R. Kannurpatti, S.M. Newman, and C.N. Bowman, (1996). "The influence of comonomer composition on dimethacrylate resin properties for dental composites." Journal of Dental Research, **75**(8): 1607-1612.

68. Tobita, H. and A.E. Hamielec, (1988). "A Kinetic Model for Network Formation in Free-radical Polymeriation." Makromolekulare Chemie-Macromolecular Symposia, **20-1**: 501-543.

69. Tobita, H. and A.E. Hamielec, (1989). "Modeling of Network Formation in Free-radical Polymerization." Macromolecules, **22**(7): 3098-3105.

70. Tobita, H. and A.E. Hamielec, (1991). "Kinetics of Free-radical Copolymerization the Pseudo Kinetic Rate Constant Method." Polymer, **32**(14): 2641-2647.

71. Tobita, H. and A.E. Hamielec, (1992). "Control of Network Structure in Free-radical Cross-linking Copolymerization." Polymer, **33**(17): 3647-3657.

72. Okay, O., (1994). "Kinetic Modeling of Network Formation and Properties in Free-radical cross-linking Copolymerization." Polymer, **35**(4): 796-807.

73. Okay, O., H.J. Naghash, and I. Capek, (1995). "Free-radical Cross-linking Copolymerization Effect of Cyclization on Diffusion Controlled T4ermination at Low conversion." Polymer, **36**(12): 2413-2419.

74. Sato, J. and V. Breedveld, (2006). "Transient rheology of solvent-responsive complex fluids by integrating microrheology and microfluidics." Journal of Rheology, **50**(1): 1-19.

CHAPTER 5

OXYGEN INHIBITION EFFECTS ON THE UV RADIATION CURING OF MULTIFUNCTIONAL ACRYLATE RESINS

5.1. Introduction

Photopolymerization is the process of converting liquid monomer doped with photoinitiator to high molecular weight polymers upon exposure to ultraviolet light. The end result of this process is usually a solid-like, highly cross-linked network that is impervious to thermal, chemical, and physical alteration or degradation. Therefore, photopolymerization is commonly used in the thin film and coatings industries to form protective barriers [1-3]. The majority of industrial applications of photopolymerization are carried out in the presence of atmospheric oxygen, which has been widely shown to interfere with free-radical polymerizations by reacting with radicals [4, 5]. This oxygen inhibition has a number of effects, including a reduction of the polymerization rate, a decrease in the polymer chain length, and the formation of a tacky surface in which full property development does not occur. For a detailed understanding of the effects of oxygen transport on free-radial polymerizations and the validation of models of this process, it is necessary to experimentally characterize it with high spatial resolution. Unfortunately, there are relatively few reports in the literature on the local effects of oxygen presence and transport in commercial monomers.

Free-radical photopolymerization generally begins with the absorption of UV light by a photoinitiator to generate active radicals. Multifunctional monomer then

combines with these initiating radicals to produce primary radicals that continue to react with the reactive groups on additional monomer to form growing polymer chains. Ultimately, this leads to the formation of a highly cross-linked three-dimensional polymer network [6]. Molecular oxygen, however, is known to strongly inhibit the reaction pathway of free-radical polymerization, and thus greatly reduces process efficiency by decreasing the polymerization rate and altering the chain length distribution. Atmospheric oxygen obstructs free-radical polymerization by reacting with initiating, primary, and polymer radicals to form peroxy radicals. These peroxy radicals do not readily reinitiate the polymerization process, and oxygen thus essentially acts as an efficient scavenger of free-radicals. In addition, the peroxy radicals can terminate with radicals present in the reaction or abstract labile hydrogen radicals [7]. Because of its efficieny as scavenger, an induction period is generally observed at the onset of polymerization, if a monomer is saturated with dissolved oxygen. Studies have shown that free radicals are more reactive towards oxygen than the reactive groups of the monomer [8], so that polymerization cannot proceed until the majority of dissolved oxygen has been consumed.

The inhibitory effects of oxygen on the kinetics of the photopolymerization process have been widely studied [6, 7]. Fluorescence quenching techniques have been used to investigate the influence of oxygen on the polymerization kinetics in photopolymer films. These studies have shown that the removal of oxygen from photopolymers prior to UV exposure leads to higher polymerization rates and a more uniform polymer distribution [9]. The main drawback of the fluorescence quenching techniques is that chromophores have to be added to the monomer system to study the material, and these additives can alter the property of material and interfere with the UV

irradiation. Pino *et al.* used photo-DSC to study the effects of oxygen inhibition on the photopolymerization of weatherfast clearcoat resins. The researchers found that the presence of oxygen greatly decreases the rate of polymerization, especially near the illuminated free surface that is in contact with the atmosphere [10]. Although the rate of polymerization can be easily obtained from photo-DSC, it is difficult to study the induction period caused by oxygen inhibition via this method because of the poor response time of the calorimeter. Nunes *et al.* utilized spatially resolved MRI spectroscopy to investigate the anisotropic effects of oxygen on the photopolymerization of dental composites [11]; again, it is difficult to monitor fast reactions using this technique. As a consequence, researchers have predominantly used real-time FTIR spectroscopy to examine the inhibitory effects of oxygen on the reaction kinetics of polymerization.

Decker *et al.* was one of the first research groups to use IR spectroscopy to investigate the inhibition of the polymerization process by oxygen. This ground-breaking research revealed that the concentration of dissolved oxygen in an oxygen-saturated multifunctional acrylate system had to drop by at least a factor of 300 before polymerization began. Using FTIR-ATR, Scherzer and Langguth determined that increasing the temperature at which the polymerization is performed shortens the the oxygen inhibition period due to oxygen being less soluble in acrylates at higher temperatures [12, 13]. Bowman *et al.* used FTIR data to show that increasing the rate of initiation, by increasing either the UV intensity or the concentration of initiator, greatly reduced the negative impact of oxygen on the polymerization kinetics and polymer

structure [14, 15]. The primary problem with spectroscopy is that it is unable to ascertain local spatial information since technique is dependent on sample volume.

On the theoretical front, Bowman and co-workers developed a comprehensive model that incorporates heat and mass transfer to study the effect of oxygen on polymerization [16]. In addition, Dickey *et al.* developed a quasi steady-state approximate kinetic model to study the effect of oxygen diffusing at the each barrier in Step and Flash Imprint Lithography [17]. It is unclear if these models can accurately be used to predict local oxygen inhibition effects since both models were parameterized and validated using volume-averaged data from spectroscopy techniques.

A significant portion of the oxygen inhibition research found in literature has focused on developing various approaches to combat the free-radical sensitivity to oxygen [18, 19]. The use of high-intensity irradiation sources and high concentrations of photoinitiator increases the production of primary radicals to the point where it overwhelms their consumption by oxygen [8, 14, 15, 20]. An alternative approach is to polymerize samples in an inert environment such as nitrogen, argon, or carbon dioxide, which eliminates oxygen from the polymerization [8, 18, 19]. Other researchers have utilized wax barrier coats [21] or performed the UV exposure under water [20] to slow down the diffusion of atmospheric oxygen into the UV-curable resin. Finally, chemical additives, such as amines, can be added that react with the dissolved oxygen and make it unavailable for radical scavenging. Although the above solutions diminish the harmful effects of oxygen, these methods increase the manufacturing cost and often create further problems in the polymerized product [18, 19, 22].

Comprehensive understanding of the fundamental impact that oxygen has on UV induced polymerizations is needed to effectively combat its inhibitory effects. In this work, the inhibitory effects of oxygen will be studied with specially designed high-resolution particle tracking microrheology experiments. The data from these experiments are also compared to the results of a numerical model that incorporates reaction kinetics and oxygen transport. Particle tracking microrheology was previously used to measure the effect of oxygen on the cure time of multifunctional acrylates. The microrheological data in Chapter 2 and 3 demonstrate that oxygen both increases the cure time and alters the scaling trend of cure time as a function of initiator concentration, suggesting a change of the reaction kinetics [23]. In this Chapter we will more specifically examine the transport and consumption of oxygen in multifunctional acrylate systems. In addition, a simple two-step model of the curing process was developed and used to analyze the obtained microrheology data. The advantage of using particle tracking microrheology to study the impact of oxygen is that it is the only direct and nondestructive technique capable of monitoring the photopolymerization process in real-time with micrometer spatial resolution.

5.2. Modeling the Kinetics of Oxygen Inhibition

Molecular oxygen is known to efficiently inhibit free-radical polymerization by reacting with initiated radicals to form peroxy radicals, which in turn do not readily reinitiate polymerization. As a result, an inhibition time will be observed when polymerization reaction is carried out in the presence of oxygen. The length of this inhibition time is dependent on the intensity of UV light, the concentrations of photoinitiator and oxygen, as well as the ability of oxygen to diffuse within the system.

The model applied in this study is based on the rather simplistic assumption that gelation in an oxygen saturated environment is a two-step process:

$$t_{gel} = t_{inhib} + t_{gel,DEOX} \tag{5.1}$$

where t_{gel} is the total time to gelation, t_{inhib} is the oxygen inhibition time during which oxygen is consumed, and $t_{gel,DEOX}$ is the time required for gelation in the absence of oxygen. The assumption that all oxygen must be consumed before the polymerization reaction can proceed is not unreasonable, given the fact that Decker *et al.* reported that the concentration of dissolved oxygen in monomer must be lowered by at least a factor of 300 before polymerization can begin.

As demonstrated in previous chapters, microrheology can be used to experimentally measure the gelation times both in the presence and absence of oxygen. The oxygen inhibition time is the difference between these experimental values and is expected to be approximated by:

$$t_{inhib} \approx \frac{[O_2]_{initial}}{R_I} \tag{5.2}$$

where $[O_2]_{initial}$ is the initial concentration of oxygen in the system and R_I is the rate of oxygen consumption, *i.e.* the rate of radical generation if the reaction kinetics is dominated by oxygen scavenging. Assuming that one radical consumes one molecule of oxygen, the polymerization reaction will not proceed until the amount of radicals generated is sufficiently high to consume nearly all of the dissolved oxygen. If R_I, the radical generation rate, is constant, Equation 5.2 could directly be used to estimate the inhibition time. However, the reaction network is slightly more complicated and requires a closer look.

Classical free-radical polymerization kinetics can be assumed to determine the concentration of dissolved oxygen in multifunctional acrylate monomers during UV induced polymerization. The simplified reaction mechanism for the photocuring of UV sensitive monomer consists of four main steps: initiation, propagation, termination, and radical scavenging, which are outlined in below.

Initiation:	$In + h\nu \longrightarrow 2R^{\bullet}$
Radical Scavenging:	$R^{\bullet} + O_2 \xrightarrow{k_o} Stable\ peroxy\ radical$
Propagation:	$R^{\bullet} + M \xrightarrow{k_p} RM^{\bullet}$
	$RM_n^{\bullet} + M \xrightarrow{k_p} RM_{n+1}^{\bullet}$
Termination:	$RM_n^{\bullet} + RM_m^{\bullet} \xrightarrow{k_{tc}} M_{n+m}$ (*combination*)
	$RM_n^{\bullet} + RM_m^{\bullet} \xrightarrow{k_{tc}} M_n + M_m$ (*disproportionation*)

In, $R^{\bullet}$, O_2, *M*, and $RM_n^{\bullet}$ represent initiator, radicals, oxygen, acrylate monomer, and growing radicals of chain length *n* respectively. M_n, M_m, and M_{n+m} correspond to the resulting polymer chains that are formed once the reaction is terminated. Photopolymerization starts with the absorption of UV light, with energy *hv*, by a molecule of photoinitiator to produce two free radicals. The generated radicals then react with molecule oxygen to form peroxy radicals, which are nonreactive towards the reactive group on the acrylate monomer. In a competitive, slower reaction, the free-radicals react with monomer to form growing polymer chains, which then continue to propagate until they encounters the radical end of another polymer chain, at which point termination occurs either by combination or disproportionation [6, 7].

In order to develop a model capable of monitoring the concentration of dissolved oxygen in the system, critical rate equations for initiation, radical scavenging, propagation, and termination need to be defined. In the expressions below, the rates have

units of mol/m^3-s and concentrations are denoted by brackets and have units mol/m^3. The rate of initiation is dependent on the concentration of initiator and the intensity of UV light delivered to the sample as follows.

$$R_i = 2(2.3\phi_i \, \varepsilon [In] I) \tag{5.3}$$

In Equation 5.3, R_i is the rate of initiation, ϕ is the quantum yield of the initiator, ε is the molar absorptivity of the initiator at 365 nm in units of m^3/mol-m, and I is the intensity of UV light in units of W/m^2, which varies across the sample due to adsorption. The value of 2.3 in the above rate equation is derived from an expression developed by Fouassier to describe the absorbed light intensity [24]. In addition, Equation 5.3 contains a coefficient of 2 because each initiator molecule forms two free-radicals upon UV exposure. This is not true for all types of initiators; however, DMPA, the initiator used in this study, is known to form two radicals. The radicals generated via the initiation step are scavenged by molecular oxygen according to the following rate.

$$R_{O_2} = -k_O [O_2][R^\bullet] \tag{5.4}$$

Here k_O is the rate coefficient of oxygen consumption in units of m^3/mol-s. Equation 5.4 implies that one radical consumes one molecule of oxygen; however, in certain reaction systems, a single radical is capable of consuming two or more molecules of oxygen since the peroxy radical can generate new radicals via hydrogen abstraction [18]. Once the concentration of oxygen in the monomer has been adequately reduced, the radicals start reacting with monomer to form polymer chains via the propagation step, which has the following kinetic expression:

$$R_p = -k_p [M][R^\bullet] \tag{5.5}$$

where k_p is the propagation rate coefficient with units of m^3/mol-s. The propagation step continues to consume monomer until the radical chain is terminated by another radical. The kinetics of the termination process are given by:

$$R_t = -2k_t[R^\bullet]^2 \tag{5.6}$$

Here $[R^\bullet]$ is the total concentration of propagating radicals and k_t is the overall termination coefficient, which represents the combined effects of combination and disproportionation. The factor of two that appears in Equation 5.6 takes into account that for each termination event two active radicals are terminated. To simplify the modeling process, the above rate equations were assumed to be independent of chain length; since we focus on oxygen inhibition, which occurs early on, this is a reasonable assumption.

Species balances for the initiator, radicals, monomer, and oxygen molecules were developed based on Equations 5.3-5.6. Mass transfer was incorporated into the model through the addition of a diffusive flux term into the following kinetic expressions:

$$Initiator: \quad \frac{d[In]}{dt} = D_{in}\frac{d^2[In]}{dx^2} - 2.3\phi\varepsilon[In]I \tag{5.7}$$

$$Radicals: \quad \frac{d[R^\bullet]}{dt} = D_R\frac{d^2[R^\bullet]}{dx^2} + 2(2.3\phi\varepsilon[In]I) - k_O[O_2][R^\bullet] - 2k_t[R^\bullet] \tag{5.8}$$

$$Oxygen: \quad \frac{d[O_2]}{dt} = D_{O_2}\frac{d^2[O_2]}{dx^2} - k_O[O_2][R^\bullet] \tag{5.9}$$

$$Monomer: \quad \frac{d[M]}{dt} = D_M\frac{d^2[In]}{dx^2} - k_p[M][R^\bullet] \tag{5.10}$$

The diffusion coefficients, D, in Equations 5.7-5.10 all have units of m^2/s. The above species balances were used, as describe in the methods section below, to simulate the concentration of dissolved oxygen in multifunctional acrylate systems during the initial phase of photopolymerization. The time required for the oxygen concentration to

decrease from atmospheric saturation by a factor of 300 was defined as the inhibition time. The simulated inhibition time was then compared to the inhibition time experimentally measured via microrheology.

5.3. Method and Materials

5.3.1. Sample Preparation

The multifunctional acrylate monomers, trimethylolpropane triacrylate (TMPTA, SR351), was obtained from Sartomer and used as received. The monomer was made sensitive to UV light by adding varying concentrations of 2,2-dimethoxy-1,2-diphenylethan-1-one (DMPA, Irgacure 651), a commercial photoinitiator, obtained from Ciba Specialty Chemicals. A small amount of micrometer-sized, inert silica based fluorescent tracer particles (< 0.03 volume%) was added to the photosensitive systems for particle tracking microrheology. Degassed samples were prepared by loading UV-sensitive systems on a Schlenk line and pulling vacuum for two hours; the container was then filled with Argon and transferred to a nitrogen-filled glove box, where the samples where loaded into the sample chamber and sealed. Samples were briefly sonicated prior to being loaded in order to minimize the aggregation of tracer particles.

The sample chambers were ca. 100 μm thick and consisted of a lithographically patterned, aluminum-coated microscope slide and cover slip (No. 1.5), separated by Parafilm spacers. The patterning (see details below) was used to spatially modulate the illumination profile of the sample. Ultraviolet light from a Hamamatsu UV spot light source (LC5) equipped with a 400 W high-pressure mercury bulb was directed through an 8 mm diameter liquid light guide, a 365 nm bandpass filter (Newport), and a high-speed electronic shutter into the sample chamber. The intensity of the incoming UV light

was measured in-situ, after passing through the microscope slide that forms the illuminated side of the sample chamber, with an EPM2000e (Coherent Inc) power meter. The light intensity was further controlled by placing neutral density filters in the optical path of the UV light and ranged from 4 to 14 W/m^2.

5.3.2. Generation of Patterned Masks

Well-defined UV illumination patterns with characteristic dimensions of tens of micrometers were generated using lithographic masks. To produce these masks glass microscope slides sputtered with 1 μm of aluminum were purchased from UVH Sputtering. A positive photoresin (Shipley 1813) was spincoated onto the aluminum side of the slides for 45 seconds at a speed of 2500 rpm. The coated slides were soft baked on hotplate at 100℃ for 5 minutes. High-resolution transparency masks with multiple line and square box patterns were printed on a Heidelberg Herkules lithographic printer. The feature size of the patterns was 50 micrometers and repeated features were spaced 50 to 300 microns apart. The masks were placed flush with the resin coated slide and exposed to UV light for 80 seconds. Following exposure, the slides were developed in Shipley 354 for two minutes and baked for 10 minutes at 70 ℃ in an oven. The exposed aluminum was etched in Transene Aluminum Etchant (Type A) for 1.5 minutes at 55 ℃ and the remaining photoresin was removed with acetone. As illustrated by Figure 5.1, the finished masks consisted of UV transparent square box and line patterns of fixed size separated by UV shaded regions with dimensions ranging from 50 to 300 microns in increments of 50 microns. Images of the masks were taken on an optical microscope (Leica DM-IRB) equipped with a CCD camera, using a 63X objective with that yielded a spatial resolution of 0.153 um per CCD-pixel. The measured dimensions of the UV

transparent patterns were found to be within five percent of the actual feature sizes printed on the mask.

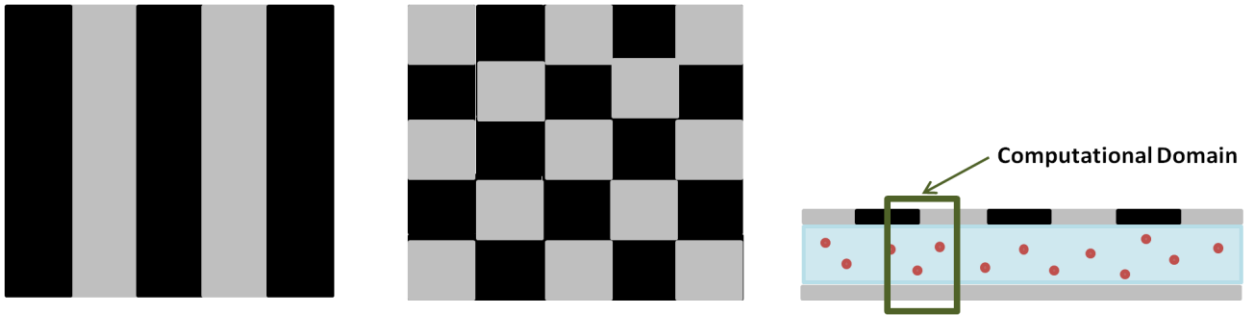

Figure 5.1: Schematic of the patterned lithographic masks used to spatially modulate the illumination profile delivered to the sample. The gray areas are UV transparent and the black areas of the masks shield UV irradiance via a thin layer of aluminum. The dimensions of the gray features were kept constant at 50 μm, while the black regions are varied from 50 to 300 microns in increments of 50 microns. The figure on the right illustrates the computational domain for the reaction-diffusion simulations.

5.3.3. Data Acquisition and Analysis

In order to perform microrheology, a filled sample chamber was placed on the inverted microscope with attached CCD camera. By flooding the sample with visible, red light, the exact location of the mask pattern with respect to the imaging optics was determined and, if necessary, adjusted without initiating polymerization. The motion of tracer particles was then recorded at a depth of 60 μm from the glass surface using a 63X oil-immersion objective and fluorescence microscopy. The images were transferred from the camera to the computer in real-time using a precision frame grabber and Openbox image acquisition software. The timing of the shutters that control the (invisible) UV exposure and the fluorescent light source for tracer imaging was computer controlled via LabView, using a fixed delay of 4 seconds after the opening of the shutter on the fluorescent light source. For a fully exposed sample without patterned mask (uniform illumination profile), previous work has shown that gelation occurs when the transient

mean-squared displacement (MSD) data first becomes independent of the lag time. In this study, the monitored area contains both UV exposed and unexposed regions due to the mask. As a result, determination of the gel point is more complicated, since the transient MSD data also varies spatially. To simplify the task, the point at which particle motion ceases in the UV exposed region was defined at the gel point. In a Newtonian liquid tracer particles are free to diffuse throughout the system; however, upon the formation of a gel network the particles are not able to move over long distances. For an unmasked sample exposed to UV irradiation, this definition of the gel point was found to be consistant with the previous definition for homogenously illuminated samples.

5.3.4. Modeling of Data

The simulation model developed for this work describes the consumption of molecular oxygen by free-radicals during the photopolymerization of TMPTA. The model allows for variation of species concentration, spatial variations in the light intensity, and light intensity throughout the thickness of the polymer sample. By entering Equations 5.7-5.10 in COMSOL Multiphysics (Burlington, MA), the oxygen inhibition time was modeled. For a fully exposed sample, diffusion of oxygen in the plane perpendicular to the incidence of UV irradiation was set to zero, resulting in a one-dimensional problem. However, for masked samples with a spatially modulated illumination profile, the transport of oxygen had to be considered in both the horizontal and vertical planes. In addition, modeling the masked samples required that a step function be introduced in the light intensity to represent the edge between light and dark areas. To solve Equations 5.7-5.10, boundary conditions for the system need to be specified. For the one-dimensional, fully exposed system, the boundary conditions for all

species concentrations were no-flux at the top and bottom of the sample. For masked systems, we took advantage of the periodicity of the mask in choosing the computational domain: from the center of an illuminated area to the center of the adjacent dark area shielded by the mask. Based on symmetry arguments, we could thus assume no-flux boundary conditions at all edges of the computational domain. The essential model parameters and the initial conditions for Eqns. 5.7-5.10 are listed in Table 5.1 along with the references from which they were obtained.

Table 5.1: List of parameters used in the model along with reference from which the value was obtained

Parameter	Description	Value	Units	Reference
D_O	Oxygen diffusion coefficient	1×10^{-10}	m^2/s	[14, 16]
$[O_2]$	Initial oxygen concentration	1.05	mol/m^3	[25]
k_o	Rate coefficient of oxygen consumption	1×10^{6}	mol/m^3-s	[26, 27]
k_t	Rate coefficient of termination	1×10^{3}	mol/m^3-s	[28]
k_p	Rate coefficient of propagation	1×10^{5}	mol/m^3-s	[28]
$[M]$	Initial monomer concentration	3700	mol/m^3	
D_M	Monomer diffusion coefficient	1×10^{-20}	m^2/s	
D_{In}	Initiator diffusion coefficient	1×10^{-20}	m^2/s	
D_R	Radical diffusion coefficient	1×10^{-20}	m^2/s	
ϕ	Quantum yield of initiator	60	%	[29]
ε	Molar absorptivity at 365 nm	20.26	m^3/mol-m	

The molar absorptivity listed in Table 5.1 was determined experimentally by performing UV spectroscopy on a dilution series of DMPA in TMPTA. Since we were primarily concerned with the transport of oxygen, the diffusion coefficients of the monomer, radical, and initiator were assumed to be infinitely slower than that of oxygen. Research has shown that the diffusion coefficient of dissolved molecular oxygen is far greater than that of any other component commonly found in the UV sensitive systems [8]. Additional assumptions were incorporated into the model: *(i)* the light source is monochromatic at 365 nm, *(ii)* the initiation reaction is assumed to generate two primary

radicals of equal reactivity and mobility, *(iii)* inhibition, propagation, and termination are chain length independent, *(iv)* each radical consumes a single molecule of oxygen, *(v)* bimolecular termination can be characterized by a single k_t term that incorporates termination by both combination and disproportionation, *(vi)* at the start of the reaction all species concentrations are uniformly distributed throughout the sample, and *(vii)* and the physical properties of the system are assumed to remain constant until the gel point.

5.4. Results and Discussion

The extent of oxygen inhibition during free-radical photopolymerization is affected by many variables, including dissolved oxygen concentration and the rate of initiation. To study the effects of inhibition during the photopolymerization UV sensitive samples were exposed to spatially modulated illumination profiles via patterned lithographic glass slides. The slides consisted of an array of UV transparent line and square box patterns with a feature size of 50 μm (see Fig. 5.1). the transparent regions were separated by a shielded area of aluminum coating ranging from 50 to 300 μm (in increments of 50 μm). These patterns allowed us to accurately control the fraction of the sample that was exposed to UV irradiance, which is simply given by:

$$Exposed\ \ Fraction = f = \frac{Area_{UV}}{Area_{UV} + Area_{Shielded}} \tag{5.11}$$

where $Area_{UV}$ is the total area exposed to UV irradiance and $Area_{Shielded}$ is the total area shielded by the aluminum coating. The square box patterns have lower exposed fractions than line patterns of similar dimensions.

The concept behind using patterned mask to study oxygen inhibition is that radicals will only be generated in the illuminated areas, and thus, oxygen in these areas

will be depleted first. Assuming that the dissolved oxygen is initially uniformly distributed and that molecular oxygen is free to diffuse around the system, oxygen from the shaded areas will try to diffuse into the light area as a result of the concentration gradients. One might therefore expect that the gel time measured by microrheology increases with decreasing exposed fraction. If the diffusion of oxygen is fast compared to the radical generation rate, all the oxygen in the system can and will be consumed before polymerization occurs. However, if diffusion of oxygen is slow, only the oxygen in exposed zones can be consumed and the inhibition time should be independent of the exposed fraction. In this scenario, masked and unmasked samples should all reach the gel point at the same time. It is important to note that in samples masked with square box patterns oxygen transport is a three-dimensional problem, while it is essentially two-dimensional problem when samples are masked with line patterns.

Figure 5.2 illustrates the dependence of the gel time on the exposed fraction for samples of TMPTA loaded with 1.0 and 2.0 wt.% DMPA. The 2.0 wt.% DMPA samples were exposed to 4 and 8 W/m^2 of UV light, while the 1.0 wt.% DMPA sample was only exposed to an intensity of 8 W/m^2. All data were collected 60 μm below the illuminated surface of the sample. Figure 5.2 clearly shows that the gel time is a strong function of the exposed fraction, and we can conclude that oxygen must be diffusing from the shaded regions to illuminated regions. Consider the data for TMPTA loaded with 2.0 wt.% DMPA exposed to 4 W/m^2 of UV irradiance: decreasing the illuminated area fraction from fully exposed to 0.50 increases the gel time by a factor of 1.4; if the exposed fraction is further reduced to 0.03, the gel time increases by a factor of 42. These results clearly show that for polymerization to occur in the illuminated area, the concentration of

dissolved oxygen in the entire system must be significantly reduced. To prove that the observed trend in the gel time data is solely the result of diffusion of molecular oxygen, samples of TMPTA loaded with 1.0 and 2.0 wt.% DMPA were degassed under vacuum and sealed in the sample chamber in an inert environment of nitrogen. As illustrated in Figure 5.2, spatially modulating the illumination profile of these degassed samples did not result in significant increases in the gel time. For a sample of TMPTA loaded with 2.0 wt.% DMPA exposed to 4 W/m^2 of UV irradiance, reducing the exposed fraction to 0.03 only increased the gel time by a factor of 1.3, whereas the oxygen saturated sample resulted in an increase of a factor of 42. The observed minor increase in the gel time of degassed sample upon masking is attributed to the presence of small amounts of polymerization inhibitors in the sample, in particular MEHQ. Although the polymerization inhibitors were removed from the monomer via a silica column prior to use, a small amount of inhibitor remains in the tracer particle stock suspension to prevent premature polymerization of this valuable resource. As a result, the prepared systems contain a small amount of polymerization inhibitor (< 50 ppm), which can also diffuse into the illuminated region to react with radicals and increase the gel time in degassed samples; because of the lower diffusion coefficient of MEHQ in comparison with oxygen, the effect is minor.

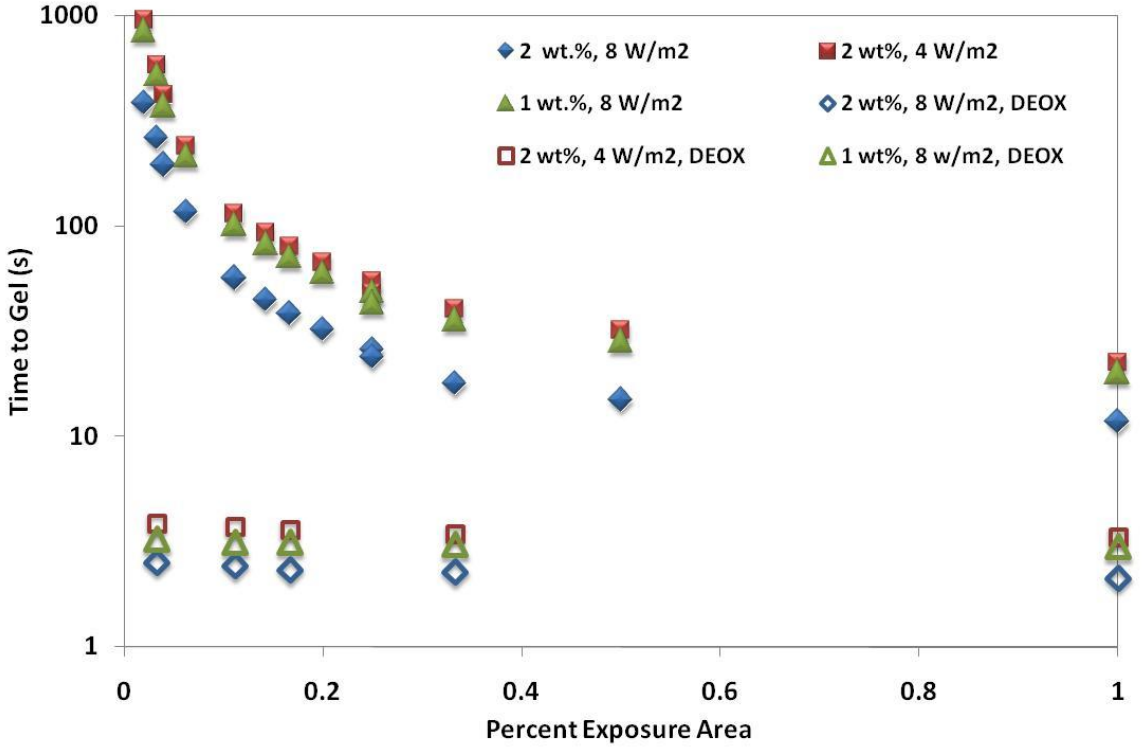

Figure 5.2: Plot of the gel time of TMPTA as a function of the percent of the sample TMPTA being exposed to UV illumination. Samples of TMPTA loaded with 2.0 wt.% DMPA were exposed to 4 and 8 W/m^{2}of continuous UV illumination at 365 nm, while 1.0 wt.% samples were exposed to an intensity 8 W/m^2. Open symbols represent degassed data and closed symbols represent oxygen saturated data.

According to Equation 5.3, the rate of initiation and generation of radicals, scales similarly with the concentration of photoinitiator and the intensity of UV irradiance. As seen in Figure 5.2, doubling the intensity delivered to a fully exposed sample of TMPTA loaded with 2.0 wt.% DMPA decreases the gel time by a factor of 2. In a similar way, one would expect samples of TMPTA loaded with 2.0 wt.% DMPA that are exposed to 4 W/m^2 of UV irradiance to gel at nearly the same time as samples of TMPTA loaded with 1.0 wt.% DMPA that are exposed to 8 W/m^2 of UV irradiance. As revealed in Figure 5.2, the 1.0 wt.% sample consistently achieves gelation more rapidly than the 2.0 wt.% samples at lower intensity. One explanation for this observation is that at higher

photoinitiator concentration, the UV is attenuated more strongly in accordance with Beer's Law, which results in additional concentration dependence to Equation 5.3. The UV light will be more attenuated in the 2.0 wt.% sample than in the 1.0 wt.% sample, and as a result, a sample with 2.0 wt.% DMPA at 4 W/m^2 will have lower rate of initiation than a sample with 1.0 wt.% DMPA at 8 W/m^2.

It is important to point out that multiple data points are reported at an exposed fraction of 0.25 for each monomer system plotted in Figure 5.2. The exposed fraction for line pattern separated by shaded areas of 150 μm is equivalent to that of a pattern of square boxes spaced on all sides by shaded areas of 50 μm, creating overlapping data points at an exposed fraction of 0.25. Although the difference between the two data points is minor and hard to observe on the logarithmic scale, the gel times for the line pattern are consistently lower than for the box pattern. This trend is likely the result of better contact between the illuminated square boxes and their shaded surroundings, experiencing oxygen transport from all four sides, whereas the line pattern experiences oxygen influx from only two sides. Based on the current design of our masks, the lowest exposed fraction that can be obtained from a line pattern is 0.14, while the maximum obtainable exposed fraction for a square box pattern is 0.25. Since there was a minimal difference between the square box and line data at an exposed fraction of 0.25, the data obtained from the individual data collected from the line and box patterns were combined to create the plots shown in Figure 5.2.

To further elucidate the effects of the rate of initiation on the consumption of oxygen, samples of TMPTA loaded with 2.0 wt.% DMPA were exposed to continuous UV illumination at intensities ranging from 4 to 14 W/m^2 in increments of 2 W/m^2. The

intensity was controlled using a series of neutral density filters that were located within the housing of the Hamamatsu UV light source. In addition to the ND filters, the UV illumination was spatially modulated using masked slides with three different line patterns. The resulting gel time data measured using microrheology are plotted in Figure 5.3. According to the figure, increasing the intensity delivered to the sample decreases the effect of oxygen inhibition. At an intensity of 4 W/m^2, decreasing the exposed fraction from 1.0 to 0.14 results in a factor of 4 increase in gel time, whereas the same decrease in exposed fraction at an intensity of 14 W/m^2 yields a factor of 3 increase in gel time. Considering that a factor on 3.5 increase in the intensity of the UV light only results in a minor decrease in oxygen inhibition, the data in Figure 5.3 shows that increasing the intensity is not highly effective at reducing the impact of oxygen inhibition on photopolymerization.

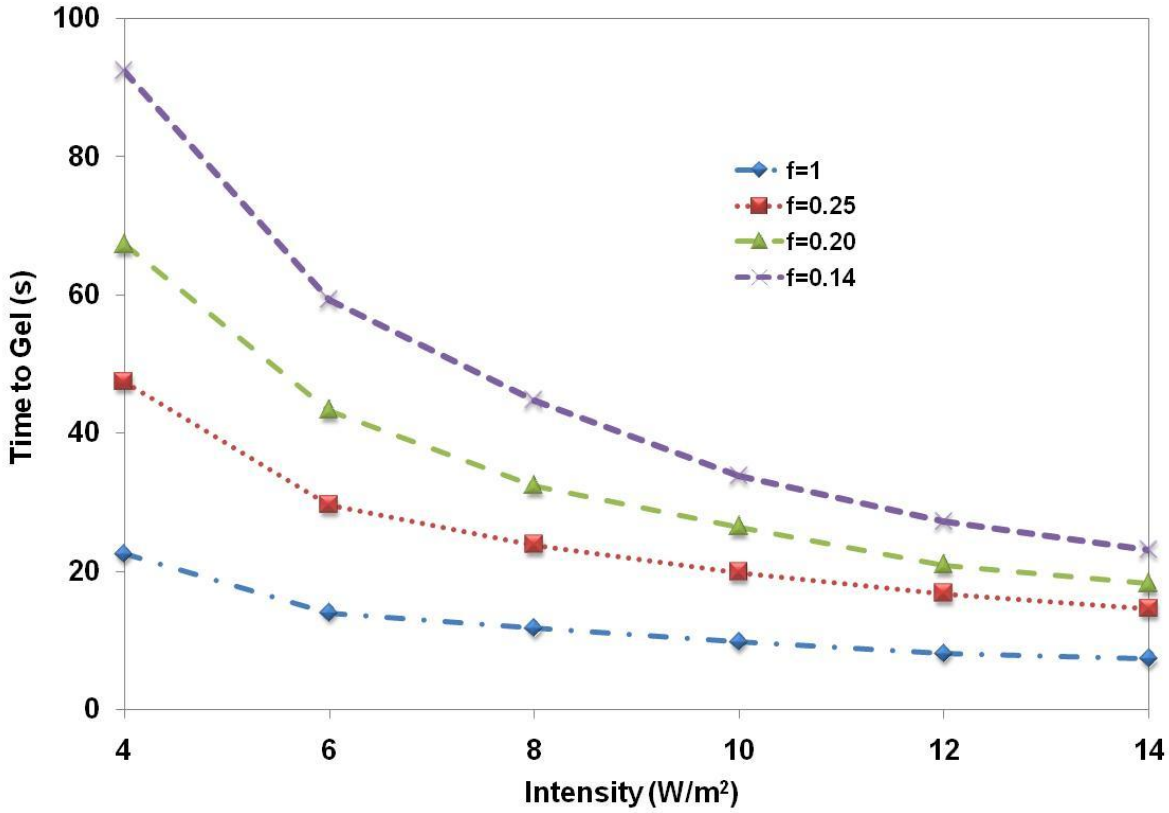

Figure 5.3: Plot of the gel time of TMPTA samples loaded with 2.0 wt.% DMPA as a function of Intensity and the fraction of area exposed to UV irradiance. All samples were exposed to continuous UV irradiance at 365 nm. The lines are to guide the eye.

The experimental data in Figure 5.3 can be used to verify the accuracy of the simple two-step polymerization model proposed in Equation 5.1. If we also assume that diffusion of oxygen is fast in comparison to the radical generation, a cross-linked network cannot form until all dissolved oxygen in the system is consumed. In the experiments carried out in this study, the time required to consume all oxygen in the system can be approximated by:

$$t_{inhib} \approx \frac{[O_2]_{initial}}{k_O [In] f I} \approx t_{gel} - t_{gel,DEOX} \tag{5.12}$$

where k_o is the rate constant for oxygen consumption and f is the fraction of the sample exposed to UV light. The equation assumes that the initiation rate is constant as a function of time and space, which is reasonable, since the initiator concentrations in our

samples (89 mol/m^3 at 2.0 wt.%) are much higher than the oxygen concentration (see Table 5.1). If one assumes that all the oxygen in the system must be consumed before forming a network, the gel time of a sample with oxygen should be the sum of the inhibition time, t_{inhib}, and the gel time of a degassed sample, $t_{gel,DEOX}$ without oxygen. The oxygen inhibition time can then be derived directly from microrheology experiments by subtracting the degassed gel times in Figure 5.3 from the times for equivalent samples with oxygen. In the experimental runs used to create the data sets in Figure 5.3, the rate constant, initiator concentration, and dissolved oxygen concentration were kept constant, while the exposed fraction and intensity were varied. As a result, according to Equation 5.12, the oxygen inhibition time for the data in Figure 5.3 should scale linearly with the inverse product of the intensity and exposed fraction. The master curve after normalization is shown in Figure 5.4 and the data appear to collapse onto a linear master curve with an intercept of zero, which validates the simple proposed model. This provides experimental proof that the oxygen diffusion is fast relative to consumption and that the polymerization is a two-step process.

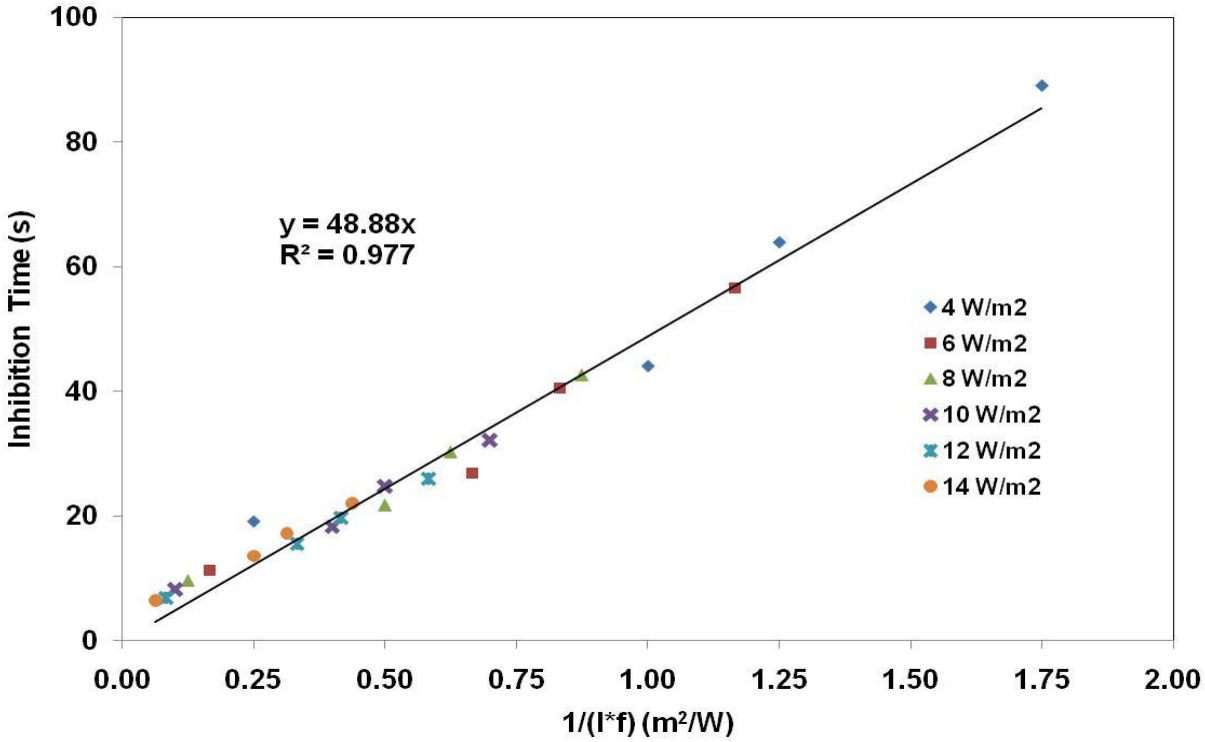

Figure 5.4: Plot of the experimentally determined oxygen inhibition as a function of the inverse product of the exposed fraction and intensity for samples of TMPTA loaded with 2.0 wt.% DMPA exposed to intensities ranging from 4 to 14 W/m^2. All samples were exposed to continuous UV irradiation at 365 nm.

The most significant deviations from the linear trendline are found in the bottom left corner of Figure 5.4. This data corresponds to the experimental measurements of the fully exposed, unmasked samples. As the fraction of the sample exposed to UV illumination is decreased, fewer deviations from the master curve are observed. When performing experiments that require an exposed fraction of one a mask with the dimensions of one mm is used to prevent bulk flow of the sample due to shrinkage. Although a sample with an exposed fraction of one is masked, it is considered fully exposed because the illuminated area of the 1 mm mask is 20 larger than the 50 micron illuminated area of the patterned lithographic masks. However, because a fully exposed sample is masked, albeit on a much larger length scale, the system will experience the

effects of oxygen transport at the edge of the mask. Given that the model proposed by Equation 5.1 assumes infinitely fast diffusion it is possible that a fully exposed sample with a mask may become inhibited by oxygen diffusing in from a far-off edge. This edge effect is the most probable explanation for the observed deviation in the fully exposed samples. One would expect the edge effect to be amplified in slow reacting systems since the oxygen would have more time to diffuse into the region of illumination where the data is recorded. Thus, the fact the largest deviation is observed at 4 W/m^2, the lowest intensity, further supports the theory that deviations are the result of the proposed edge effect. Since the data points of the spatially modulated systems fall onto the master curve, Figure 5.4 confirms the assumption that diffusion of oxygen in extremely fast. A more complete understanding of the impact of oxygen inhibition can be obtained using a model that directly incorporates the mass transport of oxygen in the reaction model, such as the COMSOL based model proposed in Section 5.2.

In Chapter 2, which examined the effect of UV penetration depth on gel time of acrylate resins, a significant difference in gelation time was also measured across a 100 μm thick sample. The dependence of gelation time on UV penetration depth was best described as linear and found to be independent of initiator concentration and monomer functionality. This linear trend was unexpected, since the attenuation of the curing light with sample depth should follow the Beer-Lambert law, and increase exponentially. An alternative explanation of this result is oxygen inhibition. Originally, depth profile measurements were performed on a samples of E4PETeA loaded with 0.25 wt.% DMPA, because the gel time of degassed samples at high initiator concentrations for this tetrafunctional monomer approached the temporal limitation of our set-up.

Unfortunately, the effects of attenuation as predicted by the Beer-Lambert law are suppressed at low amounts of DMPA. The addition of electronic shutters to our set-up significantly improved the temporal resolution and we decided to reexamine the depth profile data of TMPTA at 5.0 wt.% DMPA to investigate the effect of oxygen transport perpendicular to the illuminated surface. The experimental data can also be compared to simulated results from a kinetic model that incorporates the mass transport of oxygen.

The gel time data for the depth profiling were obtained using a Spectra-Physics 1000 W Hg(Xe) lamp with a measured intensity of 10 W/m^2 and are presented in Figure 5.4. The model data was ascertained via COMSOL using the parameter values for acrylate systems found in the literature, listed in Table 5.1. As discussed before, the inhibition time in the model was defined as the point in time when the concentration of dissolved oxygen dropped by a factor of 300. Since the experimental data in Figure 5.5 are obtained with full exposure, only oxygen diffusion parallel to the incidence of UV irradiance was considered. In order to reveal the effect of oxygen diffusion, two sets of model data are shown, one with the literature value for oxygen diffusion and one in which oxygen diffusion was stopped.

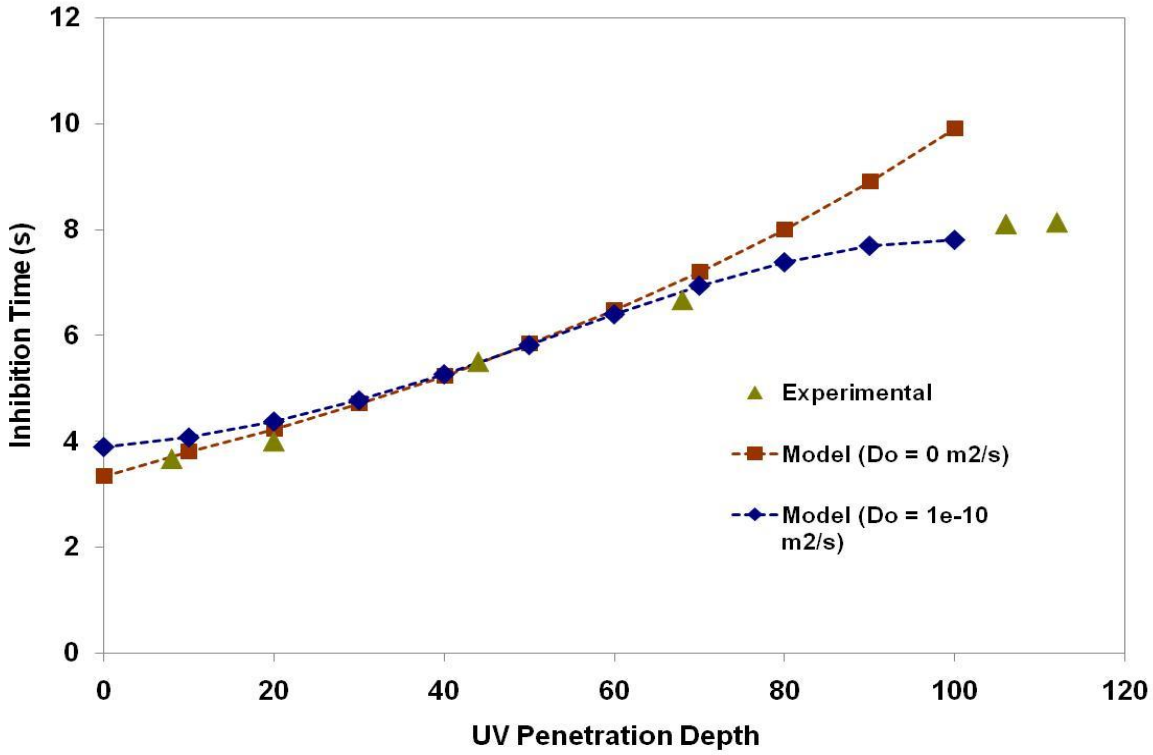

Figure 5.5: Comparison of the modeled and experimentally measured data for samples of TMPTA loaded with 5.0 wt.% DMPA continuously exposed to 10 W/m^2 of UV irradiance at 365 nm. The inhibition time is plotted against the UV penetration depth. The simulations were performed with oxygen diffusion coefficients of 0 and 1 X 10^{-10} m$^{2/}$s and a rate constant for oxygen consumption of 1 X 10^{-9} m^3/mol-s.

Figure 5.5 clearly shows that, if the mass transport of oxygen in the system is not considered, the exponential trend predicted by the Beer-Lambert law is obtained. Although the diffusion coefficient in this data set is fixed at zero, the dissolved oxygen present in the system must still be consumed for polymerization to begin. Increasing the UV penetration depth for this data set increases the gel time due to the attenuation of UV light by the polymerizing sample. Incorporating the mass transport of oxygen into the model results in a more linear dependence of the gel time on UV penetration depth. As seen in Figure 5.4, when oxygen transport is taken into consideration, the model data is in perfect agreement with the experimental data, without adjustable parameters. Close to the

interface oxygen diffusion suppresses gelation, because oxygen from the bottom of the sample diffuses upward and replenishes the top layer. As a consequence, gelation deeper into the sample is more rapid with oxygen diffusion, because part of the oxygen near the bottom has already been transported to the top and been consumed. Figure 5.5 proves that the linear trend observed in Chapter 3 is the result of mass transfer of oxygen from the bottom of the sample.

To further test the robustness of our model, the effect of varying the concentration of DMPA on oxygen inhibition time was calculated numerically and compared to the experimentally measured data from Chapter 3. Again, the oxygen inhibition time was extracted from the experimental data by substracting gel times of oxygen-free samples from the gel time of oxygen-saturated samples. At high concentration of DMPA, Figure 5.6 shows reasonable agreement between the experimental and modeled data, considering that no adjustable parameters were used. As the concentration of DMPA is decreased, the simulated data deviates significantly from the experimental results. The primary reason for the break down of the model under these conditions is that it fails to incorporate the dependence of the oxygen diffusion coefficient on exposure time, accounting for a slowly increasing sample viscosity. Research has shown that although the majority of oxygen has to be consumed for the polymerization to begin, radicals can react with monomer to form short chains in the presence of low concentrations of oxygen [8]. These small chains can affect the mechanical properties of the system, and slow diffusion of oxygen in the system. Samples loaded with low concentrations of initiator need to be exposed for extended periods of time. This extended exposure time increases the probability that a radical will react with monomer, which places limitations on the diffusion of oxygen.

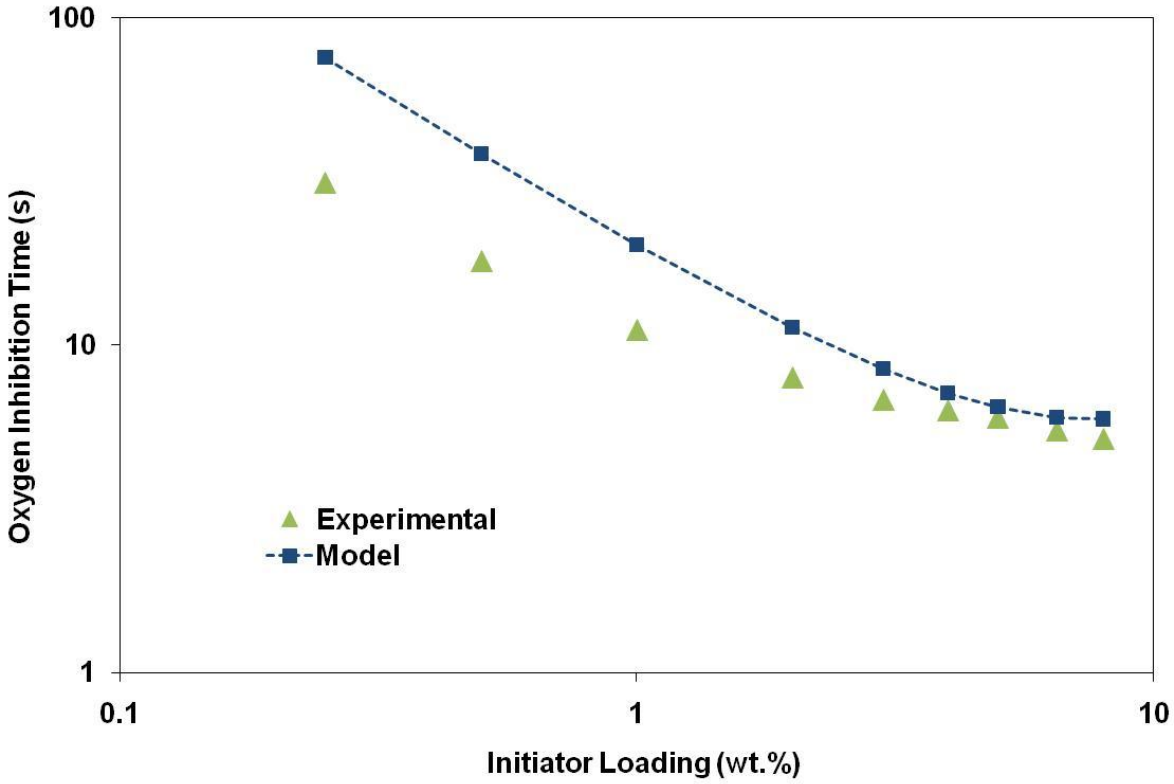

Figure 5.6: Comparison of the modeled and experimentally measured data for samples of TMPTA loaded with varying concentrations of DMPA continuously exposed to 10 W/m^2 of UV irradiance at 365 nm. The simulations were performed with an oxygen diffusion coefficient of 1 X 10^{-10} m$^{2/}$s and a rate constant for oxygen consumption of 1 X 10^{-9} m^3/mol-s.

The success of the reaction-diffusion model for the one-dimensional transport in the fully illuminated sample inspired its application to the two-dimensonsal case of the spatially modulated, masked sample. The goal was to expand the simple scaling relation behind the master curve of Figure 5.4, which assumed reaction-limited oxygen inhibition, and incorporate oxygen transport limitations. The one-dimensional model was expanded to simulate the experiments presented in Figure 5.2. Specifically, the dependence of the inhibition time on the exposed area fraction was calculated for samples of TMPTA loaded with 2.0 wt.% DMPA at 4 and 8 W/m^2 of UV irradiance. The computational domain for our numerical calculations is sketched in Figure 5.1c. The results of these

calculations and the experimental results are presented in Figure 5.7. For a fair comparison, only the data for line patterns are shown; the box patterns were left out, because they require a full three-dimensional model.

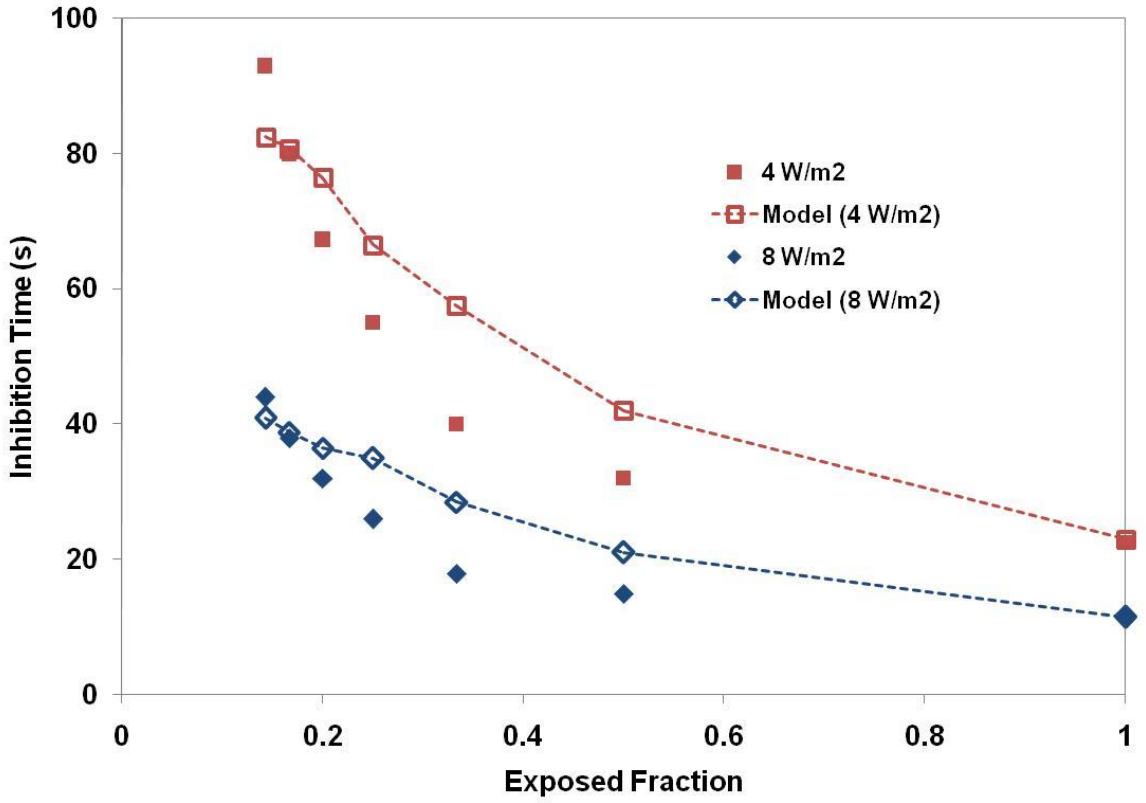

Figure 5.7: Comparison of the modeled and experimentally measured data for samples of TMPTA loaded with 2.0 wt.% DMPA continuously exposed to either 4 or 8 W/m^2 of UV irradiance at 365 nm. The simulations were performed with an oxygen diffusion coefficient of 1 X 10^{-10} m$^{2/}$s and a rate constant for oxygen consumption of 1 X 10^{-9} m^3/mol-s. The opened symbols represent modeled data, while the closed symbols represent experimental data.

Considering that the simulated data in Figure 5.7 were obtained without adjustable parameters, the model provides a reasonable first order approximation of the experimental data from microrheology. The deviations between experiment and model are of the same order of magnitude for 4 W/m^2 and 8 W/m^2, which demonstrates that the model is robust enough to capture significant changes in process conditions. Figure 5.7

also illustrates that the model is able to predict the upward trend of inhibition time with decreasing exposed fraction observed in the experimental data. However, it is apparent that the model falls short of capturing the details of the trend of the experimental data. In fact, the modeled data appear to approach a plateau in inhibition time at low fractions of exposed area, while the experimental data continues to diverge. For exposed fractions from 0.5 to 0.167, the model predicts an induction period that is greater than that measured by microrheology experiments, while at the lowest exposure fraction the model underpredicts the inhibition time.

Why does the model fail to quantitatively predict our experiments? Excellent agreement between experimental and model results was observed for the fully exposed samples in Fig. 5.7 (f = 1) and for the full depth profile in Fig. 5.5, with only one-dimensional spatial variations in the direction of illumination. Therefore, the limitations of the model in Figure 5.7 are likely due to the more complicated two-dimensional nature of the masking experiments. One explanation for these deviations could be that the model assumes a constant oxygen diffusion coefficient. As discussed above, research has shown that the formation of small polymer chains during the oxygen induction period results in a time dependent diffusion coefficient, with decreasing oxygen mobility as the polymerization process progresses [8]. In our set-up, it is feasible that the diffusion coefficient also varies as a function of location. Similar variations might be expected in the kinetic rate constants.

In addition, the microrheology experiments used to verify the two-dimensional model simulations are inherently more complex than the one-dimensional experiments and have several sources of error that could contribute to the observed differences

between experiments and model. For example, shadowing effects cannot be ruled out entirely. The aluminum masking layer was placed on the sample-side of the microscope slide and the light was collimated carefully to minimize such effects, but they cannot be ruled out entirely. The illumination profile in the model for these spatially modulated experiments is a perfect step function, but the actual intensity profile will be more complex. Finally, the line patterns of the mask were found to deviate slightly from the designed width of 50 μm, but this should not be a dominant effect. To further address these issues, experiments with variable width of the illuminated area could be performed; however, that is beyond the scope of this research.

In order to narrow the search for key parameters that could affect the results of our predictions, the sensitivity of the two-dimensional model to certain variables was investigated. The majority of the model parameters were either known molecular constants or experimentally measured in our lab (see Table 1); however, the diffusion coefficient of oxygen [14, 16] and the rate constant of oxygen consumption [26, 27] were obtained from literature. Since these literature values are merely order of magnitude estimates and not accurately known for our specific sample of TMPTA with 2.0 wt.% DMPA, we identified these parameters as our key candidates. The rate constant and diffusion coefficient were varied to obtain a more complete understanding of the process of oxygen inhibition and limitations of the model. The value of the rate constant for oxygen consumption found in literature was $1 \cdot 10^6$ m^3/mol-s. As illustrated in Equation 5.12, increasing the rate constant should result in a reduction in the observed oxygen inhibition time. Figure 5.8 shows the effects of varying the rate constant of oxygen consumption on model simulations of TMPTA samples loaded with 2.0 wt.% DMPA and

exposed to 4 W/m^2 of UV irradiance. All simulations were performed with a constant oxygen diffusion coefficient of $1 \cdot 10^{-10}$ m$^{2/}$s.

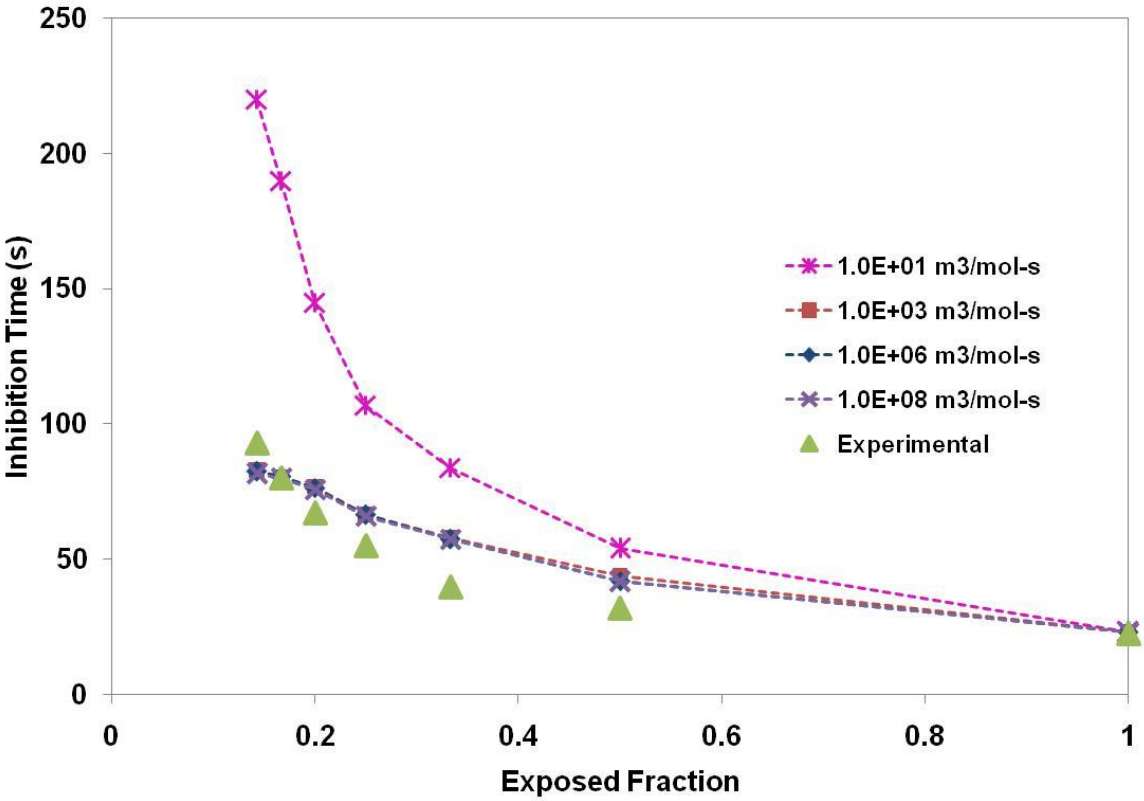

Figure 5.8: Simulation results of the inhibition time in samples of TMPTA loaded with 2.0 wt.% DMPA exposed to 4 W/m^2 of UV irradiance at 365 nm. The inhibition time is shown as a function of the fraction of the sample exposed to UV illumination and the rate coefficient of oxygen consumption. Simulations were performed with a constant oxygen diffusion coefficient of $1 \cdot 10^{-10}$ m$^{2/}$s.

The data in Figure 5.8 demonstrate that increasing the rate constant by a factor of 100 does not change the inhibition time, suggesting that the process is already diffusion-limited. In fact, even lowering the rate constant by a factor of 1000 does not result in a measureable change in inhibition time. In order to see a significant change in the inhibition time, the rate constant has to be decreased by a factor of 100,000. When the rate constant is decreased to a value of 10 m^2/mol-s, the simulation data exhibit upward curvature similar to that observed in experiments. However, at such a low value of k_o the

inhibition time from the model drastically overpredicts the time measured using microrheology. Research has shown that the rate coefficient of oxygen consumption is several orders of magnitude higher than any other reaction coefficient found in polymerization [17], thus a rate constant of 10 m^2/mol-s is highly improbable. A large oxygen reactivity coefficient is necessary to explain why no polymerization occurs in the presence of oxygen.

To determine the effect of diffusion coefficient on the oxygen inhibition time in TMPTA, the value found in literature, $1 \cdot 10^{-10}$ $m^{2/}s$, was varied over a range of limited magnitude. The diffusion coefficient determines the mobility of oxygenand depends on the temperature, viscosity of the monomer, and the size of the oxygen molecule in accordance with the Stokes-Einstein relation. Since a large diffusion coefficient indicates that oxygen molecules can freely move through the sample, increasing the diffusion coefficient in a spatially modulated system should result in a greater oxygen inhibition time. Decreasing the diffusion coefficient, on the other hand, should lead to reduced oxygen inhibition. The results of varying the diffusion coefficient in the model are shown in Figure 5.9; the kinetic rate coefficient value was kept constant at $1 \cdot 10^6$ m^3/mol-s.

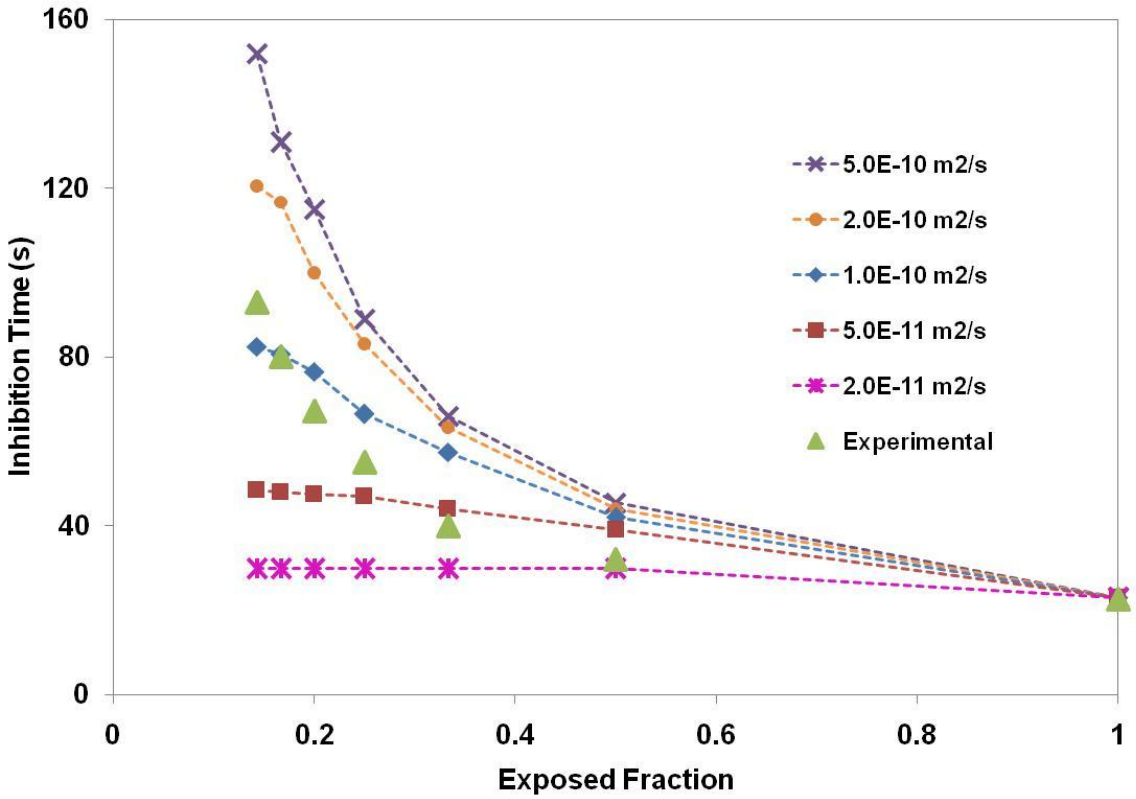

Figure 5.9: Simulation results of the inhibition time in samples of TMPTA exposed to 4 W/m^2 of UV irradiance at 365 nm. The inhibition time is shown as a function of the fraction of the sample exposed to UV illumination and the diffusion coefficient of oxygen. All simulations were performed using a constant rate coefficient value of 1 X 10^6 m^3/mol-s.

The figure clearly shows that diffusion coefficient of oxygen significantly impacts the oxygen inhibition time. Increasing the diffusion coefficient by a factor of two increases the inhibition time and changes the scaling of the modeled data. At $2 \cdot 10^{-10}$ m^2/s, the simulated data displays a pronounced upward curvature that is similar to that observed in the experimental data set. However, unlike the experimental data, even at the higher diffusion coefficient, the simulated data still approaches a plateau at low exposure fractions. This plateau is a result of the fact that a finite diffusion coefficient limits the distance over which oxygen can be transported in the illuminated sample. At low values for the diffusion coefficient, for example for $2 \cdot 10^{-11}$ m^2/s in Figure 5.9, oxygen cannot

move sufficiently to enable transport of oxygen from the masked regions into the illuminated areas. As a result, the exposed fraction has not effect on the exposed fraction any longer. For intermediate diffusion values, oxygen can only be transported into the exposed fraction of the sample from the part of the dark area that is closest; oxygen that is too far from the illuminated area cannot play a role in the inhibition process. Therefore, decreasing the exposed fraction by expanding the dark areas does not increase the inhibition time any further, leading to the plateau at low f values. Increasing the diffusion coefficient to $5 \cdot 10^{-10}$ m^2/s in the model fully eliminates and the resulting simulated data represents the qualitative features of the experimental data best, albeit at substantial longer inhibition times than measured experimentally. In addition to varying the key parameters independently, we also tried various combinations, but we were unable to reach substantially better agreement between model and experiments than was observed originally in Figure 5.7. It is therefore likely that variations of these variables as a function of time and or location must be taken into account to reproduce the experimental results.

5.5. Conclusions

The impact of oxygen on the photopolymerization of a multifunctional acrylate resin was investigated using the experimental and modeling efforts. Specifically, the transport of dissolved oxygen in TMPTA during photopolymerization was examined using particle tracking microrheology by spatially modulating the UV illumination profile with patterned lithographic masks. These masks allowed certain areas of the sample to be exposed to UV light, while at the same time, shielding other areas from illumination. As the fraction of exposed area was decreased, the overall gelation time was to significantly

increase. Since radicals are only generated in the illuminated areas, this increase in gel time was attributed to the diffusion of oxygen into the illuminated areas from the shielded areas that were not exposed to UV irradiance.

A simple two-step model for the polymerization of UV sensitive acrylate resins was developed that assumed that the time required to reach the gel point can be divided into an oxygen inhibition time and a kinetic reaction time. The model was applied in one dimension as a function of UV penetration depth. The model data was in good agreement with previously obtained microrheology data, which showed that in the presence of oxygen, the dependence of the gel time on UV penetration depth does not follow the trend predicted by Beer's Law. The diffusion of oxygen in the plane parallel to the incidence of UV irradiance results in a linear dependence of the gel time at high concentrations of photoinitiator. Considering the simplicity of the proposed model, the two dimensional results showed reasonable agreement with the experimental results obtained using microrheology. Deviations between the experimental and simulated data are likely the result of the model failure to incorporate conversion dependant diffusion coefficients. Simulations showed that the consumption of oxygen in not reaction limited, but rather diffusion limited. This work provides unique, high resolution data that cannot be obtained using the volume based methods, such as FTIR and calorimetry.

5.6. References

1. Drobny, J.G., *Radiation Technology for Polymers*. 2003, London: CRC Press.

2. Pappas, S.P., *UV Curing: Science & Technology Volume II*. 1985, Norwalk, CT: Technology Marketing Corporation.

3. Roffey, J.G., *Photopolymerization of Surface Coatings*. 1982, New York: John Wiley & Sons.

4. Decker, C., (1994). "Photoinitiated Curing of Multifunctional Monomers." Acta Polymer, **43**: 333-347.

5. Kaur, M. and A.K. Srivastava, (2002). "Photopolymerization: A review." Journal of Macromolecular Science-Polymer Reviews, **C42**(4): 481-512.

6. Odian, G.G., *Principles of polymerization*. 4th ed. ed. 2004 Hoboken, N.J.: Wiley-Interscience.

7. Mode, G. and D.H. Solomon, *The Chemistry of Radical Polymerization, Second fully revised edition*. 2006, New York: Elsevier Ltd.

8. Decker, C. and A.D. Jenkins, (1985). "Kinetic Approach of O2 Inhibition in Ultraviolet-Induced and Laser Induced Polymerizations." Macromolecules, **18**(6): 1241-1244.

9. Krongauz, V.V. and E.R. Schmelzer, (1992). "Oxygen Effects on Anisotropic Photopolymerization in Polymer Matrices." Polymer, **33**(9): 1893-1901.

10. Ruiz, C.S.B., L.D.B. Machado, J.E. Volponi, and E.S. Pino, (2004). "Oxygen inhibition and coating thickness effects on UV radiation curing of weatherfast clearcoats studied by Photo-DSC." Journal of Thermal Analysis and Calorimetry, **75**(2): 507-512.

11. Nunes, T.G., L. Ceballos, R. Osorio, and M. Toledano, (2005). "Spatially resolved photopolymerization kinetics and oxygen inhibition in dental adhesives." Biomaterials, **26**(14): 1809-1817.

12. Scherzer, T. and H. Langguth, (2001). "The effect of temperature on the induction period in the photoinitiated polymerization of tripropylene glycol diacrylate." Nuclear Instruments & Methods in Physics Research Section B-Beam Interactions with Materials and Atoms, **185**: 276-282.

13. Scherzer, T. and H. Langguth, (2005). "Temperature dependence of the oxygen solubility in acrylates and its effect on the induction period in UV photopolymerization." Macromolecular Chemistry and Physics, **206**(2): 240-245.

14. O'Brien, A.K. and C.N. Bowman, (2006). "Impact of oxygen on photopolymerization kinetics and polymer structure." Macromolecules, **39**(7): 2501-2506.

15. O'Brien, A.K., N.B. Cramer, and C.N. Bowman, (2006). "Oxygen inhibition in thiol-acrylate photopolymerizations." Journal of Polymer Science Part a-Polymer Chemistry, **44**(6): 2007-2014.

16. O'Brien, A.K. and C.N. Bowman, (2006). "Modeling the effect of oxygen on photopolymerization kinetics." Macromolecular Theory and Simulations, **15**(2): 176-182.

17. Dickey, M.D., R.L. Burns, E.K. Kim, S.C. Johnson, N.A. Stacey, and C.G. Willson, (2005). "Study of the kinetics of step and flash imprint lithography photopolymerization." Aiche Journal, **51**(9): 2547-2555.

18. Studer, K., C. Decker, E. Beck, and R. Schwalm, (2003). "Overcoming oxygen inhibition in UV-curing of acrylate coatings by carbon dioxide inerting, Part I." Progress in Organic Coatings, **48**(1): 92-100.

19. Studer, K., C. Decker, E. Beck, and R. Schwalm, (2003). "Overcoming oxygen inhibition in UV-curing of acrylate coatings by carbon dioxide inerting: Part II." Progress in Organic Coatings, **48**(1): 101-111.

20. Fouassier, J.P. and J.F. Rabek, *Radition Curing in Polymer Science and Technology Volume III: Polymerization Mechanisms*. 1993, London: Elsevier Applied Science.

21. Bolon, D.A. and K.K. Webb, (1978). "Barrier Coats Versus Inert Atomospheres Elimination of Oxygen Inhibition in Free-radical polymerizations." Journal of Applied Polymer Science, **22**(9): 2543-2551.

22. Decker, C., (1979). "Novel Method for Consuming Oxygen Instantaneously in Photopolymerizable Films." Makromolekulare Chemie-Macromolecular Chemistry and Physics, **180**(8): 2027-2030.

23. Slopek, R.P., H.K. McKinley, C.L. Henderson, and V. Breedveld, (2006). "In situ monitoring of mechanical properties during photopolymerization with particle tracking microrheology." Polymer, **47**(7): 2263-2268.

24. Fouassier, J.P., *Photoinitiation, Photopolymerization, and Photocuring – Fundamentals and Applications*. 1995, Cincinnati, OH: Hanser/Gardner Publications.

25. Gou, L.J., C.N. Coretsopoulos, and A.B. Scranton, (2004). "Measurement of the dissolved oxygen concentration in acrylate monomers with a novel photochemical method." Journal of Polymer Science Part a-Polymer Chemistry, **42**(5): 1285-1292.

26. Fouassier, J.P. and A. Merlin, (1980). "Laser Investigation of Norrish Type I Photoscission in the Photoinitiator Irgacure (2,2- Dimethoxy 2-Phenyl-Acetophenone.)." Journal of Photochemistry, **12**(1): 17-23.

27. Neta, P., R.E. Huie, and A.B. Ross, (1990). "Rate Constants for Reactions of Peroxyl Radicals in Fluid Solutions." Journal of Physical and Chemical Reference Data, **19**(2): 413-513.

28. Anseth, K.S. and C.N. Bowman, (1994). "Kinetic Gelation Model Predictions of Cross-linked Polymer Network Microstructure." Chemical Engineering Science, **49**(14): 2207-2217.

29. Tang, Y.Y., C. Henderson, J. Muzzy, and D.W. Rosen, (2004). "Stereolithography cure modelling and simulation." International Journal of Materials & Product Technology, **21**(4): 255-272.1.

CHAPTER 6

CONCLUSIONS AND RECOMMENDATIONS

In this chapter, important results of the research project will be summarized and conclusions will be drawn. Recommendations on how to use the obtained experimental results and how to improve the current experimental setup will be presented. Finally, future research in the utilization of microrheology to study photopolymerization will be proposed.

6.1. Summary

The research presented in this thesis can be summarized as follow:

- Currently, issues affecting the cure speed and overall quality of the polymer product (shape, size, and surface finish) are limiting the use of free-radical photopolymerization in certain fields.
- Microrheology has the ability to track rheological changes in photoresins with high resolution as a function of both time and location; and therefore, can provide a better understanding of the overall process.
- Significant variations in the gelation time were observed as a function of UV penetration depth over a 100 micron sample.
- The energy threshold model fails to accurately predict the gelation time at low intensities and in thick samples.

- Performing the photopolymerization on oxygen saturated samples changes the kinetic scaling from an exponential to a power law decay.
- Microrheology can accurately be used to monitor the polymerization front with high spatial and temporal resolution.
- A spike in the structural heterogeneity of polymerization occurs at the gel point and this heterogeneity increases with increasing monomer functionality.
- Exposing a sample to multiple pulses of UV light separated by periods of darkness reduces the amount of UV exposure required to achieve gelation.
- Post UV exposure reactions in multifunctional acryaltes were found to be insignificant after one second.
- Removing dissolved oxygen from the acrylate sample significantly increased the effectiveness of the measured dark reaction.
- The consumption of oxygen by radicals was found to be limited by diffusion and not by reaction kinetics.
- In the presence of oxygen, the dependence of gel time on UV penetration depth was determined to be linear and not exponential as predicted by Beer's Law.
- Modeling the photopolymerization process as a simple two step process yielded reasonable agreement with experimentally obtained data.
- Microrheology provides unique, high resolution data that cannot be obtained using other techniques commonly employed to study photopolymerization.

6.2. Conclusions

Despite the importance and widespread use of photopolymerization in numerous industrial applications, limitations that result from a general lack of understanding about the process continue to exist. Specifically, spatial variations of photopolymerization and oxygen inhibition impose significant limitations on applications that require high spatial resolution and an ultra fast processing time. Past studies of photo-induced polymerization have been performed using spectroscopy, calorimetry, and rheology. Although previous research by these technologies has expanded the knowledge of the photopolymerization process, the techniques used in these studies lack the ability to monitor photopolymerization with both high spatial and temporal resolution.

To address these issues, the emerging technique of microrheology was employed to study and monitor the photopolymerization process in-situ. The initial results prove the ability of microrheology to track rheological changes in samples of photoresins as a function of both time and location. Through this research, a better understanding of both the kinetic behavior and spatial variations of acrylate photoresins is achieved.

A significant increase in the gelation time was observed as a function of UV penetration depth. The trend was found to be independent of monomer functionality and UV intensity. These results show that microrheology has the potential to provide considerable insight into the spatial inhomogeneities that plague many applications. In addition, the presence of oxygen was found to significantly in the cure time of acrylate resins. Removing the dissolved oxygen from acrylate samples, resulted in a shift in reaction kinetics from a power law decay in oxygen saturated samples to an exponential decay in degassed samples.

The results of the intensity study not only show that decreasing the UV intensity decreases the gelation time, but also that the simple energy threshold model is not accurate at empirically predicting photopolymerization at low intensities of UV irradiation or in deep samples. The intensity study also provides insight into the rate constant of the initiation mechanism. In addition, the experimental data can be used to validate and strengthen models that are currently being developed to predict the outcome of photopolymerization. The results give a good understanding of how the reaction kinetics, shown in Equations 1.1-1.13, are affected by changing system parameters. This information could be used to test the predictive powers of current models and aid in the development of new models. For instance, it is expected that the data in Figures 3.1-3.4 could be used to develop an accurate model that is able to balance the initially dominant initiation and inhibition (oxygen and polymerization inhibition) kinetics and the propagation and termination kinetics that determine the later stage of the process.

The variation of the illumination profile with time provided information about the location of the polymer front, the extent of post UV exposure reaction, and structural heterogeneity. The reaction of radicals in the dark was found to be insignificant after one second. Removing the dissolved oxygen from the system was found to significantly increase the effectiveness of the post UV exposure reaction. The polymerization front was mapped with respect to time and location. This data shows that in the middle of a sample the liquid-to-gel transition occurs over 300 ms. In addition, a maximum in the structural heterogeneity in a polymerizing system was found to occur at the gel point.

Spatially dependent microrheology experiments demonstrated that the diffusion of oxygen in multifunctional acrylate systems was remarkably fast. The proposed model,

which assumed gelation of acrylate resins is simple two-step process, consisting of oxygen inhibition and network formation, was shown to give a reasonable first-order approximation of the process. In samples loaded with high concentrations of photoinitiator, the observed linear dependence of the gel time on UV penetration depth was determined to be a result of oxygen inhibition.

In conclusion, microrheology is an effective tool for monitoring the photopolymerization process. The research offered in this thesis uniquely expands the understanding of photo-induced free-radical polymerization. Microrheology allows for the optimization of process formulations and provides important kinetic information that could be used to advance modeling efforts. The presented research achieves the goals set forth by the objective and gives the basis and direction for future work.

6.3. Recommendations

The above presented research has proven without a doubt that particle tracking microrheology is capable of monitoring the UV induced polymerization of acrylate resins with unprecedented spatiotemporal resolution. This technique, however, does not provide information about the chemical conversion of the monomer. The majority of comprehensive polymerization models in literature are designed to predict the conversion of the monomer double-bond [1-3]. During photopolymerization, polymer is formed at the expense of the monomer double-bond, thus techniques such as photo-DSC [4, 5] and FTIR [6, 7] are commonly used to measure the decrease in double-bond concentration with time. In order to compare microrheological measurements of the gel point to a model that predicts conversion, one could calculate critical conversion at the gel point using the Flory—Stockmayer statistical theory of gelation. Research, however, has

shown that the assumptions made by the Flory—Stockmayer theory are not valid for fast reacting systems of high functionality [8, 9]. As a result, the gel point calculated using the Flory—Stockmayer theory may not be equivalent to the gel point measured by a rheometer. An alternative approach is to use a spectroscopy based technique to directly measure the monomer conversion at gel point specified by microrheology data. If the FTIR data is obtained under the same conditions used in microrheology, the measured conversion at the gel point can be directly compared to modeled predictions.

Thus it is recommended that the experimental data obtained using microrheology be compared to FTIR data obtained under the same conditions. In order to directly match the conditions of the microrheology experiments, FTIR analysis will have to be performed on samples cured outside the instrument. One drawback of this approach is that the sample may change from the one obtained directly after irradiation due to dark curing. In Chapter 4, we extensively studied the post UV exposure reactions in the acrylate systems and found them to be insignificant after one second, and thus, the effects are known. Preliminary FTIR analysis of EEA loaded with 5.0 wt.% DMPA is presented in Figure 6.1.

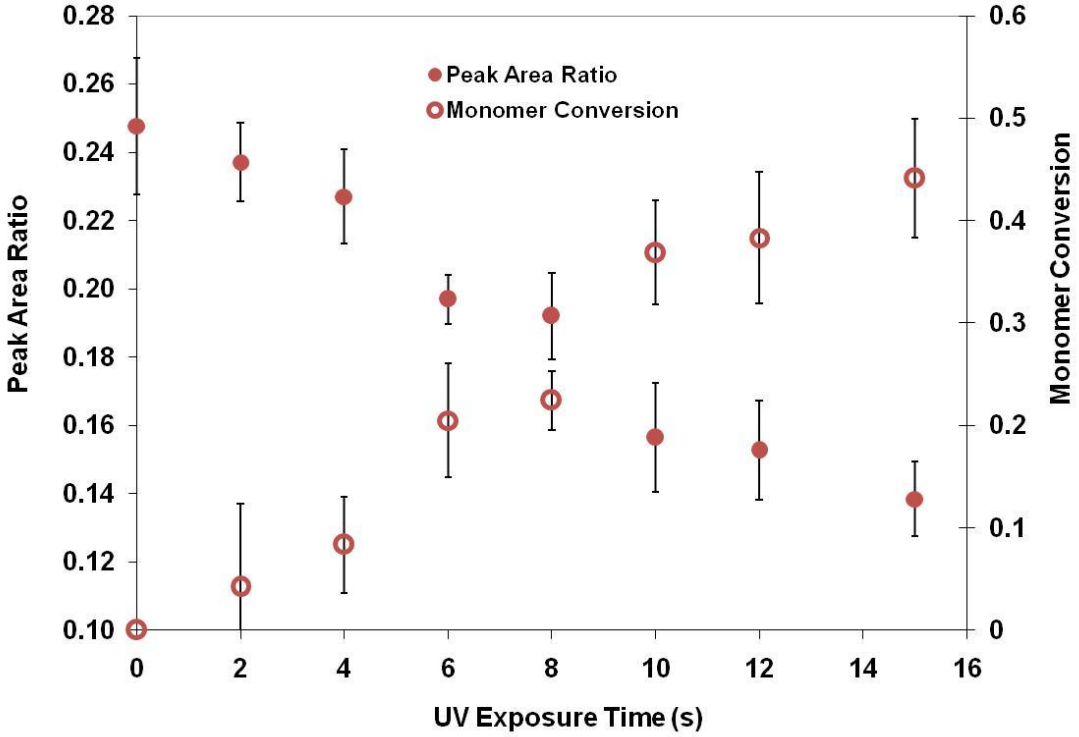

Figure 6.1: Double-bond conversion and the peak area ratio of the double-bond to the carbonyl plotted as a function of UV exposure time for EEA loaded with 5.0 wt.% DMPA. The photosensitive systems were saturated with oxygen and exposed to continuous UV illumination at 365 nm. Microrheology shows gelation of the sample occurs at 23 seconds.

Since the concentration of the carbonyl group does not change with exposure time, the peak area ratio of the double-bond to carbonyl group was used to standardize the analysis of double-bond concentration. As seen in Figure 6.1 the peak area ratio, and thus the double-bond concentration, decreases with exposure time. Although conversion in EEA, a linear monomer, is expected to approach a value of one, the fact that the conversion is only at 0.45 after 15 seconds is not unexpected considering the gel time measured using microrheology was found to be 23 seconds. It is important to note that the conversion data in Figure 6.1 is averaged over the entire sample volume, whereas, the data obtained using microrheology are not volume averaged. This may result in minor

discrepancies between the FTIR and microrheology data. The preliminary data in Figure 6.1 shows that FTIR is capable of monitoring the conversion of EEA as it approaches the gel point determined by microrheology; however, further analysis is necessary to obtain a complete understanding. Complementing microrheology results with FTIR data has the potential to increase understanding of UV induced cross-linking reactions and optimize process models.

A fundamental source of error in this research was the loss of resolution associated with the photobleaching of the embedded silica particles. Photobleaching made images difficult to analyze toward the end of the experiment and resulted in artifacts for some data sets. In addition, the high density silica particles sedimented relatively quickly and aggregated at the bottom of the sample chamber, especially for low-viscosity monomers. As a result, fewer particles were available for statistical analysis and the contrast and clarity of the images were reduced. Using less dense, more fluorescently stable particles, such as commercial produced polystyrene particles, would greatly reduce error in the image analysis. Polystyrene particles, however, swell and leach fluorescence in the current system of acrylate monomers. As a result, alternative methods like growing a thin silica layer on a polystyrene particle need to be investigated.

The experimental data obtained from this research has the potential to positively impact efforts to model and control the process of photopolymerization. The empirical threshold model is the least complicated model applied to photopolymerization. The model is based on the idea that polymerization reaches percolation after a certain amount of critical energy is delivered to the sample. The model neglects to consider the kinetics of free-radical polymerization, listed by Equations 2.13-2.22, and the heat and mass

transfer associated with photo-induced polymerizations. Consequently, the simplicity of the model is lost in the fact that new values of the energy threshold must be determined for each experimental formulation and geometry. Subsequent models have been developed that incorporate both reaction kinetics and transport processes. The data ascertained in this research could be used to strengthen and validate current and future models.

6.4.Future Research

Acrylate and methacrylate monomers are highly reactive; as a result theses systems are by far the most widely used in free-radical photopolymerization processes. Compared to cationic polymerization, free-radical polymerization exhibits significantly more polymerization shrinkage. Shrinkage results in a 5-25% loss in volume (2-8% in linear dimensions) [10, 11] caused by the formation of covalent bonds during the photopolymerization process. Covalent bonds decrease the distance between monomer molecules by approximately half compared to two molecules experiencing Van der Waal's forces. In literature shrinkage is usually given as a percentage change in volume and is often quantified as:

$$S = \frac{\Delta V}{V + \Delta V} \times 100 \tag{6.1}$$

where V is the volume of the cured species and ΔV is the difference between the volumes of the uncured and cured species [12]. Shrinkage causes stress in the polymer parts, which ultimately affects the performance and quality of the final product. Product failure such as coating delamination, gaps in dental fillings, and mismatch of the mold and embossed polymer dimensions in UV embossing all result from shrinkage [12].

Polymerization shrinkage is a major problem that significant burdens industry and obstructs the expanded use of photo-induced curing.

Understanding the development of shrinkage during the photopolymerization process is principle to reducing costs, optimizing productivity, and increasing product quality. As a result, there are several experimental devices for active measurement of polymerization, including: dilatometry (mercury [13] and water-based [14, 15]), buoyancy test, interferometry [16-18], strain gage techniques [19-21], optical scanning [22] and direct linear displacement transducer measurements [23, 24]. Each of these techniques has its advantages and disadvantages. Mercury based dilatometry has potential health hazards [14], is very sensitive to thermal fluctuations [13] and being opaque to radiation, it is unsuitable for use with photocured materials [24]. Water-based dilatometry is also dependant on temperature stability [15] and may be influenced by water absorption by the resin. Both dilatometry techniques are labor intensive [25]. Buoyancy techniques are reasonably insensitive to temperature changes, but are very sensitive to air bubbles attached to the resins surface or to the suspending wire. Techniques based on measuring linear shrinkage using contact displacement transducers are much less labor intensive [25], but may have potential errors associated with the effect of gravity or the load of the measuring system on the result of non-uniform shrinkage [25].

The current setup, which utilizes a mask with a single millimeter-sized gap, was also used to explore the spatial resolution of the microrheological setup. The trifunctional SL resin, TMPTA enhanced with 1.0 wt.% DMPA was exposed to UV light for approximately 1 minute; afterwards, UV illumination was terminated and

measurements of microrheology were performed at the edge of the masked area. The resulting curves of MSD as a function of position are shown in Figure 6.2. The inset shows the full trajectories of all tracer particles in the field of view. From the trajectories, it is clear that the particles to the right of the phase boundary are unable to move because they are trapped in the cross-linked gel network, while the tracer particles to the left of the boundary are able to diffuse without constraint. The observation is clearly supported by the MSD data in Figure 6.2. On the left side of Figure 6.1 the transient MSD curves depend on lag time, which is a characteristic of a viscous liquid, while on the right the MSD is independent of lag time, indicating a gel. The mask used in the current experimental setup is sufficient to minimize the effects of shrinkage, but not to study the process of shrinkage quantitatively.

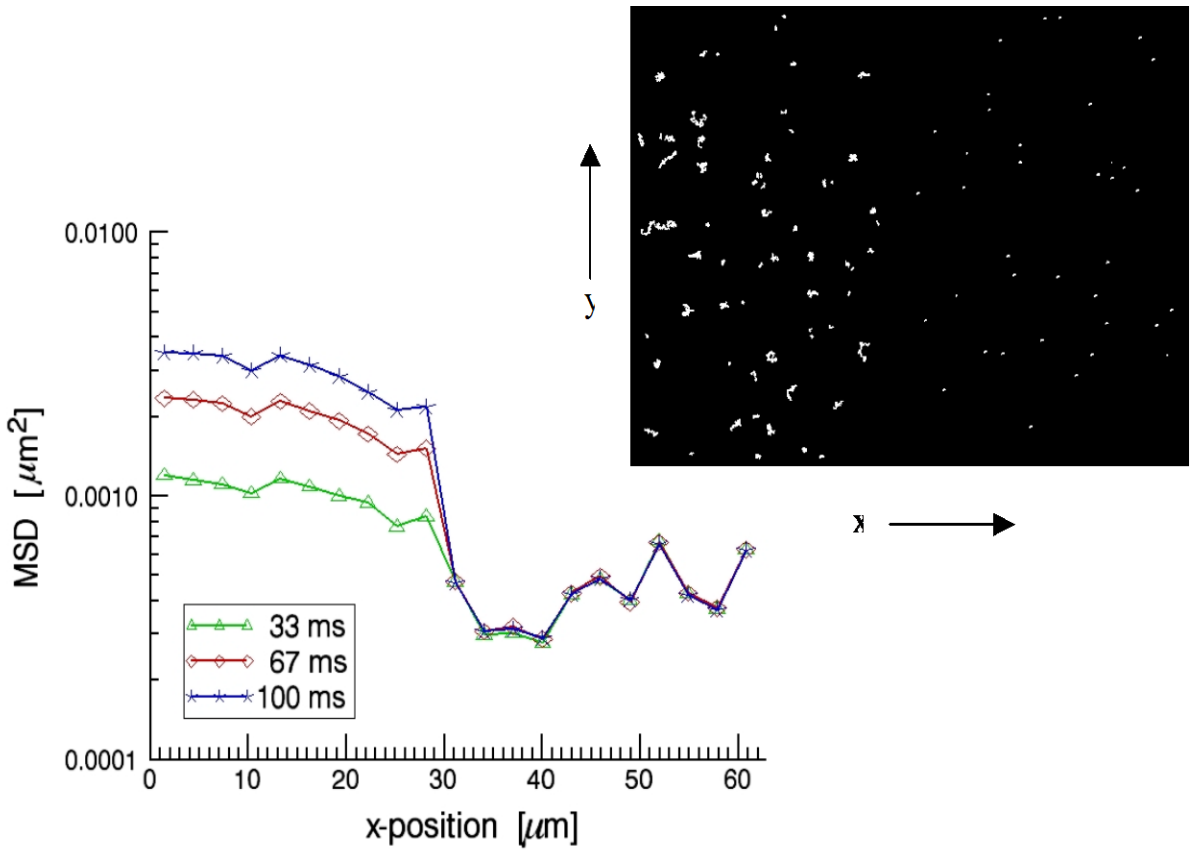

Figure 6.2: Spatial variations of tracer particle MSD in a partly exposed cured sample of trimethylolpropane triacrylate with 1.0 wt% DMPA.

The above results prove that the current experimental setup has the high spatial resolution necessary to further study the effects of shrinkage. By varying the illumination profile as a function of space detailed information about the local effects of polymerization shrinkage can be obtained using an experimental setup similar to that outlined in Chapter 5. Since polymerization shrinkage is often inhomogeneous within light-cured materials, the ability to monitor the process on a local level using microrheology would greatly enhance and expand current knowledge of shrinkage. As illustrated in Figure 6.3, various patterned lithographic mask with micrometer-sized line spacings and patterns can be fabricated and used in conjunction with videomicroscopy to study spatial effects. The masking experiments are expected to enable quantitative

characterization of shrinkage effects during photopolymerization. Information such as the origin of shrinkage in the sample as well as real-time measurements of the velocity profiles can be obtained by performing statistical analysis of the bulk motion recorded during the gelation process. The velocity can readily be determined using the recorded particle trajectories by dividing the total particle displacement (in both the x direction and y direction) by the time interval between images. In addition, the study would provide three-dimensional profiles of gelation by using microscopy to examine the sample at the boundaries of the mask pattern.

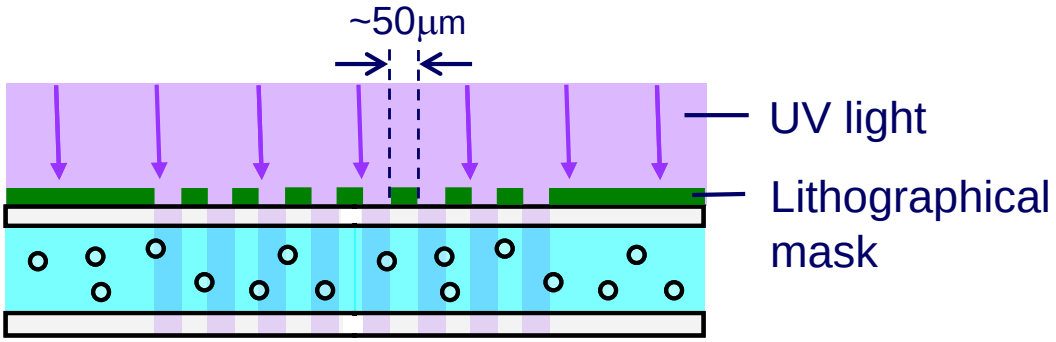

Figure 6.3: Experimental design for spatial patterned photo-masks.

The above design will allow the variation of several parameters including illumination area, spacing between illuminated area, incident intensity, and photoresin composition. It is expected that exposing a larger area to UV irradiation will lead to more shrinkage. By varying the spacing between exposure gaps it is anticipated that the direction of shrinkage can be altered. If a large area of unexposed sample surrounds exposure gap shrinkage may become more unidirectional since when contraction occurs the exposed area can draw in as much sample as necessary. It is hypothesized that having

exposure gaps separated by a smaller amount of unexposed area will cause sample to be drawn in from multiple directions during contraction. Decreasing the incident intensity and resin functionality is expected to increase the amount of shrinkage. Areas where shrinkage occurs can be determined by examining the velocity profiles; areas where no shrinkage occurs would have a zero velocity. This type of analysis could allow for the determination of the origin of contraction. In addition, since velocity is a vector, the direction of shrinkage can be determined. Experimental data obtained from the proposed research can be used to validate and strengthen models that are currently being developed to predict shrinkage.

The ultimate future goal would be the commercial implementation of microrheology as a tool for high-throughput screening and in-line quality control monitoring. The ability to use microrheology to perform high-throughput screening has already been well-established [26] and preliminary results prove that microrheology has the ability to accurately perform in-situ process monitoring. The current experimental setup which uses video microscopy is almost certainly too slow for high-throughput screening and in-line quality monitoring; therefore, different microrheological techniques need to be investigated. The implementation of microrheology in commercial processes has the potential to improve product quality and uniformity, as well as lower process cost associated with manual quality control.

The focus of this investigation will be on the microrheological technique of diffusing wave spectroscopy (DWS) since it has been shown to have necessary accuracy and temporal resolution required to perform high-throughput screenings [27]. DWS is a multiple scattering technique that can detect particle displacements at the sub-nanometer

level [26, 27]. Weitz and coworkers laid the foundation for DWS in the late 80's [28]; the technique has since developed into an effective tool for investigating dynamics of concentrated, highly scattering systems such as foams, emulsions, and colloidal suspensions [26]. DWS is based on the assumption that laser light used to illuminate a sample will experience a large number of scattering events before it exits the sample. The light leaving the sample is collected in either the forward or backward scattering direction before being projected onto a traditional dynamic light scattering detection apparatus. A DWS setup consists of a laser, optical collection tube, photomultiplier tube, amplifier-discriminator, digital correlator, and a computer.

The intensity correlation function can be directly transformed into a time-dependent MSD via the application of the Siegert relation, careful calibration of the DWS set up with reference sample, and basic numerical analysis [26]. The simplicity and speed of this process gives DWS an advantage over video microscopy based microrheology, which requires time-consuming image analysis. The inherent ensemble averaging of DSW, however, disables the advanced statistical treatment that is possible with single particle trajectories, which ultimately limits local spatial resolution. As a result, DWS requires a higher concentration of probe particles compared to video microscopy based techniques [26].

It is important to note that DWS is not a substitute for video microscopy based microrheology, but rather a complementary technique. The key advantages that DWS has over the particle tracking microrheology setup described in previous sections are Angstrom level spatial resolution and temporal resolution up to 10 MHz [26]. The principal disadvantage of DWS is that the technique relies on ensemble averaging over

the entire sample, which greatly increases efficiency of data acquisition and analysis. As a result, the local spatial information obtained using the setup currently being employed in this research is lost. The benefit of extremely high temporal resolution greatly outweighs the disadvantages of DWS when the technique is applied to high-throughput screening of process formulations.

6.5. References

1. Goodner, M.D. and C.N. Bowman, (2002). "Development of a comprehensive free radical photopolymerization model incorporating heat and mass transfer effects in thick films." Chemical Engineering Science, 57(5): 887-900.

2. Anseth, K.S. and C.N. Bowman, (1994). "Kinetic Gelation Model Predictions of Cross-inked Polymer Network Microstructure." Chemical Engineering Science, 49(14): 2207-2217.

3. Boots, H.M.J., J.G. Kloosterboer, G.M.M. Vandehei, and R.B. Pandey, (1985). "Inhomogeneity during the Bulk-Polymerization of Divinyl Compounds Differential Scanning Calorimetry Experiments and Percolation Theory." British Polymer Journal, 17(2): 219-223.

4. Sandner, B., N. Kotzian, J. Tubke, S. Wartewig, and O. Lange, (1997). "Photocalorimetric monitoring of the polymerization of an oligo(ethylene glycol) dimethacrylate in oligo(ethylene glycol) dimethyl ethers." Macromolecular Chemistry and Physics, 198(9): 2715-2727.

5. Clark, S.C., C.E. Hoyle, S. Jonsson, F. Morel, and C. Decker, (1999). "Photopolymerization of acrylates using N-aliphaticmaleimides as photoinitiators." Polymer, 40(18): 5063-5072.

6. Corcione, C.E., A. Greco, and A. Maffezzoli, (2004). "Photopolymerization kinetics of an epoxy-based resin for stereolithography." Journal of Applied Polymer Science, 92(6): 3484-3491.

7. Priola, A., G. Gozzelino, F. Ferrero, and G. Malucelli, (1993). "Investigation on the Structure-Property Relationships for Films Obtained from UV Curable Coatings." Progress in Organic Coatings, 22(1-4): 301-314.

8. Lovestead, T.M., A.K. O'Brien, and C.N. Bowman, (2003). "Models of multivinyl free radical photopolymerization kinetics." Journal of Photochemistry and Photobiology a-Chemistry, 159(2): 135-143.

9. Okay, O., H.J. Naghash, and I. Capek, (1995). "Free-radical Cross-linking Copolymerization Effect of Cyclization on Diffusion Controlled Termination at Low Conversion." Polymer, 36(12): 2413-2419.

10. Drobny, J.G., *Radiation Technology for Polymers*. 2003, London: CRC Press.

11. Kaur, M. and A.K. Srivastava, (2002). "Photopolymerization: A review." Journal of Macromolecular Science-Polymer Reviews, C42(4): 481-512.

12. Cook, W.D., M. Forrest, and A.A. Goodwin, (1999). "A simple method for the measurement of polymerization shrinkage in dental composites." Dental Materials, 15(6): 447-449.

13. Penn, R.W., (1986). "A Recording Dilatometer for Measuring Polymerization Shrinkage." Dental Materials, 2(2): 78-79.

14. Lai, J.H. and A.E. Johnson, (1993). "Measuring Polymerization Shrinkage of Photo-Activated Restorative Materials by a Water-Filled Dilatometer." Dental Materials, 9(2): 139-143.

15. Bandyopadhyay, S., (1982). "A Study of the Volumetric Setting Shrinkage of Some Dental Materials." Journal of Biomedical Materials Research, 16(2): 135-144.

16. Dudi, O. and W.T. Grubbs, (1999). "Laser interferometric technique for measuring polymer cure kinetics." Journal of Applied Polymer Science, 74(9): 2133-2142.

17. Fogleman, E.A., M.T. Kelly, and W.T. Grubbs, (2002). "Laser interferometric method for measuring linear polymerization shrinkage in light cured dental restoratives." Dental Materials, 18(4): 324-330.

18. Fano, V., W.Y. Ma, I. Ortalli, and K. Pozela, (1998). "Study of dental materials by laser beam scanning." Biomaterials, 19(16): 1541-1545.

19. Sakaguchi, R.L., A. Versluis, and W.H. Douglas, (1997). "Analysis of strain gage method for measurement of post-gel shrinkage in resin composites." Dental Materials, 13(4): 233-239.

20. Sakaguchi, R.L., C.T. Sasik, M.A. Bunczak, and W.H. Douglas, (1991). "Strain-Gauge Method for Measuring Polymerization Contraction of Composite Restoratives." Journal of Dentistry, 19(5): 312-316.

21. Sakaguchi, R.L., M.C.R.B. Peters, S.R. Nelson, W.H. Douglas, and H.W. Poort, (1992). "Effects of Polymerization Contraction in Composite Restorations." Journal of Dentistry, 20(3): 178-182.

22. Hudson, A.J., S.C. Martin, M. Hubert, and J.K. Spelt, (2002). "Optical measurements of shrinkage in UV-cured adhesives." Journal of Electronic Packaging, 124(4): 352-354.

23. Watts, D.C. and A.J. Cash, (1991). "Determination of Polymerization Shrinkage Kinetics in Visible-Light-Cured Materials - Methods Development." Dental Materials, 7(4): 281-287.

24. Watts, D.C. and A.J. Cash, (1991). "Kinetic Measurements of Photopolymerization Contraction in Resins and Composites." Measurement Science & Technology, 2(8): 788-794.

25. Degee, A.J., A.J. Feilzer, and C.L. Davidson, (1993). "True Linear Polymerization Shrinkage of Unfilled Resins and Composites Determined with a Linometer." Dental Materials, 9(1): 11-14.

26. Breedveld, V. and D.J. Pine, (2003). "Microrheology as a tool for high-throughput screening." Journal of Materials Science, 38(22): 4461-4470.

27. Waigh, T.A., (2005). "Microrheology of complex fluids." Reports on Progress in Physics, 68(3): 685-742.

28. Pine, D.J., D.A. Weitz, P.M. Chaikin, and E. Herbolzheimer, (1988). "Diffusing-Wave Spectroscopy." Physical Review Letters, 60(12): 1134-1137.